UNIVERSITY OF SOUTHAMPTON

FACULTY OF ENGINEERING, SCIENCE AND MATHEMATICS

SCHOOL OF PHYSICS AND ASTRONOMY

Optical and X-ray Studies of Be/X-ray Binaries in the Small Magellanic Cloud

Matthew Peter Edward Schurch

Thesis for the degree of Doctor of Philosophy

April 20, 2009

UNIVERSITY OF SOUTHAMPTON

ABSTRACT

FACULTY OF ENGINEERING, SCIENCE AND MATHEMATICS

SCHOOL OF PHYSICS AND ASTRONOMY

Doctor of Philosophy

OPTICAL AND X-RAY STUDIES OF BE/X-RAY BINARIES IN THE SMALL MAGELLANIC CLOUD

by Matthew Peter Edward Schurch

High-mass X-ray binaries (HMXBs) have proved to be some of the most interesting X-ray sources in the sky. The growing population of Small Magellanic Cloud (SMC) Be/X-ray binaries is monitored weekly with two 15ks *RXTE* observations. My thesis focuses on presenting the analysis of the X-ray data and the optical follow-up that enhances it. I present detailed studies of the Hα emission features in several prominent Be/X-ray binaries in the SMC and examine their outbursting nature by combining the OGLE optical light curves with the *RXTE* light curves. This has culminated in an orbital solution for SXP18.3 as well as measured orbital periods for SXP2.37, SXP172 and SXP202B. Through detections of quasi-periodic variations in the optical light curves, the details of interactions taking place between the Be star's circumstellar disk and the neutron star are being revealed. These data are providing the building blocks that may help explain the physical processes that produce the circumstellar disk. In addition, the optical counterpart to SXP15.3 is discussed in the light of recent *XMM-Newton* results, raising doubt over the true optical counterpart.

Contents

Declaration

I hereby declare that no part of this thesis has been previously submitted to the University of Southampton or any other university as part of the requirements for a higher degree. The work described within was conducted by the author, whilst in consultation with M.J. Coe. Where I have consulted the published work of others, this is always clearly attributed.

Matthew Schurch
20^{th} April 2009

Publication

Parts of this work have previously appeared in the following publications:

Schurch M. P. E., Coe M.J., McGowan K. E., McBride V. A., Buckley D. A. H., Galache J. L., Corbet R. H. D., 2007, MNRAS, 381, 1561
Schurch M. P. E., Udalski A., 2008, ATel, 1611, 1
Schurch M. P. E., Udalski A., Coe M., 2008, ATel, 1670, 1
Schurch M. P. E., et al., 2009, MNRAS, 392, 361

Acknowledgements

I have been extremely fortunate during the course of my PhD. I've been lucky to have a number of our SMC sources do some weird things but most importantly I've been able to use the opportunities offered to me in the name of science to visit some of the most amazing places in the world, which would otherwise have taken me many years, and many pounds, to do! However, throughout these trips one thing has always stuck in my head, that pretty much where ever I was, I was in a warmer climate than those friends I'd left behind. All this travelling has however not been in vain. On my many returns I've managed to enlighten the lives of many friends and family with wonderful stories of places visited and people met, but most importantly, I've had an audience for the odd picture I've taken along the way. But, this has not pleased everyone, with the common saying amongst friends being "When are you going to stop messing around and get a real job like the rest of us?" Well I can now answer that question... To the guys back home, when I regain the memory of the second half of my 18th birthday! Tim, when you take my badminton crown off my head, and Dr Bussey, well, you have no leg to stand on. To everyone else, never!

In all seriousness though, I've had amazing time here in Southampton, and there are a few people I would like to thank. Firstly, my supervisor Malcolm, without his continued guidance and encouragement I would not be writing this at the moment. When Malcolm wasnt around there were always two people that I could turn to for help, Katie and Vanessa, thank you both for your ever present ear. Jose, deserves a special mention. You passed on many scripts that have aided me throughout my work, I would like to thank you for leaving all those "deliberate" mistakes in your code to test me. Lee, have fun finding the rest of those deliberate mistakes, and I hope I taught you how to have a successful, incident free, observing run. A massive thank you must go to the tea ladies of my office, Mark and Elmar. I surely would have fallen asleep on countless occasions without the almost non stop use of the

kettle. Cheers Martin, for the sage financial advice, I particularly liked your use of eBay when shopping for radio telescopes! To all the others who are or have at one point been part of the furniture in 4075 and the rest of the astronomy group, thanks for all the help.

Lastly, without the help and support of those closest to me none of this would have been possible. Emma, you have been there every step of the way right from the beginning with my interview in Cape Town. You've always offered me the best advice and encouragement and for that I cannot thank you enough. A word or two for my brothers, Chris, the bar has been raised and it's your turn. Nick, can you please stop raising that bar! Lastly, Mum and Dad. Where on Earth would I be without you two? After a decidedly dicey entrance into this world, you have guided, and helped me, albeit with the odd bump on the way, into becoming the person I am today. Thank you.

Cloth Cat, Ice Pop and Pippin, my silent comrades

Prologue

Two fuzzy blobs floating in the Southern sky have for years provided people with their first glimpse of another galaxy. The Large and Small Magellanic Clouds have played a crucial role in advancing astronomy ever since man first started studying the celestial bodies. Today, they are a hot-bed of scientific research in all areas of astronomy, being studied by teams of scientists distributed all over the world using the most up-to-date instruments. An unusual feature of the Small Magellanic Cloud is that it is host to an unusually large population of X-ray binary systems for a galaxy of its size. It is these exotic X-ray binary systems that the research in this thesis is focused on. Chapter 1 will present an overview of the types of X-ray binaries that are commonly found in any galaxy, including our parent galaxy the Milky Way and in the Magellanic Clouds. Chapter 2 will discuss the evolutionary history of the Large and Small Magellanic Clouds (LMC and SMC) and how it has played an important role in producing the large unexpected population of Be/X-ray binaries.

Discovering new X-ray binaries is very important if the population is to be studied as a whole. Over the past few years many X-ray observations have been made of the SMC in an attempt to boost the number of known X-ray binaries. One such study by *Chandra* recently discovered a number of new X-ray sources in the Wing of the SMC. Chapter 3 presents the optical spectral classification of the counterparts to these sources as well as a study of the X-ray and Hα emission. This combined multi-wavelength approach has allowed a detailed study of the characteristics of

these systems.

The majority of the high-mass X-ray binary sources in the SMC appear to be extremely transient in nature. These sources have been monitored through an extensive observational campaign with the Rossi X-ray Timing Explorer for over 10 years. There are a few systems where X-ray outbursts are seen to occur periodically but the large majority of sources rarely go into X-ray outburst. SXP18.3 was one of these systems, until it started what was to become the longest Type-II X-ray outburst ever seen in the SMC. Chapter 4 presents a detailed analysis of the 36 week outburst through studies of both the X-ray and optical light curves. The unprecedented length of the outburst has for the first time allowed an extensive study of the pulse timing of an SMC pulsar enabling a full orbital solution to be calculated.

Monitoring the X-ray activity of the SMC sources tells only one side of the story. Thanks to the excellent Optical Gravitational Lensing Experiment, extensive optical light curves covering almost all the SMC X-ray binary sources for approximately the past 12 years are now available. Chapter 5 explores a number of these optical light curves where they have been searched for orbital periods and quasi-periodic variations. A comparison of the optical and X-ray emission has revealed essential clues regarding the nature of the binary systems and the fundamental emission processes involved.

Finally, Chapter 6 will draw all these findings together and present possible routes forward in the understanding of these X-ray binary sources.

Chapter 1

Introduction

1.1 X-ray Binaries

It is generally thought that approximately 50% of the stars in galaxies are in binary systems (Cherepashchuk, Sazhin, & Trifalenkov 1995). The life cycle of these stars is extremely dependent on many features of the binary system; the individual masses of the stars, eccentricities, orbital separation and orbital period are some of the more major features that will affect their evolutionary path. During the lifetime of the binary, at least one, if not both, of the stars will die creating a binary system where at least one star is a remnant. The exact nature of the remnant i.e., whether it is a white dwarf, neutron star or black hole is dependent on the mass of the progenitor star. Most of these binary systems will eventually create an extreme environment where complex interactions can take place between the two stars, often resulting in energy being released across the electromagnetic spectrum; in particular the optical, X-ray and γ-ray luminosities are often seen to increase dramatically.

These systems are known collectively as X-ray binaries (XRBs). In the vast majority of XRBs the compact remnant star which gives rise to the X-ray emission is a

neutron star. However, a small number of systems are believed to harbour black hole candidates. These systems can be further divided into distinct groups and sub-groups according to many parameters such as outburst frequency. However, the main classification is into two groups; high-mass and low-mass X-ray binary systems (HMXBs and LMXBs). This classification is based solely upon the mass of the secondary star or optical counterpart. Generally, LMXBs have counterparts with a mass similar to that of the Sun ($< 4\,M_{\odot}$); an example of such a system is Scorpius X-1. HMXBs like Cygnus X-1, have counterparts with a mass far greater than the Sun (typically $> 10\,M_{\odot}$). A third group is that of the rare Intermediate mass X-ray binaries (IMXBs) where the counterpart has a mass between the two other groups. However, only a handful of such sources are known; Her X-1 and Cyg X-2 (Lewin & van der Klis 2006) are both IMXBs containing a neutron star. The emission behaviour and evolutionary paths of all these XRB groups are significantly different and will be discussed later.

Binaries containing a white dwarf (WD) and a low mass companion are not generally referred to as part of the XRB group, even though they are binary systems containing a remnant star that is detected as an X-ray source. They are weaker X-ray sources than binaries containing neutron stars or black hole candidates and as a result are grouped separately. Their classification as Cataclysmic Variables (CVs) is due to the large variations in their observed brightness caused by nova events. Motch et al. (2007) have recently identified a group of very low level X-ray emitting sources that are associated with Be stars. These systems have X-ray and optical properties very similar to the unusual X-ray source γ Cas, namely, early optical counterparts in the spectral range B0.5-B1 and hard X-ray spectra. Motch et al. (2007) propose that these systems may represent the previously undiscovered population of Be/WD X-ray binaries. Kahabka et al. (2006) discovered a super soft X-ray source in the LMC emitting at a similar level to γ Cas. As a result of the optical analysis they propose that this source is a Be/WD X-ray candidate. These γ Cas sources are currently the mostly likely candidates for the missing population of Be/WD binaries, as predicted

by the generally accepted binary evolution theory (Raguzova 2001), but currently none have been confirmed as containing a WD.

1.1.1 Low-Mass X-ray Binaries

LMXBs are interacting binary star systems where a neutron star or a black hole is present, along with a normal low mass counterpart. The optical emission from the low mass companion is dwarfed by that arising in the extremely hot accretion disk around the compact object. It is this hot disk that is the primary generator of the X-ray emission. LMXBs are generally persistent sources due to matter being continually stripped off the optical counterpart. As a result the life time of the system is governed by the evolutionary path of the optical counterpart. Typically LMXBs can exist for around $100 - 1000$ Myr (Majid, Lamb, & Macomb 2004). They tend to form a close binary, with a short orbital period, generally < 20 days (Lewin & van der Klis 2006). This allows for a continuous stream of matter to flow from the Roche lobe filling counterpart through the inner Lagrangian point. This matter forms an accretion disk around the compact companion. It is here in the accretion disk that the gas is heated through frictional forces to extreme temperatures, giving rise to the majority of the optical and X-ray emission.

1.1.2 Intermediate-Mass X-ray Binaries

Only a few IMXBs are known to exist. This discrepancy is possibly due to their accretion rates, which result in them being very short lived. van den Heuvel (1975) suggested that the X-ray emission in IMXBs is due to Roche lobe overflow as opposed to mass capture from a stellar wind. This is because the optical counterparts do not have a strong enough stellar wind to allow a sufficient level of mass transfer to generate the level of X-ray emission seen. For the optical counterpart to transfer matter through Roche lobe overflow then the time spent as an active X-ray binary

will be short due to the high mass transfer rates and relatively small amount of fuel. Typically the X-ray phase of these systems may last for a few 1000s of years (Lewin & van der Klis 2006).

1.1.3 The High-Mass X-ray Binary Family

HMXBs are in general the most numerous class of XRBs in any given galaxy. However, this general classification covers a wide range of observational characteristics which result in it being sub-divided into three classes based on the mass transfer method and the spectral type of the counterpart. Firstly, in the classical HMXBs, the optical counterpart, typically a supergiant, fills its Roche lobe. This allows accretion to take place via Roche lobe overflow, in a similar fashion to the LMXB systems. SMC X-1 is a classical HMXB and is the only one of its type currently known in the SMC (Wilson & Wilson 1976). These sources tend to be bright and persistent with $L_x \sim 10^{38}\,\mathrm{erg\,s^{-1}}$.

The second class of HMXB are the Be/X-ray binaries. The optical counterpart in these systems is a Be star that is rotating very close to the speed at which the centrifugal force at the equator is equal to the gravitational force; this rotation speed is known as its critical rotation speed. They are usually main sequence stars in the spectral range 09e−B3e (luminosity class III to V). The typically wide and eccentric orbit only permits the neutron star to accrete as it passes through periastron, hence these sources are typically seen exhibiting X-ray and optical outbursts. They are all transient sources sometimes outbursting periodically but, more often than not, they appear to be randomly regulated. They form the largest sub class of HMXB. These systems will be discussed in more detail in §1.1.3.1.

The third class is the supergiant X-ray binaries (SGXBs), where accretion is a result of matter captured from the stellar wind. The counterpart is typically a massive early type OB supergiant (luminosity class I or II). Recently the supergiant systems

have been further subdivided into two categories: the persistent wind-fed systems, and the fast X-ray transient systems (SFXT) (Sguera et al. 2005). These SFXTs exhibit extremely short lived outbursts sometimes lasting only a few hours, and are predominately seen at very high energies, in particular as γ-ray sources. These features have made these systems hard to find, and it has only been through recent observations with telescopes such as *INTEGRAL* that the extent and details of this population are being uncovered. Currently there are around 12 known SFXT systems (Walter & Zurita Heras 2007). Observations of the optical counterparts have revealed them all to be highly reddened early-type OB supergiants. These systems are still very poorly understood, and the exact processes that give rise to their extremely short outbursts are not fully known. Some systems, such as IGR J11215-5952 (Sidoli, Paizis, & Mereghetti 2006), show recurrent outbursts which are most likely related to an orbital period. In comparison the persistent SGXBs have a fairly well established model. The compact remnant accretes material directly from the strong out flowing stellar wind, producing a low-luminosity persistent source with very short temporal variations, typically with $L_x \sim 10^{36}\,\mathrm{erg\,s^{-1}}$.

Negueruela et al. (2008) propose that all these types of supergiant systems are in fact comprised of similar stellar objects and that their differing outburst characteristics can be explained in terms of a differing orbital configuration within a clumpy stellar wind. The transition from persistent SGXB to SFXT takes place around two stellar radii ($2\mathrm{R}_*$) where the density of clumps changes dramatically. Figure 1.1 shows two possible orbital configurations for SFXTs. In relation to these diagrams a SGXB system will be formed if the orbit is extremely tight (more so than in the left hand panel) and circular. Hence it can continually accrete throughout the orbit from the clumpy stellar wind; making them persistent sources. In contrast to this, the SFXTs spend the majority of their orbit in free space, only accreting when they randomly approach a clump. This orbital model fits with the observation that all known SGXBs have compact objects orbiting at $r \lesssim 2R_*$.

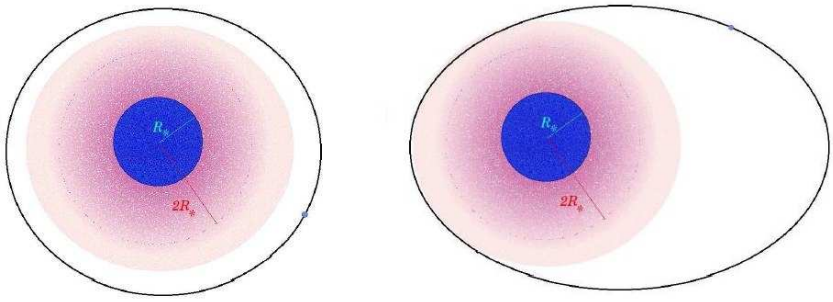

Figure 1.1: Possible schematic configurations for an SFXT. The coloured region depicts the area where the clumped wind density is high. The left hand panel depicts an intermediate low luminosity system. The right hand panel shows a highly eccentric system with extremely orbitally modulated outbursts. (Taken from Negueruela et al. 2008)

1.1.3.1 Be/X-ray Binaries

The vast majority of HMXBs fall into the Be/X-ray binary class, which is to say the optical counterpart is an early type Be star. In almost all these systems the compact remnant is a neutron star. Figure 1.2 shows an artists impression of a typical Be/X-ray binary system. The diagram represents all the key features of the system, in particular the extremely unusual large circumstellar disk responsible for the Hα and infrared emission. McBride et al. (2008) have recently shown that the spectral population of Be/X-ray binaries in the SMC is consistent with that found in the Milky Way, with a peak in the distribution at B0 as shown in Figure 1.3. Unlike Be stars found in isolation, where the spectral distribution continues down to B9, the HMXB distribution is sharply cut off at B3.

X-ray observations of these systems have shown that they are extremely transient in nature. Often a source can lie dormant and undetected for many years. Occasionally these sources will suddenly begin an outburst, as was the case for A1118-616 (Coe et al. 1994) in 1992 when an unexpected second X-ray outburst was detected 27 years after the initial X-ray detection by Ariel 5 (Eyles et al. 1975). As with isolated Be stars the circumstellar disk can change quite dramatically and, accordingly, the observed X-ray activity is often correlated with changes in the state of

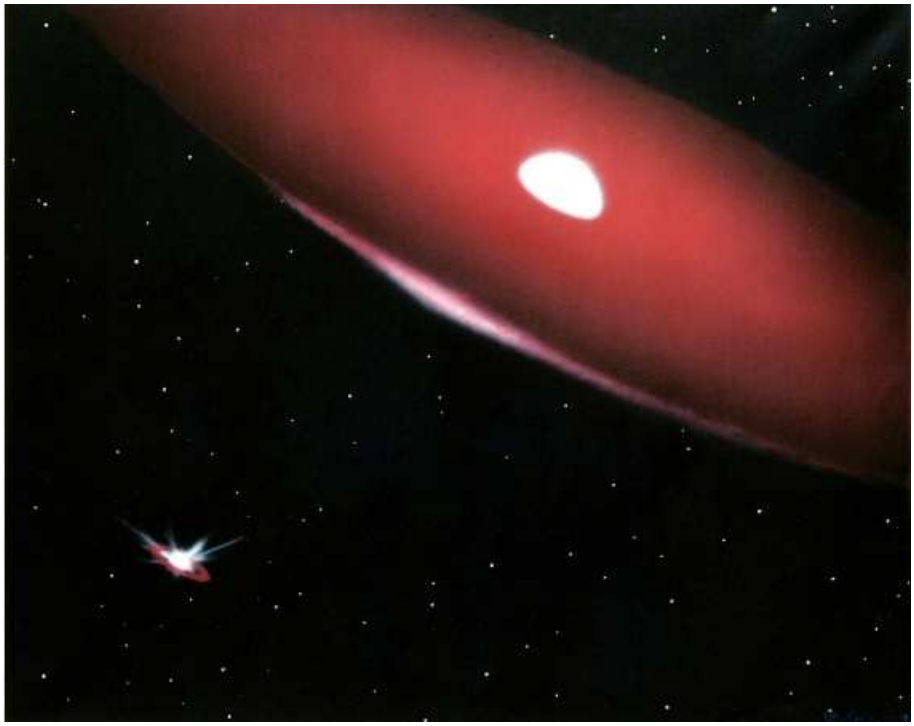

Figure 1.2: Artists impression of a Be/X-ray system.

the circumstellar disk. Typically three types of X-ray emission are observed from Be/X-ray binaries (Stella, White, & Rosner 1986; Negueruela 1998):

- Type-I outbursts: The Be star is in a steady phase where the circumstellar disk is truncated relatively close to the star. The neutron star can only interact with the circumstellar disk when it is close to periastron. Hence the outburst pattern appears to be orbitally modulated. Typically these outbursts reach luminosities of $L_x \approx 10^{36-37}\,\mathrm{erg\,s^{-1}}$.

- Type-II outbursts: These are associated with Be star phases when the circumstellar disk has grown to cover most, if not all, of the orbit. Hence the neutron star can continue to accrete material throughout its orbit producing a continuous outburst often lasting months. There is no sign of orbital modulation. These outbursts are typically brighter, reaching luminosities of $L_x \gtrsim 10^{37}\,\mathrm{erg\,s^{-1}}$.

- Quiescence: A persistent low X-ray state can be detected from many sources

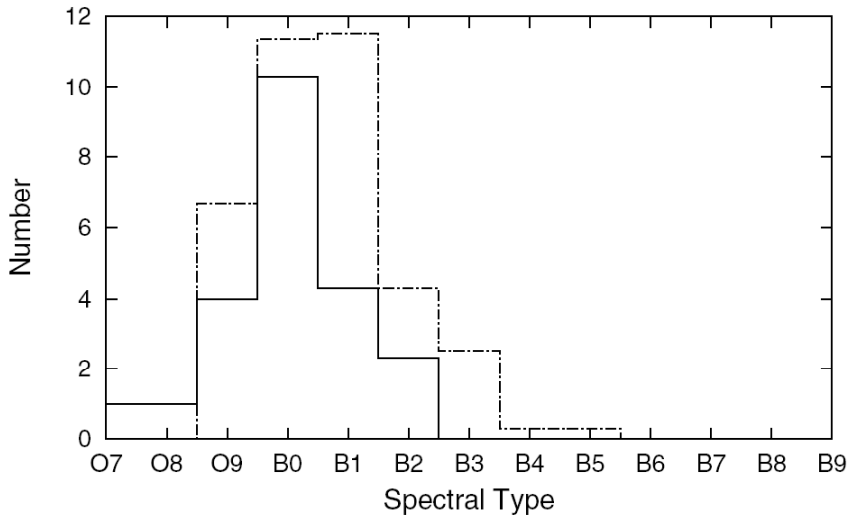

Figure 1.3: Spectral distribution, determined from blue spectra of ∼40 Be/X-ray binaries in the SMC (dot dashed) as compared the distribution of Be/X-ray binaries in the Milky Way (solid). (Taken from McBride et al. 2008)

in-between periods of outburst. Generally this state is believed to be due to accretion directly from the stellar wind when the neutron star is away from the circumstellar disk. Typically the quiescent X-ray luminosity is $L_x \lesssim 10^{34}\,\mathrm{erg\,s^{-1}}$.

Although the majority of outbursts can be identified as one of the above two types, some have been observed at times least expected. Outbursts when the neutron star is passing through apastron may even take place. They have been observed occasionally; although they are not necessarily seen directly as a distinct outburst but can often become extremely clear when the X-ray light curves are folded on the orbital period. This emission is generally thought to be due to an increased level of capture of matter from the slower moving stellar wind. Outbursts occurring during other orbital phases are seen but are still very poorly understood. They could possibly be attributed to sudden changes in the circumstellar disk structure.

1.1.4 Binary Formation and Evolution

The evolution of binary star systems, in which one or both of the progenitor stars is a Be star, leads to some of the most exotic star systems in the Universe. The evolution of these stars, culminating in the formation of a compact remnant (typically a neutron star), was fist described by Paczyński (1967). It is in the latter stages of their evolution where either one or both objects will form a compact remnant, typically a neutron star. If both stars were sufficiently massive, and the evolution of the binary system is such that neither of the stars are ejected during a supernova, then a double neutron star binary system can form. Recent reviews of the evolutionary processes and stages can be found in Vanbeveren, De Loore, & Van Rensbergen (1998) and Tauris & van den Heuvel (2006).

The principal stages of Be binary evolution (as discussed in the literature) are illustrated in Figure 1.4. As shown, the two massive (typically $\geq$8 $M_{\odot}$) zero-age main sequence stars (ZAMS) evolve first into a HMXB. Initially the two stars evolve through the normal evolutionary tracks independently, both stars burning hydrogen. The more massive star evolves faster and is thus the first to expand, filling its Roche lobe. This expansion allows mass to be transferred through the inner Lagrangian point (L_1) onto the less massive star. This transfer of mass also carries with it angular momentum. This additional angular momentum will act to increase the angular velocity of the mass-gaining star (spinning it up). The redistribution of mass also alters the orbital period and separation. Mass transfer continues until the initially more massive star is completely stripped of its hydrogen shell. The resultant stage is now a helium star with a now massive OB star companion. Eventually the helium-burning star exhausts its supply of fuel and explodes as a supernova. The result is a compact neutron star remnant. It is at this point that the properties of the HMXB are established. The spin period of the neutron star is largely determined by the amount of matter that is removed from the star during the supernova. The supernova will also disrupt the orbital motions. The supernova kick velocity acts to

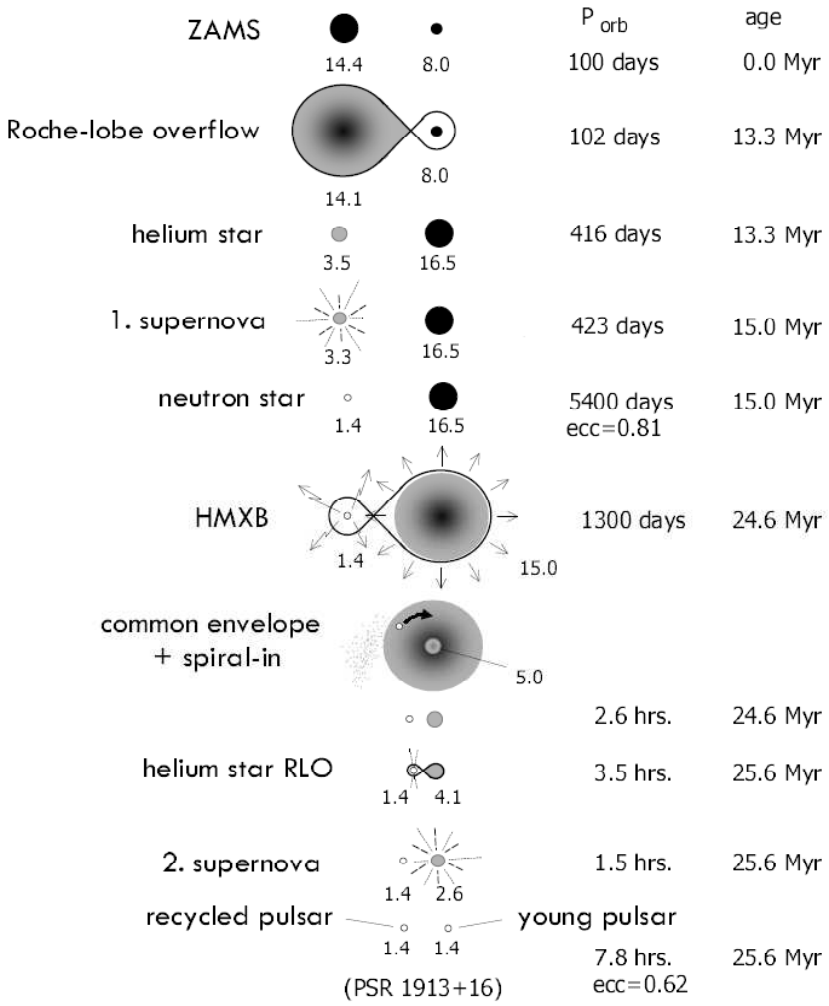

Figure 1.4: Evolution of a HMXB. (Taken from Lewin & van der Klis 2006)

increase the orbital separation of the two stars and greatly increase the eccentricity, assuming that the binary system survives in the first place. At this point the system can start to behave as a typical HMXB behaving as previously described in §1.1.3.1. Figure 1.4 shows a SGXB accreting through a strong stellar wind.

No matter which HMXB is formed, the massive OB star continues to evolve. Some matter is inevitably lost to the orbiting neutron star, but it eventually evolves into a red giant. At this point the expansion of the outer layers of the star may engulf a large part if not all of the orbit of the neutron star. This phase is known as the

common envelope stage. During this period, the neutron star interacts strongly with the outer layers of the red giant, leading to heightened levels of X-ray emission. The orbit slowly shrinks due to the drag force between the envelope and neutron star. Eventually the red giant loses its outer envelope entirely and becomes a helium star in a close binary orbit with the neutron star. At this point Roche lobe overflow of the helium star can take place, continuing the X-ray phase. Ultimately, the helium star also undergoes a supernova explosion, creating the second neutron star in the binary system. However, the state of the binary system at this point is largely dependent on the quantity of mass that is lost during the supernova. If more than half of the mass of the system is lost then the binary is disrupted, freeing the two neutron stars of each other.

It is clear from the evolution of the binary system that X-ray emission is only seen during particular periods of evolution. In particular, the primary period is during the evolution of the companion Be star. As previously mentioned, for a Be/X-ray binary system the companion is a massive early-type OB star. As a consequence the predicted lifetime of these stars (and the X-ray active phase) is relatively short, $10^6 - 10^7$ years. The consequence of this is that their distribution within galaxies is restricted to areas with high star formation rates. Galaxies such as the SMC have a particularly favourable environment for the formation of Be/X-ray binaries.

1.1.5 Accretion Process

A key stage of the evolution process is the transfer of matter from the companion star to the neutron star. Once the material has been captured by the neutron star (through one of the many possibilities discussed earlier), it can create an accretion disk. The outer orbit of the accretion disk initially forms at the point of lowest energy for the particular angular momentum of the gas that has passed through the L_1 point given by:

$$R_{circ} \cong 4(1+q)^{4/3}[0.500 - 0.227 \log q]^4 P_{day}^{2/3} R_{\odot} \tag{1.1}$$

where q is the mass ratio of the binary and P is the binary period (Frank et al. 2002). This radius can form anywhere between the neutron star's surface and the edge of its Roche lobe, but is typically of the order of $R_{\odot}$. Internal viscosity within the disk redistributes both energy and angular momentum throughout the disk material, allowing the material to flow inwards towards the compact star at the disk centre. The inner cut off point of the disk is dependent on the strength of the magnetic field of the neutron star. This point is know as the Alfvén radius (r_A) and is defined as

$$r_A = \left(\frac{\mu^4}{2GM\dot{M}^2}\right)^{1/7} \tag{1.2}$$

where the magnetic pressure balances the ram pressure of the in-falling matter (Frank et al. 2002). It is at this point that the accretion flow moves away from the disk and becomes guided by the magnetic field lines towards the magnetic caps of the neutron star, as shown in Figure 1.5. However, this process is restricted by the radius of co-rotation (R_c),

$$R_c = \left(\frac{GMP_{spin}^2}{4\pi^2}\right)^{1/3} \tag{1.3}$$

defined as the radius where the accretion disk's rotational period equals the neutron stars spin period (Bildsten et al. 1997). If $r_A > R_c$ then the magnetic field lines are in effect rotating faster than the material that is trying to move along them. This results in the material being flung away. As a consequence some of the neutron star's angular momentum is lost, causing its angular velocity to decrease (spinning it down). This process is known as the propeller effect. However, if $r_A \leq R_c$ then the accretion flow can move freely along the magnetic field lines. Since the flow is

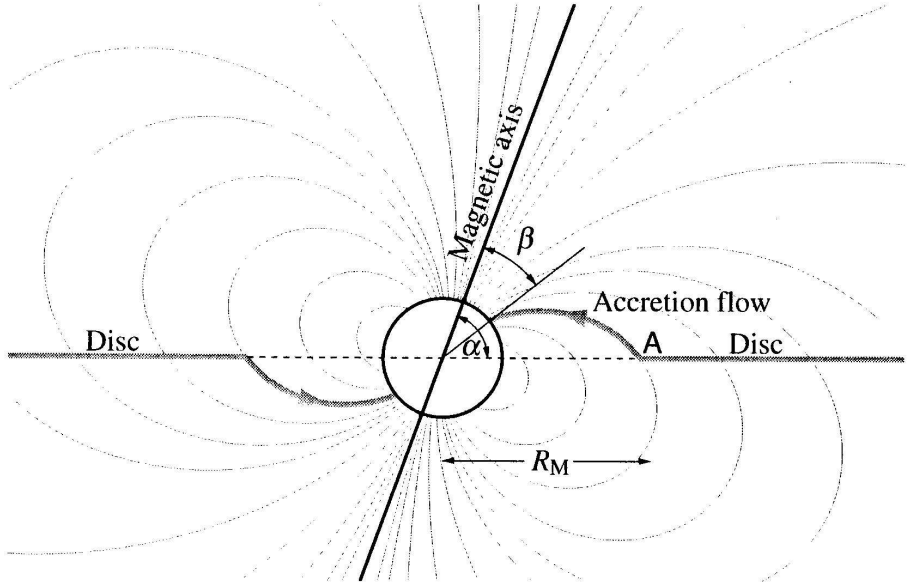

Figure 1.5: Schematic showing an accreting neutron star and disk. At the point where $r_A = R_c$ material leaves the disk and follows the magnetic fields lines towards the magnetic poles of the neutron star. (Taken from Jaschek & Jaschek 1990)

now decoupled from the disk motion it can no longer pass its angular momentum outwards, instead it has to impart its angular momentum to the neutron star. This accretion torque causes the neutron star to increase its spin period (Pringle & Rees 1972).

Accretion then takes place onto the magnetic poles. As the matter is pulled out of the accretion disk it becomes guided along the magnetic field lines. If all the associated kinetic energy of this in-falling matter is converted to radiation at the neutron stars surface, then the associated accretion luminosity is given by

$$L_{acc} = \frac{GM\dot{M}}{R_*} \tag{1.4}$$

where R_* is the radius of the neutron star (Frank et al. 2002). This value however cannot exceed the Eddington luminosity

$$L_{Edd} = \frac{4\pi G M m_p}{\sigma_T} \simeq 1.3 \times 10^{38} (M/M_\odot) \,\mathrm{erg\,s^{-1}} \tag{1.5}$$

where σ_T is the Thompson cross-section, which is set by equating the radiation and gravitational forces acting on the in-falling matter (Frank et al. 2002). However, in deriving this limit many assumptions have been made, chief amongst which are that the accretion is spherical and steady. Both of these assumptions are not valid in the accretion method described for Be/X-ray binaries. However, this value will act as an order-of-magnitude estimate, since any refinements would require many quantities for magnetically controlled accretion onto a neutron star to be known.

1.1.6 Spin/Orbit Relation – The Corbet Diagram

The majority of the known Milky Way and Magellanic Cloud Be/X-ray binaries now have well known orbital periods derived from the analysis of the X-ray and optical data. Many of these orbital periods have come from X-ray pulse timing analysis, but more recently the long term optical and X-ray light curves have revealed many new periods due to the repetitive nature of Type-I outbursts. The systems are not confined to a narrow range of orbital periods, but rather they show an extremely wide distribution, ranging from a few days to hundreds of days (Liu et al. 2005). Corbet (1984) noticed that there is a strong correlation between the observed orbital and spin periods of the neutron star. Since this early observation, the orbital-pulse period plane has been investigated thoroughly, not only for Be/X-ray binaries, but for all the other XRB systems. Figure 1.6 (known commonly as the Corbet diagram) depicts how the orbital-pulse period plane can be used to provide a rough estimation of the type of system based on these two parameters. As can be clearly seen, the Be systems occupy a region to the far right of the plane. The relation between the two parameters for the Be/X-ray binaries is roughly governed by Equation 1.6 (Corbet 2006, private communication), and can be used to predict the expected orbital period

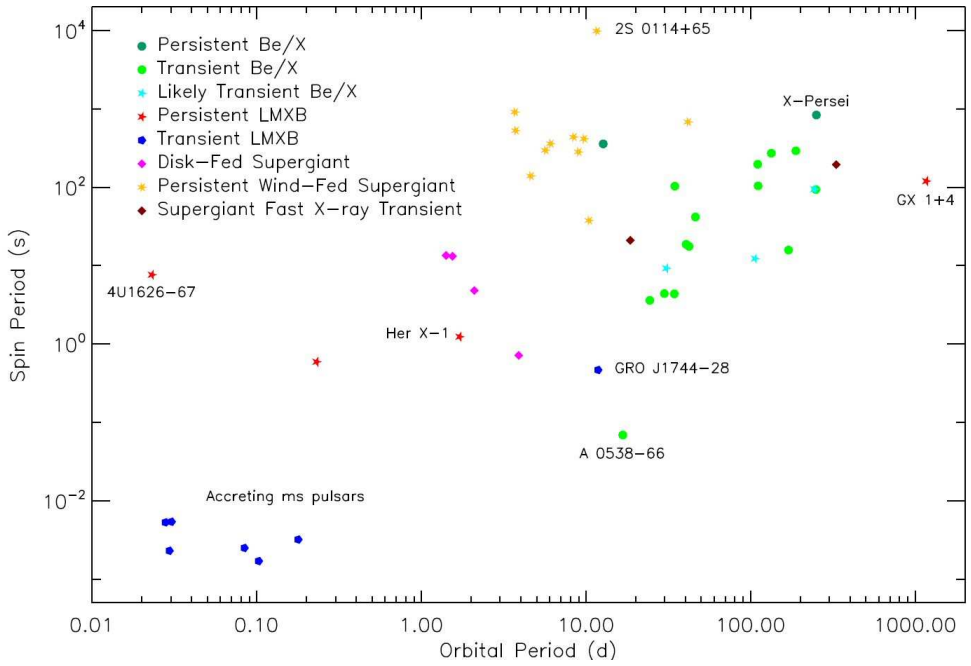

Figure 1.6: Corbet Diagram. Private communication from Corbet (2006).

(P_{orb}) when new pulsating X-ray sources are suspected to be Be systems.

$$P_{orb} = 18 \times (P_{pulse}^{2/5}) \tag{1.6}$$

The conventional view for the existence of this relation is due to the time spent spinning up and down the neutron star. It is generally expected that neutron stars are born with fast rotation periods. As discussed, this short spin period inhibits the accretion of any extra matter due to the Alfvén radius being larger than the co-rotation radius. This allows the neutron star to spin down. Once the neutron star is spinning slowly enough to allow accretion, then the system enters a quasi-equilibrium period when it is continuously and alternately spinning up and down. Eventually the neutron star reaches an equilibrium, which is largely dependent on the orbital period as it spends the majority of its time away from the optical companion spinning down.

1.1.7 Optical Properties and Variability of Be/X-ray Binaries

In addition to the X-ray activity, Be/X-ray binaries exhibit significant optical emission that can vary over time. This emission is dominated by the massive Be star counterpart. Key characteristics of the binary system can be revealed through optical studies.

1.1.7.1 Be Stars

The first reported Be star was γ Cas (Secchi 1878). Since then, these intriguing objects have been well studied, but are still poorly understood. The distinguishing and classifying feature of a Be star is the presence of Balmer line emission, in particular at Hα (Jaschek, Slettebak, & Jaschek 1981). This is also accompanied by a strong continuum infrared excess. Both of these effects are believed to be a result of emission from a circumstellar disk. The infrared excess has been shown by Woolf, Stein, & Strittmatter (1970) and Dachs & Wamsteker (1982) to originate from free-free hydrogen emission in the circumstellar disk. The nature of a Be star is one that is continually changing, as the disk can be completely expelled from the system. The same star can change from B to Be and back again, but is continually classified as a Be star once the emission lines have been seen. O and A stars that show the same behaviour are customarily referred to as Be stars, but supergiant stars are not included, since they exhibit Hα emission without the presence of a disk (Jaschek, Slettebak, & Jaschek 1981).

1.1.7.2 Optical Spectroscopy

Classifying the Be star in Be/X-ray binaries is possible due to the relative brightness of the two stars. In particular, optical spectroscopy of a range covering the Hα line

is crucial. Normal B stars show the Hα spectral line to be in absorption; this is due to the hot ionised outer surface layers of the star making the star optically very thick. However, if the cooler, un-ionised circumstellar disk is large enough, then the Hα absorption line can be partially or even fully filled, producing the classifying emission line.

Further classification issues arise due to the Be phenomenon. The fast rotation speeds of the Be star broadens the observed absorption lines, often causing the edges to merge. In addition the emission features from the Balmer lines and other elements like iron can cause the smaller classifying lines to be lost. The key classifying lines that are typically used are H, He, Si and Mg, in their various ionisation states (Walborn & Fitzpatrick 1990). However, classification in the SMC is made more difficult due to the weakness of many of the metal lines. This is a result of the metal-poor environment that the stars are born in. Classification of Be stars in the SMC follows the methodology outlined in Lennon (1997) and Evans et al. (2004).

As mentioned, the absorption lines are typically broad. Studies of them by Townsend, Owocki, & Howarth (2004) have shown that Be stars can be rotating at or near their critical break up velocity ($v_{equator}/v_{crit} \simeq 0.95$). It is this fast rotation that possibly causes the development of a circumstellar disk. Internal Be star non-radial pulsations may provide sufficient energy and angular momentum to the outer layers of the star, allowing material to escape, forming a disk (Townsend, Owocki, & Howarth 2004).

1.1.7.3 Circumstellar Disks

Be stars, both in isolation and in binaries, exhibit periods when the circumstellar disk is present, and periods when the disk appears to be lost. Clark, Tarasov, & Panko (2003) present 18 years of high resolution Hα spectroscopy of the Be star *o* And. During these observations it was found that the star lost and then rebuilt its

disk. The formation of the disk occurred gradually over 1000's of days. In a similar manner to the formation, it was also found that the loss of the disk began at the inner radii and moved outwards. Both these observations are consistent with the viscous disk model of Lee, Osaki, & Saio (1991). In this model, angular momentum is transferred to the outer layers of the disk through the viscosity of the matter, thus increasing its size. If, for some reason, the input of material is halted, then the disk will slowly dissipate. This type of viscous model produces a disk that is rotationally dominated in a quasi-Keplerian orbit (Okazaki & Negueruela 2001). What is still largely speculative is exactly how the material is passed to the inner edge of the disk. As mentioned above, the fast rotation of the Be star is certainly important, but exactly how non-radial pulsations (Osaki 1986) play a part is not fully understood. Other models have also been proposed to explain the formation of the circumstellar disk, in particular, the magnetically compressed disk model of Cassinelli et al. (2002). The primary concern with this model is the required magnetic field strength. A B2V star would require a magnetic field of $\sim$300 G, increasing to unacceptable levels ($\sim 10^3$ G) for earlier classifications. In order to confirm this model, accurate supporting measurements of the magnetic fields in a number of isolated Be and binary Be stars are required (Hubrig et al. 2007).

Reig, Fabregat, & Coe (1997) noticed that in Be/X-ray binaries the maximum reported equivalent width of the Hα line was proportional to the orbital period. They also noted that the equivalent width of the Hα line in isolated neutron stars is on average larger than those in Be/X-ray binaries. These effects are interpreted as a truncation of the circumstellar disk by the orbiting neutron star (Reig, Fabregat, & Coe 1997), where as the Be stars in isolation can continue to develop their disks. More recent observations have confirmed this relation (Reig 2007) and monitoring of these sources over long periods has shown that the Hα emission lines reach a maximum width, for example GRO J1008-57, which reaches a maximum equivalent width of $\sim$ 20Å (Coe et al. 2007). Okazaki & Negueruela (2001) presented a model for the circumstellar disk to help explain the main types of X-ray outbursts and the

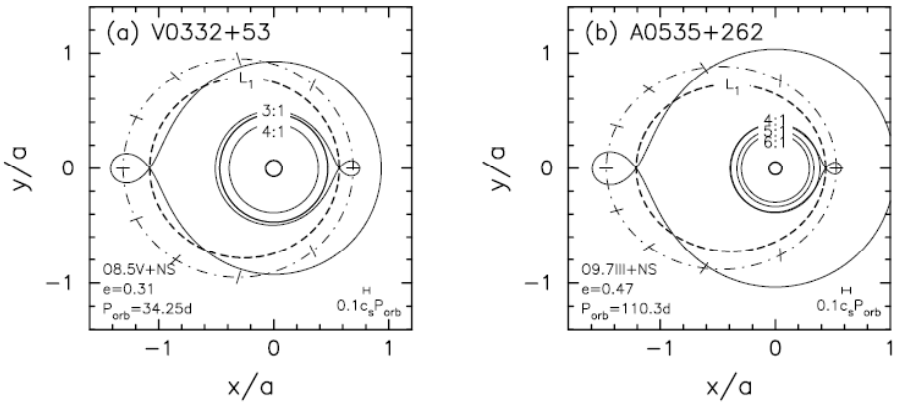

Figure 1.7: Circumstellar disk truncation models for the two Be/X-ray binary systems V0332+53 and A0535+262. The orbit of the neutron star is marked by the dot-dashed line. The solid thin lines represent the critical lobes of the two stars at apastron and periastron. The labelled solid lines represent the radii at which the disk will truncate for various points during the binary orbit. (Taken from Okazaki & Negueruela 2001)

truncation effects. They found that a viscous disk acting under the Shakura-Sunyaev viscosity prescription (Shakura & Syunyaev 1973) will be naturally truncated. Since the physics of accretion disks and decretion disks under this prescription is the same, then it would be expected, for mass ratios within the range $0.05 - 0.25$, that the disk would become truncated at a radius which is in a 3:1 resonance with the orbit (Osaki 1996).

As is clearly seen in Fig 1.7, the model predicts a truncated circumstellar disk for both systems. Various truncation radii exist, since the binary orbits have moderate levels of eccentricity. For Be/X-ray binaries the mass ratio (typically ≤ 0.1) is within the above range and so the expected truncation for most systems would be the 3:1 resonance radius. For highly eccentric systems the neutron star spends a large fraction of its time away from the disk, and so larger resonance states are available. However, those systems with low orbital eccentricities are also truncated at the 3:1 resonance radius. Type-I outbursts can take place when the resonance radius is close to, or at, the Roche lobe radius, allowing matter to be transferred to the neutron star (Okazaki & Negueruela 2001). Type-II outbursts are harder to explain using this geometry; one possibility is that the truncation radius cannot contain the disk

matter as it builds up. The disk would become dynamically unstable eventually transferring the matter to the neutron star.

1.1.7.4 Optical Variability

In addition to the X-ray variability of these sources, the optical emission can also be highly variable. Since the Hα emission is generated in the circumstellar disk, any interactions with the neutron star can cause variations in the line profile. The basic Hα profile falls into one of two broad categories, largely dependent on the inclination angle:

- High inclination (viewing the disk edge on): produces a symmetrical double-peaked structure. This is an effect of the rotation of the circumstellar disk.
- Low inclination (viewing the disk from above): produces a single-peaked smooth profile.

At intermediate angles a combination of the two effects can be seen. An estimate of the inclination angle is particularly useful when trying to calculate the orbital parameters of the system (Wilson et al. 1997). A central absorption feature is also common to many disks, these are classified as shell-type.

Optical variability in individual systems can take place on many time scales, from hours, to days, to progressive year long variations. Generally, the size of the magnitude changes are closely linked to the time scale. Short-term variations produce relatively small luminosity changes, whereas the longer term variations can produce changes up to a few magnitudes. These physical changes in the size of the disk are reflected in the equivalent width of the line. This is closely related to the line full width at half maximum (FWHM) since both are driven by the outer layers of the disk (Hanuschik, Kozok, & Kaiser 1988). Variations in the ratio of the heights of

the blue and red peaks of the emission line are known as the V/R variation. These variations are not thought to be related to the star, since the periods are significantly longer than the rotational period. Okazaki (1991) explained these variations in terms of a low frequency global one-armed oscillation of the disk. These density waves are produced by variations away from Keplerian motion, possibly a consequence of the recent passage of a neutron star. The V/R variation in LSI+61°303 is seen to vary significantly during 5 years of monitoring (Liu & Yan 2005), as shown in Figure 1.8. The authors also note an additional emission component, which arises in the centre of the profile as the neutron star passes through periastron. They suggest this emission is from an accretion disk that has formed. The viscous disk model used for modelling the truncation radii also reproduces the observed V/R variations (Lee, Osaki, & Saio 1991).

Zamanov & Martí (2000) also reported the first direct correlation between the activity of the neutron star and the circumstellar disk in LSI+61°303. They found that the radio outburst is shifted in phase by a quarter of its $\sim$4 year modulation with respect to the variations in Hα equivalent width.

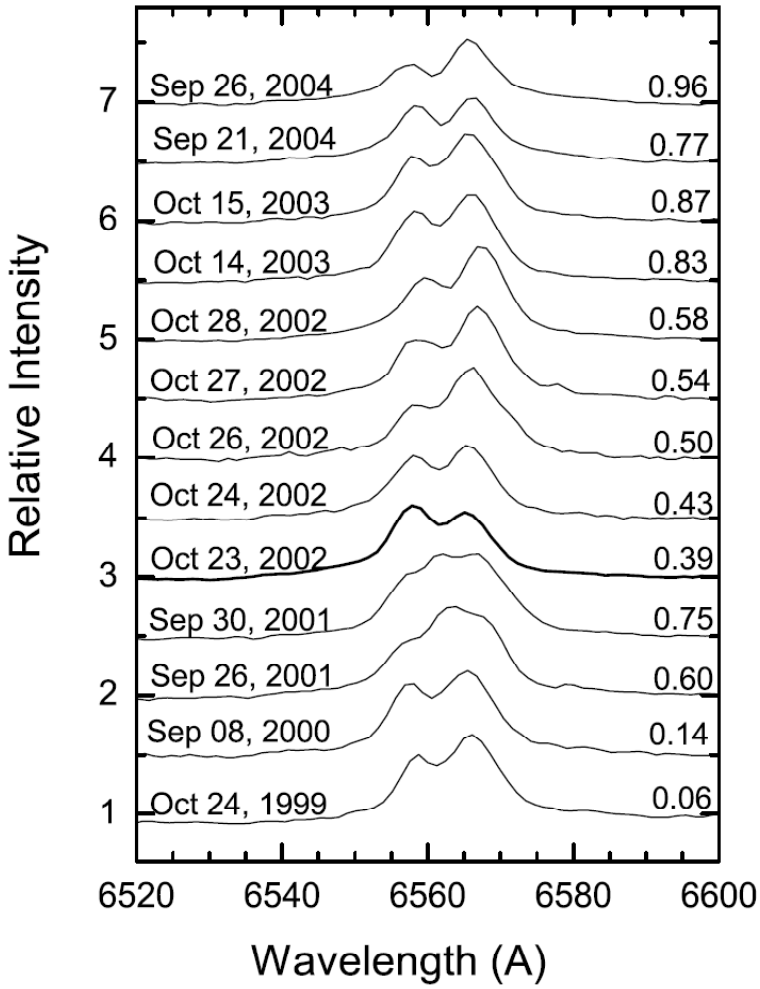

Figure 1.8: Selected Hα spectra of LSI+61°303 showing the V/R variation during the period 1999 to 2004. All spectra have had the continuum level normalised and are offset vertically to allow direct comparison. The corresponding radio phases are given in the right-hand side. (Taken from Liu & Yan 2005)

Chapter 2

The Magellanic Clouds

2.1 The Magellanic Clouds

Our galaxy, the Milky Way, is only one of a number of galaxies in our Local Group. Two of our nearest neighbours in galactic terms are the Large and Small Magellanic Clouds, otherwise known as the LMC and SMC. Found in the Southern Hemisphere, these two galaxies are clearly visible with the naked eye on a clear night. The first true observations of the Magellanic Clouds were performed by William Herschel between 1834 and 1838 from the Royal Observatory at the Cape of Good Hope.

Since these early observations they have become two of the most studied astronomical objects in the sky. Both the LMC and SMC are dwarf irregular galaxies with classification types **SB(s)m**[1]. The Magellanic system however has several other elements, which although not clearly visible to the naked eye bind the galaxies together. The Magellanic Bridge (shown in Figure 2.1), Stream and Leading Arm are the names given to the complex neutral hydrogen features that are between the two galaxies, emanating behind the SMC and in front of the LMC, respectively. These

[1]http://nedwww.ipac.caltech.edu/

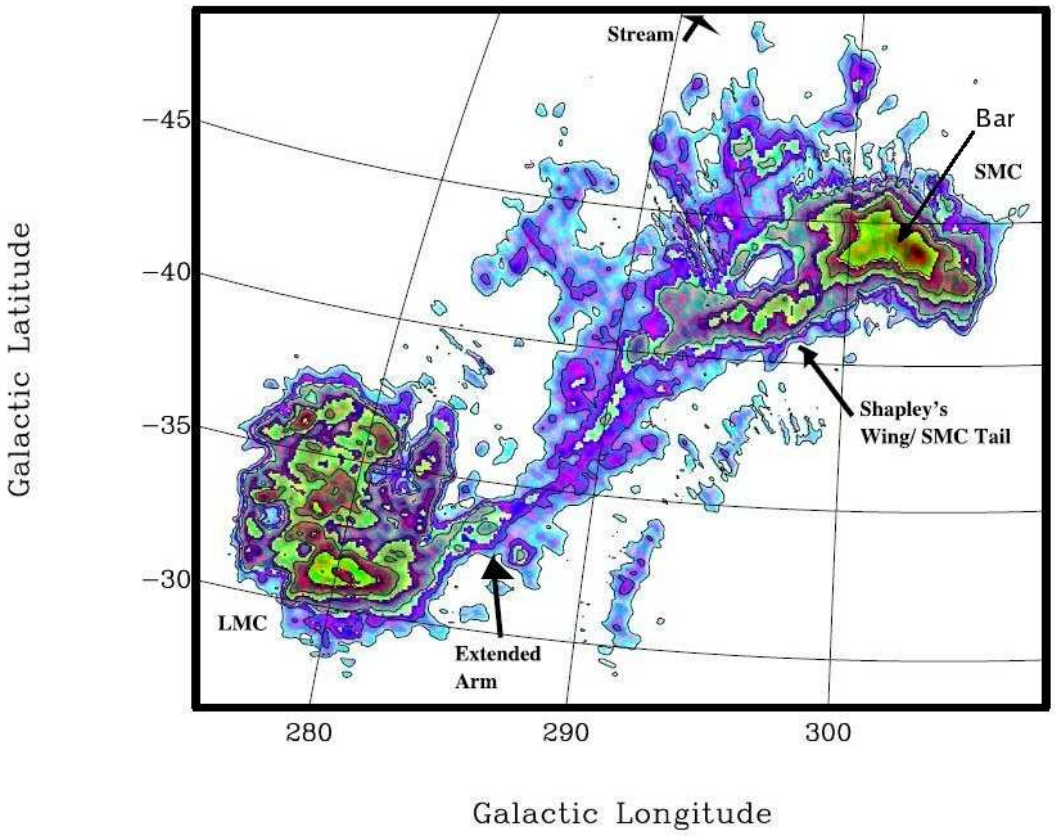

Figure 2.1: Neutral hydrogen column density map of the Magellanic Cloud system. Clearly visible is the Bridge which joins the LMC and SMC. (Taken from Putman 2000)

structures reveal much of the interaction history that has taken place between these two galaxies and the Milky Way. They are primarily visible at radio wavelengths and also in Hα.

The most obvious evidence for past interactions between these objects is the $\sim 10^8\,M_\odot$ filament known as the Bridge. Tidal models have successfully reproduced the formation of the Bridge during a close encounter between the clouds approximately 0.2 Gyr ago (Figure 2.2) (Gardiner & Noguchi 1996). Even though recent work by Besla et al. (2007); Kallivayalil, van der Marel, & Alcock (2006); Kallivayalil et al. (2006) (discussed in §2.3) challenged the findings of Gardiner & Noguchi (1996), the interaction that caused the formation of the Bridge is not disputed and

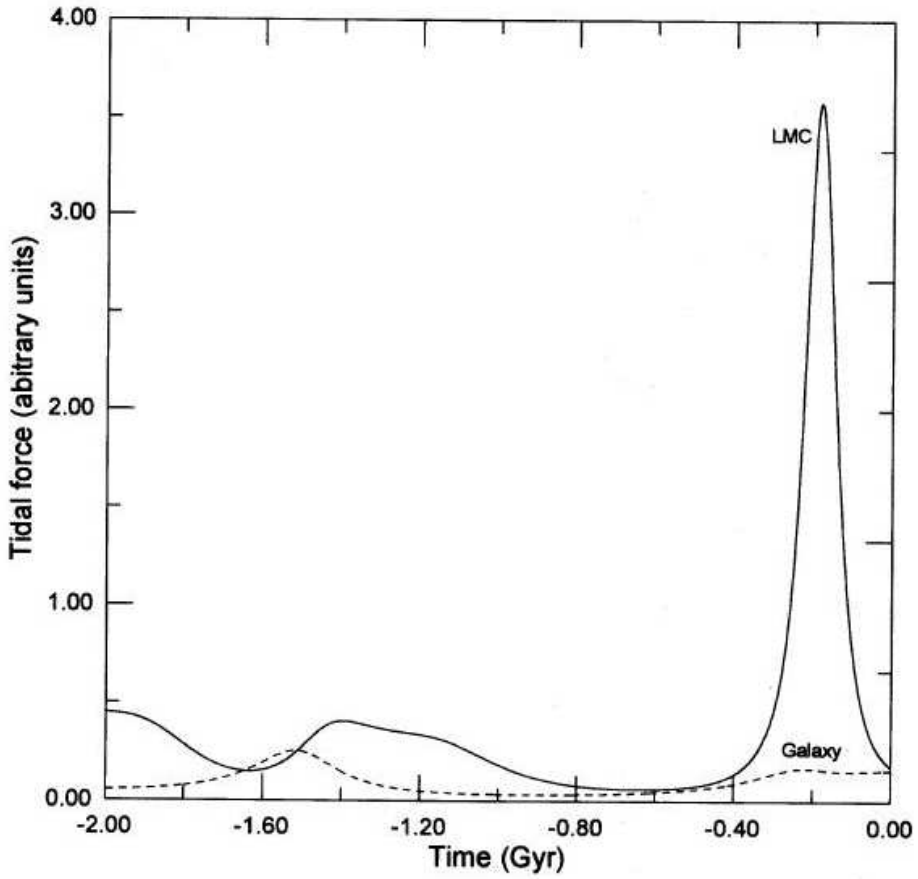

Figure 2.2: The tidal force exerted on the SMC by the Milky Way and LMC as a function of time. (Taken from Gardiner & Noguchi 1996)

remains primarily between the SMC and LMC. However, these new studies have made explaining the other features visible in the HI images far more complex. It is these close encounters that are likely to have caused periods of extreme star formation activity, hence the short-lived Be/X-ray binaries can be dated back to these periods.

2.2 The X-ray Population

Even though the SMC and LMC are linked and have been subjected to similar tidal interactions in the past, they exhibit vastly different source populations. The LMC

Table 2.1: Distribution of identified HMXBs.

Galaxy	Total	Pulsars	Ref
Milky Way	114	66	Liu et al. (2006)
LMC	36	7	Liu et al. (2005)
SMC	92	56[1]	Liu et al. (2005), Coe et al. (2005)

[1]http://www.astro.soton.ac.uk/∼mjc/

(the largest object in the system, ∼1/10 the mass of the Milky Way) contains a distribution of sources typical of any galaxy, with all the main types of X-ray binary present. In contrast, the much smaller SMC (∼1/100 the mass of the Milky Way), has an extremely large X-ray population entirely made up of HMXBs. No LMXBs have been found in the SMC to date. Over the past 20 years the number of known HMXBs located in the SMC has been steadily increasing with the majority being found in the Bar region (Haberl & Pietsch 2004; Coe et al. 2005). Table 2.1 shows the distribution of known HMXBs in the Milky Way, LMC and SMC. Clearly, the SMC is extremely unusual in that approximately half of the 129 known pulsating HMXBs are located in this small galaxy. This feature has made the SMC one of the best places to study HMXBs since they are all contained within a relatively small area on the sky and at an approximately uniform distance of 60 kpc (Harries, Hilditch, & Howarth 2003).

2.2.1 SMC X-ray Sources

There are 56 identified X-ray pulsar HMXB systems in the SMC (Table 2.1). Within the SMC all but one system (SMC X-1, which has a B0I counterpart) have been found to have a main sequence Be star counterpart. As noted earlier, McBride et al. (2008) find that the spectral distribution of these counterparts is consistent with the distribution found in the Milky Way, as shown in Figure 1.3.

A large amount of X-ray telescope time on *Chandra* , *XMM-Newton* and *RXTE* has been devoted to the study of the SMC Be/X-ray binaries. The majority of these observations have focused on the Bar region (Figure 2.1) due to the large fraction

of HMXBs that are located in this region (see, for example, Haberl & Pietsch 2004; Edge et al. 2004; Shtykovskiy & Gilfanov 2005; Haberl et al. 2008a). However, until recently the only major X-ray study of the Wing pulsar population was through the *RXTE* monitoring campaign led by Robin Corbet (see Laycock et al. 2005; Galache et al. 2008, for details). Coe et al. (2005) analysed the locations of the known X-ray pulsars and postulated that a relationship between the HI intensity distribution and the distribution of the pulsars existed. This prompted a large survey of the Wing of the SMC using *Chandra*. A total of 20 individual pointings were made of approximately 10 ks each. The survey was successful in finding two new pulsars (SXP65.8 and SXP967) and detecting two previously known pulsars (SXP101 and SXP348). However, the lack of a sizeable Wing population would seem to refute the proposed connection between the HI and pulsar distribution. Due to *Chandra's* high spatial resolution the counterparts to all four sources were identified (SXP348's was previously known). A detailed description of the survey can be found in McGowan et al. (2007). The follow-up observations to this work are presented in Chapter 3.

Until recently there was only one known HMXB in the bridge, RX J0209.6-7427 (Kahabka 2000). But, observations by *INTEGRAL* during December 2008 detected a second suspected HMXB, IGR J015712-7259 (Coe et al. 2008b). Follow-up observations by *SWIFT* localised the source to a star with an USNO R1 magnitude of 15.4 mag. ToO observations by *RXTE* detected an 11.6 s pulse period. This is the first confirmed detection of a pulsating HMXB in the bridge. This is particularly interesting due to the extremely low number of stars in the bridge and opens up another previously unexplored area for study.

2.3 New Thought on the History of the SMC

Studies of the Magellanic Cloud system by Gardiner & Noguchi (1996) have shown the system to be gravitationally bound to the Milky Way and have completed several

orbits during a Hubble time. However, recent research studying the proper motion of both the LMC and SMC by Besla et al. (2007) has raised doubts over these earlier findings. Kallivayalil et al. (2006); Kallivayalil, van der Marel, & Alcock (2006) measured the proper motions of stars in both the SMC and LMC using two data sets taken by the Advanced Camera for Surveys on board the *Hubble Space Telescope*. The authors compared the positions of the cloud stars to 21 LMC and 5 SMC background quasars, the relative shifts in position between the two observations providing the proper motion values. The determination of the proper motion of the LMC was made to better than 5% accuracy and a four-fold improvement was made in the accuracy of the SMC value. It was found that the 3D velocities of the Magellanic Clouds are substantially higher, by $\sim$100 km/s, than the previously estimated values from Gardiner & Noguchi (1996). Besla et al. (2007) used these new values to evaluate their implications for the evolutionary history of the Magellanic Clouds.

Due to the mass difference between the LMC and the SMC, they concentrated their study primarily on the interactions between the LMC and the Milky Way. Initially the authors use the same formulation as the previous studies and model the Milky Way as an isothermal sphere (Gardiner & Noguchi 1996). This produces a similar result to Gardiner & Noguchi (1996) with the orbits of the clouds being quasi-periodic with a decaying maximum distance from the Milky Way, the primary difference being that the most recent close approach of the systems happened significantly longer ago than previously thought. Due to work suggesting that the dark matter halo of the Milky Way has been evolving, the authors reanalysed the data this time modelling the Milky Way in greater detail. A 4-component model for the Milky Way was used, basically a disk with a central bulge, surrounded by a dark matter halo that is in hydrostatic equilibrium with a halo of hot gas. This model is consistent with known observational constraints. Their reanalysis of the orbital history of the Milky Way and Magellanic Clouds is shown in Figure 2.3.

It is clear that, in comparison with the previous orbital histories of the Magellanic

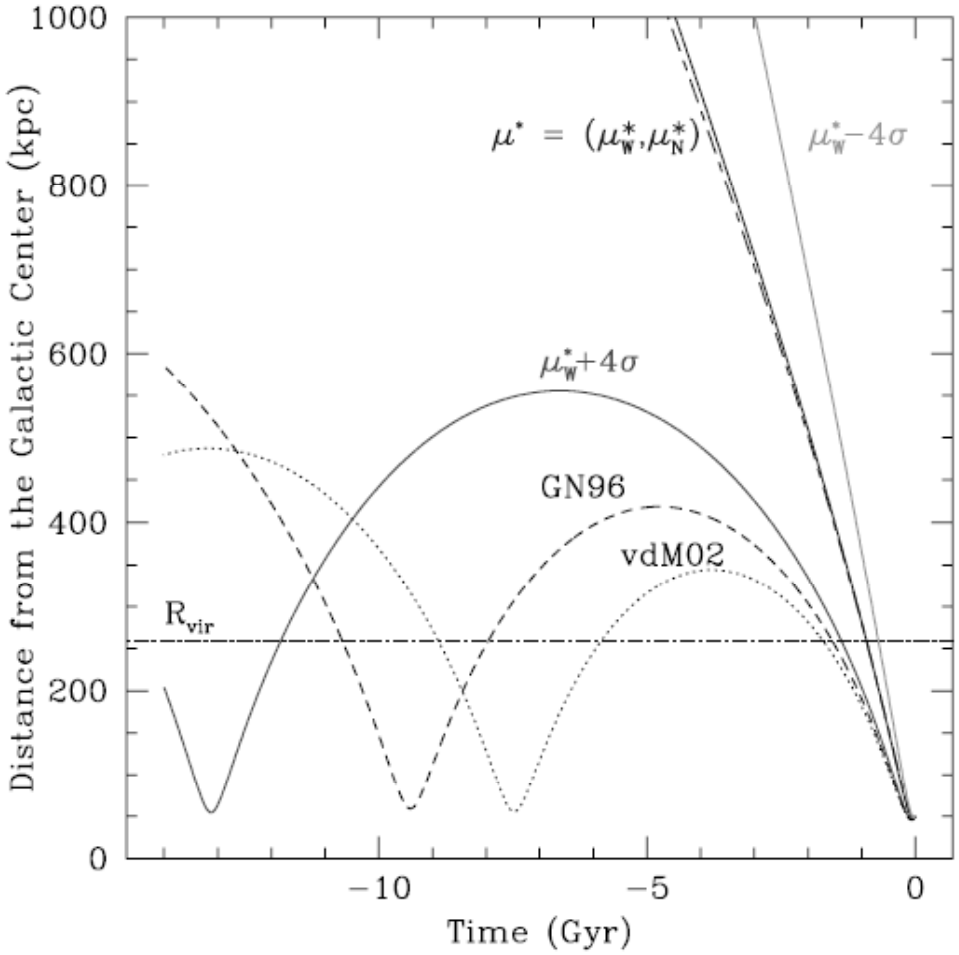

Figure 2.3: Orbital evolution of the LMC plotted as a function of time in the past, where T = 0 corresponds to today. All allowed orbits are constrained by the lines marked $\mu^*_w \pm 4\sigma$. The model proposed by Gardiner & Noguchi (1996) falls outside of the allowable values proposed by these recent measurements. (Taken from Besla et al. 2007)

Clouds, the new proper motion measurements produce a history that may be extremely different. The 4σ upper and lower limits suggest that the Magellanic Clouds could either be bound to the Milky Way or completely free and just passing by. Even in the bound state, the previous closest approach is now around 13 Gyr ago compared to the Gardiner & Noguchi (1996) value of 7 Gyr. Besla et al. (2007) conclude that the new Milky Way model, combined with the most recent and accurate proper motion values, suggests that the Magellanic Clouds are on their first passage about the Milky Way and that they are currently at perigalacticon. They also compare

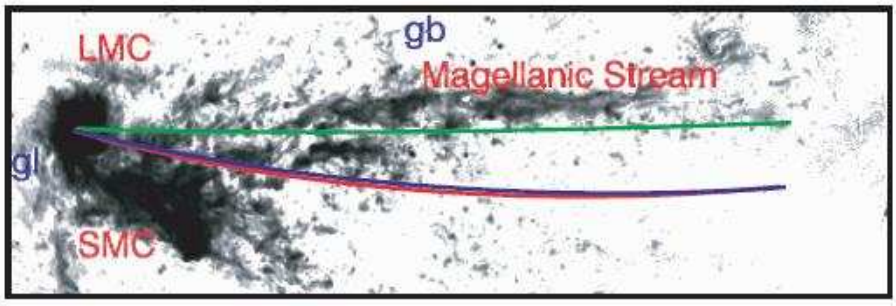

Figure 2.4: HI distribution of the Magellanic Stream from the data of Putman et al. (2003). The green line traces the orbit theoretically determined by Gardiner & Noguchi (1996). The red line shows the path traced by the mean Kallivayalil, van der Marel, & Alcock (2006) proper motions for the fiducial MW model. These new predicted paths deviate by 10° from the location of the Magellanic Stream. (Taken from Besla et al. 2007)

their orbital predictions to the Magellanic Stream (Figure 2.4). In previous studies, the Magellanic Stream was used to fix the northern component of the proper motion since it is believed to be an artefact left due to stripping of gas from the clouds as they passed through the Milky Way halo. As can clearly be seen in Figure 2.4, the predicted path of the LMC does not follow the observable position of the Magellanic Stream, unlike the work of Gardiner & Noguchi (1996). This discrepancy could be due to the uncertainty over the formation process of the Magellanic Stream. However, both the ram pressure and tidal stripping models predict that the Magellanic Stream should trace the paths of the SMC and LMC for at least some portion of their past movements.

One key ingredient that has so far been overlooked in their evaluation is the presence and effect that the SMC has on the predicted orbit. It is generally accepted that the SMC and LMC have maintained a binary state for quite some time due to the presence of the bridge material and a common envelope of gas surrounding the two clouds. Besla et al. (2007) find that the additional mass of the SMC (approximately one tenth that of the LMC) has little impact on the overall results. Figure 2.5 shows the predicted paths of both the SMC and LMC in this new formulation, as well as that predicted by Gardiner & Noguchi (1996). The new orbital path of the

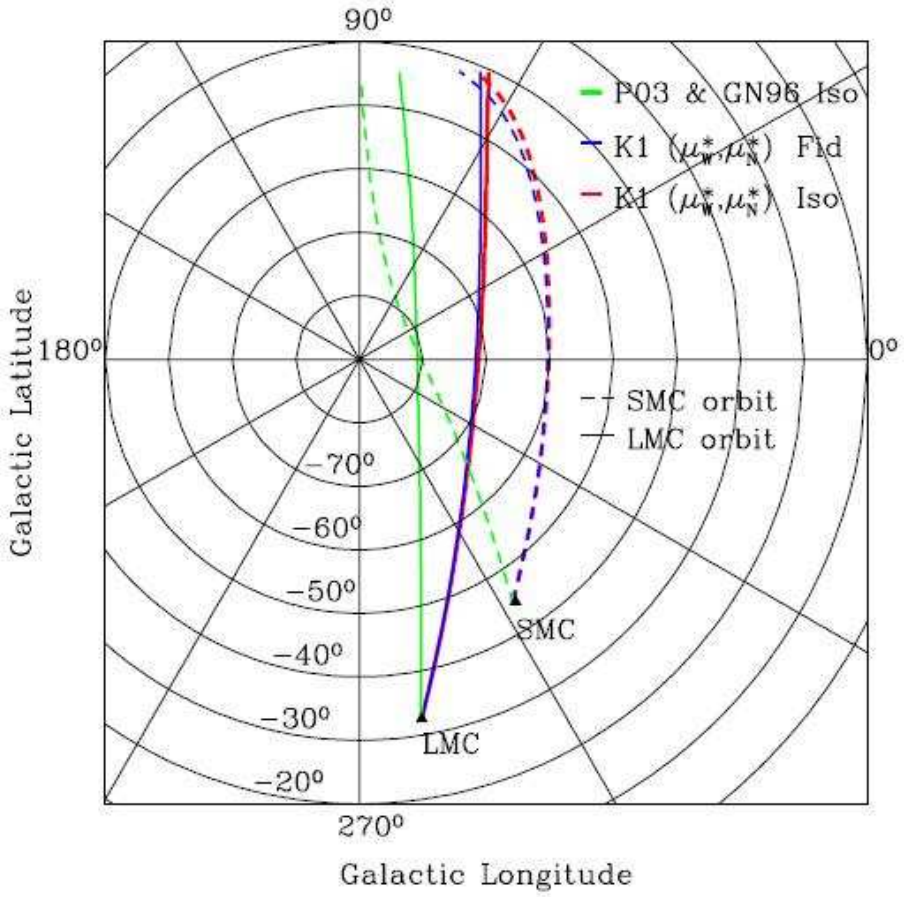

Figure 2.5: Possible orbits of the LMC (solid lines) and SMC (dashed lines) mapped out as a polar projection in galactic (l,b) coordinates. The green lines represent the orbits as implied by Gardiner & Noguchi (1996) with the dashed line also representing the Magellanic Stream. The red/blue lines represent orbits predicted by the isothermal and proposed Milky Way model for the longest lived binary state if the LMC is moving at the mean proper motion velocity from Kallivayalil et al. (2006). (Taken from Besla et al. 2007)

SMC clearly deviates from the Magellanic Stream, unlike in the model of Gardiner & Noguchi (1996).

More observations using *Hubble Space Telescope* are being made in order to strengthen this new orbital history of the Magellanic Clouds, but it seems almost certain that a rethink of the formation processes behind many of the key features of the system will be necessary. However, these new orbital models do not change the results by Zaritsky & Harris (2004) that show that the SMC has a high recent star formation

rate, with recent burst episodes occurring 0.06, 0.4 and 2.5 Gyr ago. This is because the primary cause of these bursts is not through tidal interactions with the Milky Way but through interactions with the outer gas envelope of the LMC.

Chapter 3

Optical Follow-up of New SMC Wing Be/X-ray Binaries

Until recently the majority of X-ray observations by *Chandra*, *XMM-Newton* and *RXTE* have concentrated on the Bar, since the large fraction of HMXBs are located in this region. Coe et al. (2005) analysed the locations of the known X-ray pulsars and believed there to be a relationship between the HI intensity distribution and the distribution of the pulsars. This prompted a large survey of the Wing of the SMC using *Chandra*. A total of 20 individual pointings were made of approximately 10 ks each. The survey was successful in finding two new pulsars (SXP65.8 and SXP967) and detecting two previously known pulsars (SXP101 and SXP348). Due to *Chandra's* high spatial resolution the counterparts to all four sources were identified (SXP348's being previously known). Table 3.1 shows the positions and V band magnitudes of the counterparts to the detected pulsars. A more detailed description of the survey can be found in McGowan et al. (2007). Classification of the counterparts is necessary in order to evaluate where these new pulsars lie in relation to the Galactic and SMC spectral distribution of Be/X-ray binaries. This chapter will investigate the optical counterparts of these recently discovered Be/X-ray binaries in the Small Magellanic Cloud. Many optical ground-based telescopes have been

utilised to follow up the X-ray observations, providing coverage in both the red and blue bands.

3.1 Optical Data

Since the *Chandra* observations were completed in March 2006, a number of telescopes have been used for the optical follow-up observations. Table 3.2 presents a list of the data collected for each of the sources. The telescope configurations and reduction processes used are as follows:

- AAT - 3.9m telescope, Anglo-Australian Observatory, Australia. The AAOmega optical spectrograph was used, fed by the 2 Degree Field (2dF) robotic fibre positioner covering a 2 degree field at prime focus with 392 fibres. Each observation consisted of three 1800 s exposures made on 31 August 2006. The data reduction was performed using the latest 2dfdr package version 3.46. All traces were extracted using a tram line optimisation. The spectra were then corrected for the detector response, and the red and blue arms were scaled and stitched together by forcing them to meet at 5900Å allowing the complete range to be viewed. These tasks were performed using the AAT package. The red arm has a dispersion of 1.5Å/pixel and the blue of 1.03Å/pixel. The total wavelength range covered is approximately 3700Å-8800Å. There are several bad columns in the AAT CCD. These columns have been removed and appear as spaces in the spectra.

- SALT - 11m Southern African Large Telescope, SAAO, South Africa. The Robert Stobie Spectrograph was used in conjunction with two gratings in long slit mode.

  - Blue : 2300 l/mm grating at an angle of 30.125°. This gives a dispersion of 0.34Å/pixel and a wavelength range of approximately 3800Å-4880Å.

Table 3.1: New HMXBs in the Wing

SXP ID	X-ray and Optical Names	Coordinates	V Mag	Classification
SXP101	RX J0057.3-7325, MACS J0057-734 10	00:57:27.08 -73:25:19.5	14.9[1]	B3-B5 Ib-II[4]
SXP967	CXOU J010206.6-714115, [MA93] 1301	01:02:06.69 -71:41:15.8	14.6[2]	B0-B0.5 V
SXP348	SAX J0103.2-7209, [MA93] 1367	01:03:13.94 -72:09:14.4	14.8[3]	B0-B0.5 V
SXP65.8	CXOU J010712.6-723533, [MA93] 1619	01:07:12.63 -72:35:33.8	15.0[1]	B1-B1.5 II-III

[1]McGowan et al. (2007), [2]Massey (2002), [3]Hughes & Smith (1994),
[4] Luminosity classification based solely on method of Wegner (2006).

  - Red : 1800 l/mm grating at an angle of 36.5°. This gives a dispersion of 0.40Å/pixel and a wavelength range of approximately 5930Å-7210Å.

  The SALT detectors consist of three chips aligned along the dispersion axis each separated by a small gap (evident in the spectra). Full data reduction and mosaicking of the three chips were performed using the SALT IRAF pipelines and the standard IRAF packages in version 2.12.1 provided by the NOAO. No flux calibration has been performed.

- ESO - 3.6m telescope, La Silla, Chile. The EFOSC2 faint object spectrograph was used combined with a grism with 600 l/mm. The data reduction was performed using standard IRAF packages. The spectra have a dispersion of 1.99Å/pixel and a wavelength range of approximately 3080Å-5100Å, although the useful range is only from 3700Å.

- SAAO - 1.9m telescope, SAAO, South Africa. The unit spectrograph was used combined with a 1200 l/mm grating and the SITe detector. Data reduction was performed using standard IRAF packages. The dispersion of the spectra has been fairly consistent over the years since the same set up has been used, approximately 0.43Å/pixel. The wavelength range has varied slightly due to small changes in the grating angle; the wavelength range covered in all spectra used here is approximately 6230Å-6970Å. A few cosmic rays have been removed by hand.

  All the spectra, except those from ESO (due to their lower resolution), have been smoothed with a boxcar average of 5 pixels. An arbitrary offset has been applied to some of the spectra to allow visual comparisons of the spectral lines.

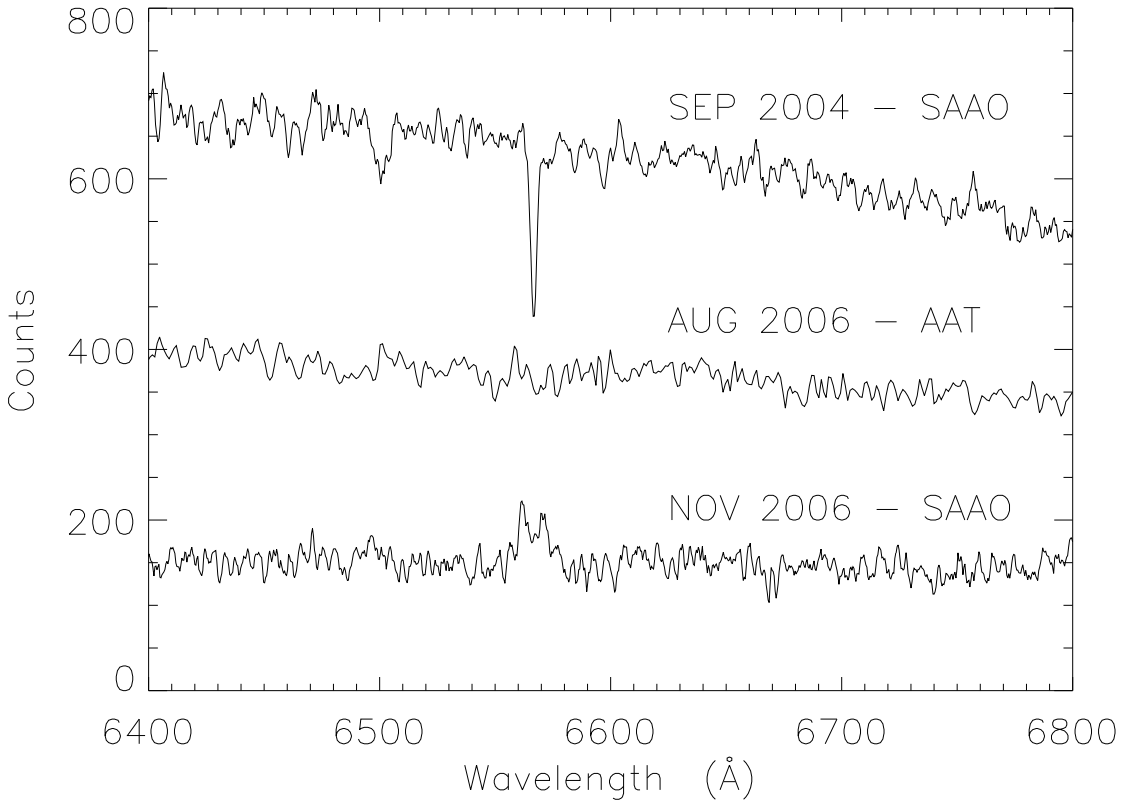

Figure 3.1: Hα spectra of SXP101. Spectra dates top to bottom: 07 Sep 2004, 31 Aug 2006, 10 Nov 2006.

3.2 Observations

3.2.1 Classification Method

Spectral classification of Be stars in the SMC is particularly difficult. Classification of Be stars in the Milky Way relies on using the ratios of many metal lines (Walborn & Fitzpatrick 1990), but the metallicity of SMC stars is lower than those in the Milky Way, and so these metal lines appear extremely weak and are often not present. There is also the added difficulty that the Balmer lines, in particular, become rotationally broadened and hence obscure any comparisons to neighbouring lines. Other difficulties are added when the effect of the circumstellar disk is considered. Strong Hα emission is seen to originate from the circumstellar disk, but as mentioned in §1.1.7.2 the circumstellar disks can have an effect on the higher

Table 3.2: Observations

SXP ID	Telescope	Date	Exposure Time (s)	Hα EW (Å)	Hβ EW (Å)
SXP101	SALT Red	-	-	-	-
	SALT Blue	10 Oct 2006	450	-	0.0 ± 0.7
	ESO	14 Sep 2006	2400	-	1.1 ± 0.2
	AAT	31 Aug 2006	5400	0.2 ± 0.3	4.7 ± 0.3
	SAAO	07 Sep 2004	2×1000	1.7 ± 0.2	-
	SAAO	10 Nov 2006	2×1500	-2.9 ± 0.5	-
SXP967	SALT Red	15 Oct 2006	600	-13.4 ± 0.1	-
	SALT Blue	16 Oct 2006	600	-	-1.0 ± 0.1
	ESO	13 Sep 2006	2400	-	-0.7 ± 0.1
	AAT	31 Aug 2006	5400	-13.4 ± 0.2	-0.8 ± 0.2
	SAAO	10 Nov 2006	1800	-12.9 ± 0.4	-
SXP348	SALT Red	-	-	-	-
	SALT Blue	-	-	-	-
	ESO	14 Sep 2006	1800	-	0.3 ± 0.2
	AAT	-	-	-	-
	SAAO	12 Sep 2004	2500	-8.7 ± 0.9	-
	SAAO	30 Oct 2005	1000	-2.9 ± 0.6	-
	SAAO	08 Nov 2006	1200	-6.3 ± 0.5	-
SXP65.8	SALT Red	-	-	-	-
	SALT Blue	-	-	-	-
	ESO	13 Sep 2006	2000	-	1.2 ± 0.1
	AAT	31 Aug 2006	2×5400	-21.3 ± 0.3	0.9 ± 0.2
	SAAO	13 Nov 2006	1800	-13.5 ± 0.6	-

order Balmer lines through in-filling. This increases the difficulty when using weak metallic lines around the Balmer lines. Consequently, the classification criteria and methods as set out by Lennon (1997) and Evans et al. (2004) have been used. These methods use the presence of HeII lines to restrict the classification to B0 and earlier. For the later spectral types, classifications is based on the relative strengths of the silicon lines, when they are identifiable. Comparisons of the silicon lines to MgII, HeI and the OII bands can provide additional classification constraints. Table 2 in Evans et al. (2004) details the classification scheme.

For the luminosity, classification methods set out in Walborn & Fitzpatrick (1990) have been adopted. However, since this method relies on line ratios, the same difficulties as previously mentioned are faced. A check on this luminosity classification was made by comparing the absolute magnitude of the source in the V-band with

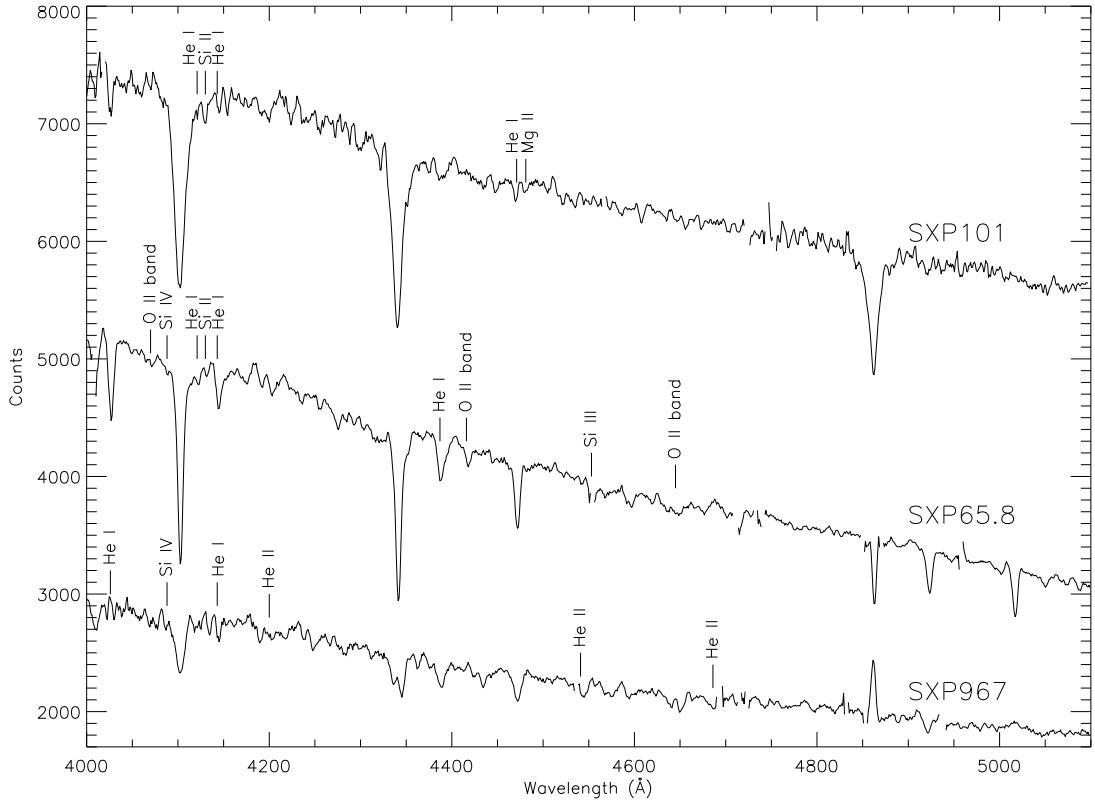

Figure 3.2: AAT spectra taken on 31 Aug 2006. Top to bottom: SXP101, SXP65.8, SXP967, (smoothed with gaps for dead pixels).

the spectral classification obtained. Here a distance modulus for the SMC of 18.9 (Harries, Hilditch, & Howarth 2003) was adopted, and the relevant tables in Wegner (2006) were used. These tables are based on absolute magnitudes from HIPPARCOS data. Although the luminosities of Be stars in the SMC may differ somewhat to those in the Milky Way, the method was adopted as a check, and it is recognised that in some cases the results obtained may be uncertain.

3.2.2 SXP101

This source was detected by both ROSAT (RX J0057.3-7325) and *ASCA* (AX J0057.4-7325; Kahabka et al. 1999; Torii et al. 2000). Coherent pulsations were first detected in the *ASCA* data at a period of 101.45 ± 0.07 s. The resultant overlapping error circles allowed for some counterparts to be tentatively assigned (Edge

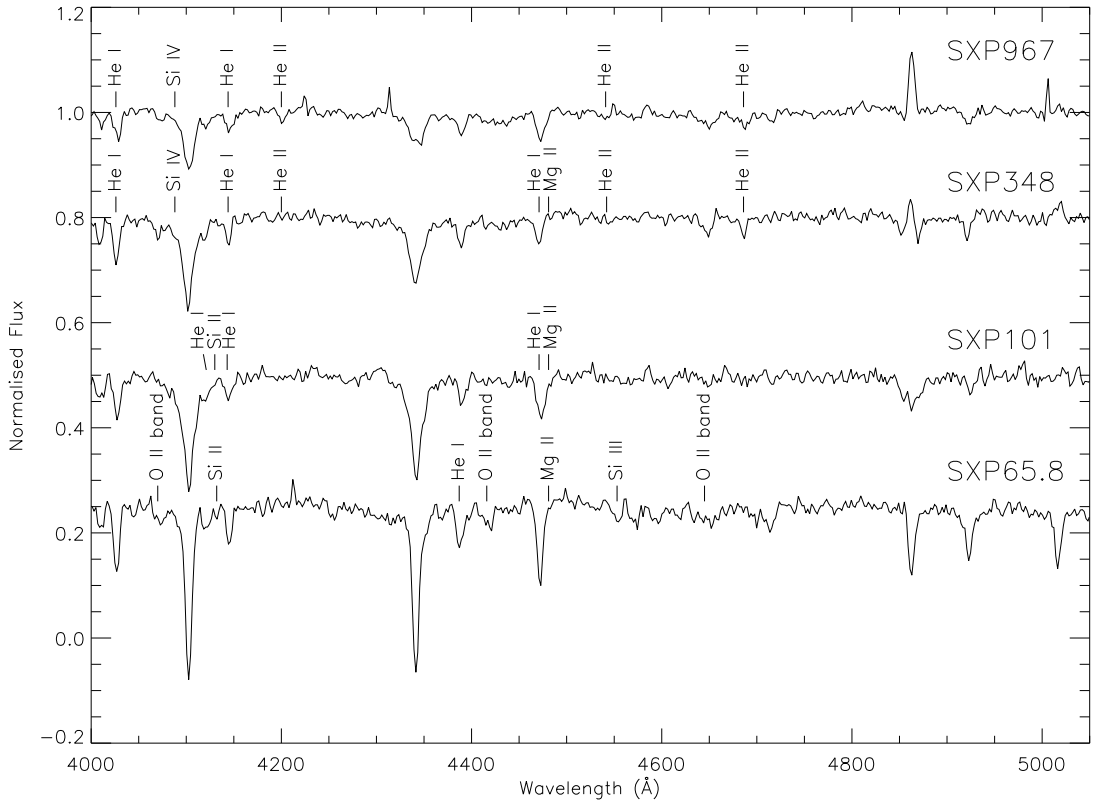

Figure 3.3: ESO blue spectra taken on 14 Sep 2006. Top to bottom: SXP967, SXP348, SXP101, SXP65.8 (no smoothing).

& Coe 2003). The detection of pulsations at 101.16 ± 0.26 s in the *Chandra* data (McGowan et al. 2007) has allowed the counterpart to be clearly identified as the source previously labelled E in Figure 3 of Edge & Coe (2003), MACS J0057-734 10 (Tucholke et al. 1996). This source had first been identified as a possible counterpart in January 2000 due to its r-Hα colour revealing an excess of Hα. Subsequently this source was observed 4 years later (in 2004) using the 1.9m SAAO telescope. Two spectra taken on the night have been co-added and are shown in Figure 3.1. The Hα line is clearly seen in absorption, hence the source was not considered to be a prime candidate. Strangely the AAT spectrum (Figure 3.1) shows neither absorption or emission in Hα. In fact it is perfectly filled in. Curiously, the higher order Balmer lines in the AAT spectrum (Figure 3.2) show no signs of infilling: they are all clearly in absorption with no peculiar features. A third red spectrum (Figure 3.1) was taken recently at SAAO in November 2006. Two spectra were taken consecutively and have been co-added to increase the signal to noise ratio. The Hα profile

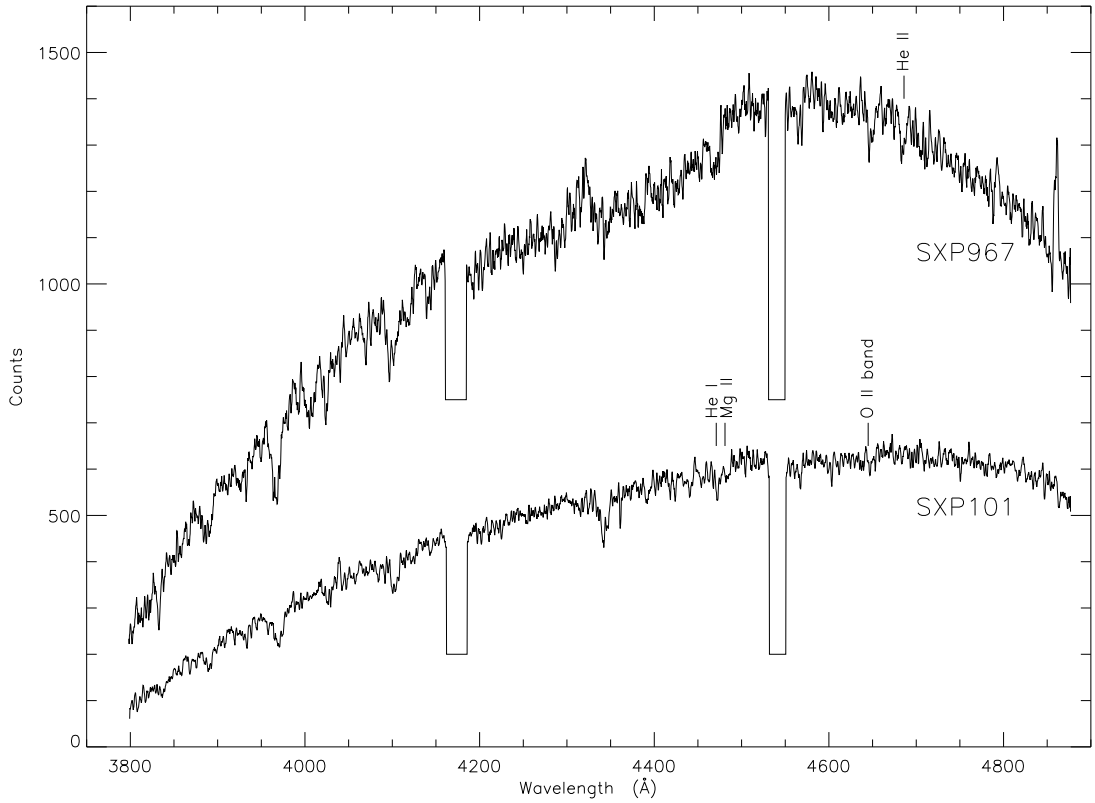

Figure 3.4: SALT blue spectra of SXP967 (16 Oct 2006) and SXP101 (10 Oct 2006) (chip gaps are clearly visible).

now appears to be slightly in emission, suggesting its Be nature. There have been several observations of the Hβ emission line during the last few months of 2006 (Figure 3.2, 3.3, 3.4). These observations appear to show that in the course of little more than one month the line has completely filled itself in.

Classification has been made using blue spectra taken by AAT, ESO and SALT (Figures 3.2, 3.3, 3.4). The counterpart is extremely difficult to classify due to a severe lack of metallic lines. No HeII lines are visible, hence the counterpart must be B1 or later (Lennon 1997). There is some evidence for the presence of the OII 4640-50Å band in the SALT spectra, however it seems to be lacking in the other spectra. Comparison of all three spectra with those given in Figure 4 of Evans et al. (2004) would seem to place the counterpart in a broad spectral range of B1-B5. MgII 4481Å is possibly present in all three spectra, in particular the SALT and AAT ones. However, the resolution of the ESO spectra is not sufficient to deblend the

line from the neighbouring HeI line. If the presence of this line is to be believed, then combined with the lack of SiIII 4553Å a earlier classification limit of B3 can be assigned (Lennon 1997). Visible in the AAT spectra is the SiII blend of 4128/4132Å and HeI line at 4143Å. HeI 4121Å is possibly visible on the red shoulder of the Hδ line. However, it is heavily obscured and cannot be used for classification. The ratio of SiII to the HeI line would suggest a classification around B8 (Evans et al. 2004). This line ratio is not seen in the ESO spectra, in fact, SiII is barely seen and the HeI line appears strongly, suggesting a classification more like B5. A classification range of B3-B5 would agree with the Balmer lines appearing very broad and deep which is typical of a mid range Be star. The luminosity classification method of Walborn & Fitzpatrick (1990) only goes as far as classifying B2 stars, hence only the estimate from the V-band magnitude is used. The luminosity class is estimated to be about Ib-II from Table 10 presented in Wegner (2006). A luminosity class of Ib-II would make the counterpart a supergiant and not a Be star. This luminosity classification should be treated cautiously due to the methods used.

3.2.3 SXP967

The first X-ray detection of this pulsar was in the SMC *Chandra* Wing survey on 06 February 2006. McGowan et al. (2007) performed timing analysis on the source revealing a 700 s period. They noted that the data were carefully examined to ensure that this period was unrelated to the 707 s period associated with the dithering pattern in the Z direction, the source was named SXP700. However, a subsequent *XMM-Newton* detection on 04 June 2007 (Haberl et al. 2008a) revealed a source at the same position with an X-ray period of 966.97 ± 0.47 s. Due to the unlikely case that there could be two independent sources, Haberl et al. (2008a) re-examined the *Chandra* data. The authors found that the 700 s period was a result of missing columns crossing the source during the dithering. When these columns are included in the analysis the 700 s period vanishes. The authors searched for

the 967 s period in the *Chandra* data but were unsuccessful, possibly due to the relatively short length of the observation (9.4 ks). The source was thus renamed SXP967 to reflect the true X-ray period.

The *Chandra* source is coincident with [MA93] 1301 (Meyssonnier & Azzopardi 1993). Three red follow-up spectra, taken within a few months of each other by SALT, AAT and SAAO, reveal the counterpart star to have a very strong Hα line in emission (Figure 3.5). This strongly suggests the identification of this object as a Be/X-ray binary. The three observations were spaced roughly a month apart from each other. It can be seen in Table 3.2 that the equivalent width of Hα has barely changed over the course of these observations, indicating that the circumstellar disk was in a fairly stable state.

Classification of the counterpart has been possible through the three blue spectra taken by AAT, ESO and SALT (Figures 3.2, 3.3, 3.4). Weak HeII at 4686Å can be seen in all the spectra; using the classification guide set out by Evans et al. (2004), this immediately places the object as earlier than B1. No other HeII lines are visible in either the AAT or SALT spectra, but HeII 4200Å is present in the ESO spectrum. This, combined with the lack of HeII 4541Å, allows the classification of B0-B0.5 to be made (Evans et al. 2004). Hβ can also be seen to be strongly in emission in all three blue spectra. A luminosity classification can be made by comparing the ratio of SiIV 4089Å to both HeI 4026Å and 4144Å. The ESO spectrum shows strong HeI lines compared with slight evidence of SiIV in the blue shoulder of the Hδ line. Using the ratio of these lines results in a luminosity class of V (Walborn & Fitzpatrick 1990). Using the method based upon the V-band magnitude yields a classification of III-V.

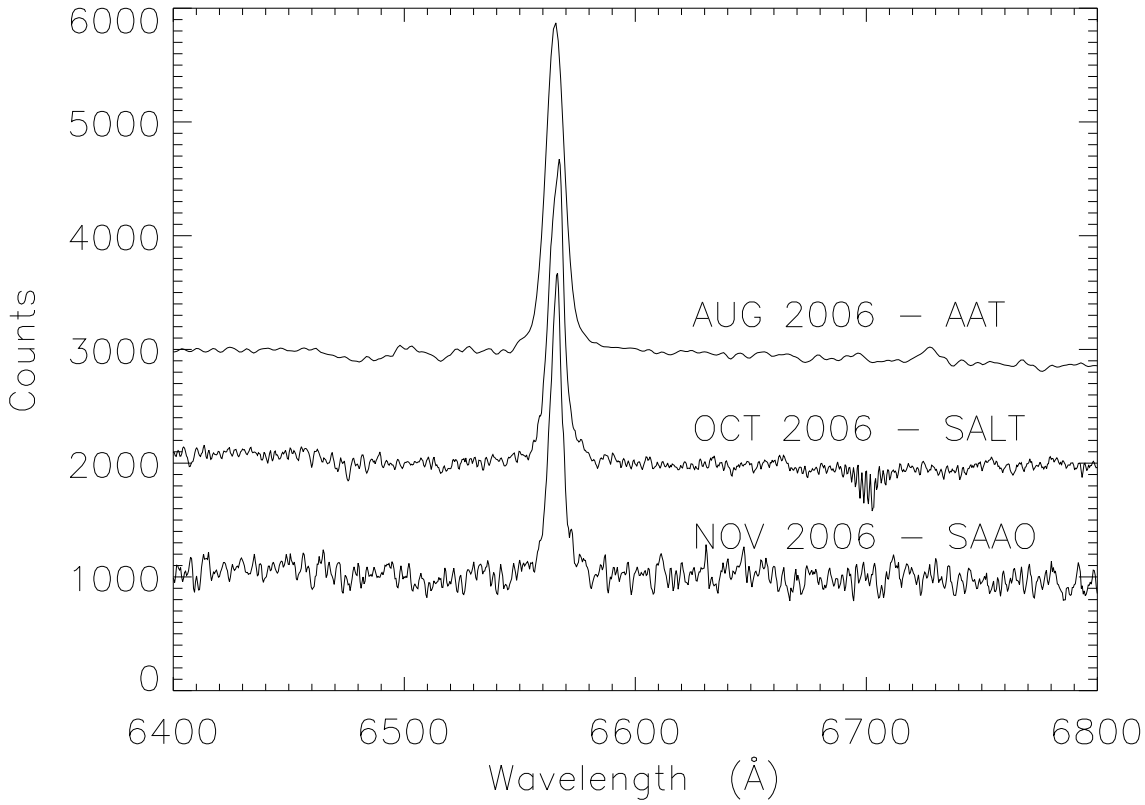

Figure 3.5: Hα spectra of SXP967. Spectra dates top to bottom: 31 Aug 2006, 15 Oct 2006, 10 Nov 2006 (this spectrum has been scaled to allow the comparison of the Hα profile).

3.2.4 SXP348

This is the only detected pulsar from the *Chandra* Wing survey which has a previously known counterpart. It was first detected by *BeppoSAX* in 1998 (Israel et al. 1998) with a pulse period of 345.2 ± 0.1 s. The *Chandra* source is coincident with [MA93] 1367 (Meyssonnier & Azzopardi 1993), a Be star (Hughes & Smith 1994; Israel et al. 1998). Spectra taken in 2004 and 2005 by the 1.9m SAAO telescope (Figure 3.6) show that the Hα line has been varying over recent years. In 2004 the line was strongly in emission with a small second peak on its red shoulder. Just over a year later, in 2005, the line appears to have dropped in strength and displays a shell profile. A recent spectrum (Figure 3.6), taken on 08 November 2006, shows Hα to be back in emission, this time with a slightly more prominent feature on the red shoulder, making it appear more double-peaked. The ESO spectrum (Figure 3.3),

taken near to this most recent red spectrum, shows the Hβ line to be largely filled in with an emission peak at its centre. The Hα profile has also weakened quite dramatically since it was first observed in 1992 (Hughes & Smith 1994). They reported an equivalent width of -22Å; however, they did not note anything about the shape of the emission line. The Hβ line has also weakened since 1992, when they reported an equivalent width of -1.7Å.

From the ESO spectra (Figure 3.3), a strong HeII line at 4686Å is seen; this firmly restricts the spectral class to earlier than B1. Further constraints can be established, based on the presence of very weak HeII at 4541Å and 4200Å in the ESO spectrum. A spectral classification of B0-B0.5 can be placed on this counterpart (Evans et al. 2004). This agrees with the spectral range of O9-B1 (V-III) determined by Hughes & Smith (1994), where they estimated the spectral class to around B0, based on the strength of HeI 4471Å relative to its neighbour MgII 4481Å. The presence of HeII 4686Å was uncertain in their spectrum due to a flat fielding correction. Using the same HeI and SiIV lines in the ESO spectrum for the luminosity classification, as used for SXP967, yields a very similar situation, strong HeI lines and a moderate bump representing SiIV on the shoulder of Hδ. Using this ratio a luminosity classification of V is made (Walborn & Fitzpatrick 1990), which is consistent with the range of III-V estimated from the V-band magnitude.

3.2.5 SXP65.8

3.2.5.1 Optical

SXP65.8 is the second of the new pulsars detected in the SMC Wing survey on 10 February 2006. The *Chandra* source is coincident with the emission line star [MA93] 1619 (Meyssonnier & Azzopardi 1993). Follow-up red spectra were taken by SAAO and AAT (Figure 3.7). The counterpart was observed twice with the AAT on the same night, roughly one hour apart. Each observation was 5400 s long. Since these

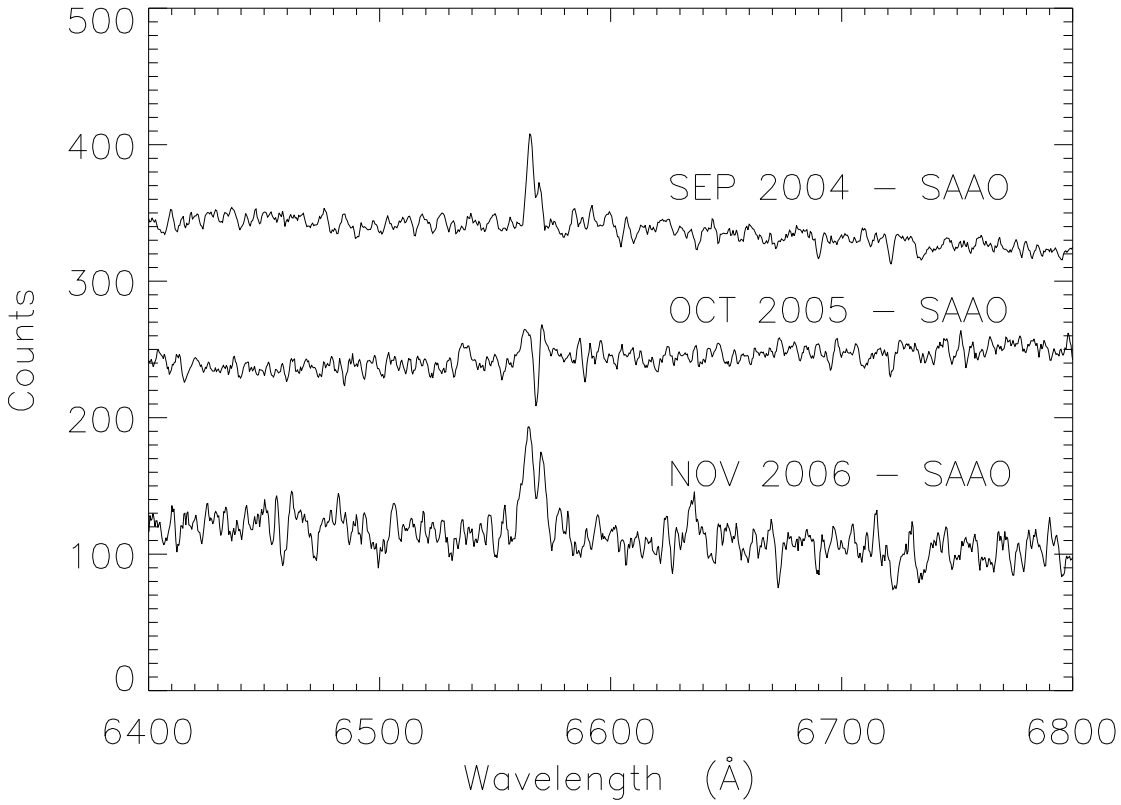

Figure 3.6: Hα spectra of SXP348 observed at SAAO. Spectra dates top to bottom: 12 Sep 2004, 30 Oct 2005, 08 Nov 2006.

spectra are both of high quality and show no astrophysical difference, only one is included here. The strong Hα emission line present in the AAT spectrum strongly suggests that the counterpart is indeed a Be/X-ray binary. In the few months between the AAT and SAAO spectra the Hα line profile has changed significantly. It is now extremely double-peaked. This would indicate that the circumstellar disk has shrunk in size and now the absorption in the stellar photosphere is becoming a more dominant effect.

The classification for this counterpart has been based on AAT and ESO blue spectra (Figures 3.2, 3.3). Clear OII absorption bands visible at 4640-50Å, 4415-17Å and 4070Å are present in both spectra, and the HeII lines have also completely disappeared. These features allow a classification of B1-B3 to be made (Evans et al. 2004). Several silicon lines help to refine the classification. The presence of a strong SiIII 4553Å line in the AAT spectrum is dubious, since it falls on a dead

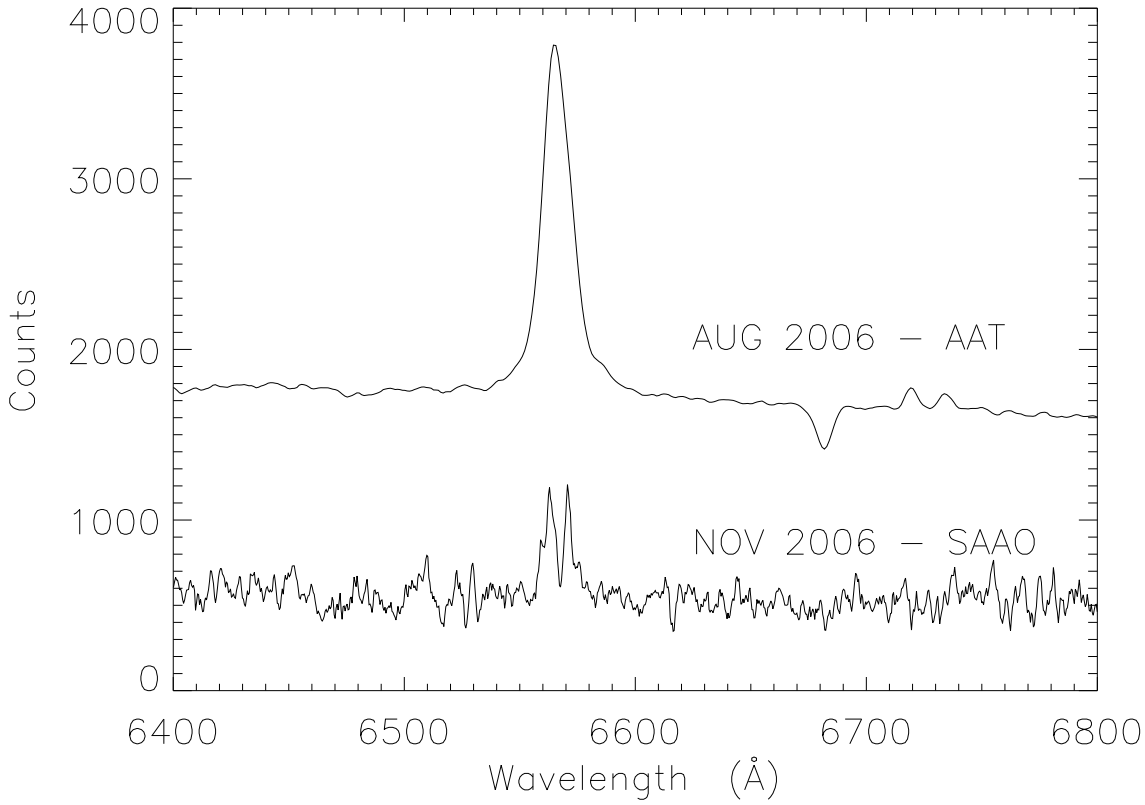

Figure 3.7: Hα spectra of SXP65.8. Spectra dates top to bottom: 31 Aug 2006, 13 Nov 2006 (this spectrum was scaled to allow the comparison of the Hα profile).

pixel, but, the continuum does appear to take a strong dip just before and then rise just after, suggesting the line is indeed present. Also visible in the AAT spectrum is weak SiIV 4088Å and SiII 4132Å. The ESO spectrum confirms the presence of SiIII and SiII, but SiIV only appears as a slight bump on the shoulder of Hδ. There is the possibility of very weak MgII 4481Å absorption seen on the shoulder of the HeI line in the ESO spectrum. Comparing the strengths of SiIII to MgII implies a classification earlier than B2 (Lennon 1997). By using the detections of the other lines, it is clear that OII is stronger than SiIV 4088Å, which refines the classification to B1-B1.5. SiIV 4116Å is unresolvable in both spectra, due to the width of the Hδ feature. Since it is not certain whether this line is present or absent, a final classification of B1-B1.5 is made. There are also notable FeII lines in absorption at 4924Å and 5018Å. Using the ratio of SiIII to HeI 4387Å a luminosity classification of II-III (Walborn & Fitzpatrick 1990) is made, which agrees with that obtained

using the magnitude method.

3.2.5.2 X-ray

Using *Chandra* data (for more details see McGowan et al. 2007) a phase-resolved spectrum for SXP65.8 was extracted using CIAO v3.4 standard tools. The spectra were regrouped by requiring at least 10 counts per spectral bin. The subsequent spectral fitting and analysis were performed using XSPEC v12.3.0. A phase binned light curve was created (Figure 3.8) based on MJD 53776.82172 and a pulse period of 65.78 s (McGowan et al. 2007). The two phase binned spectra were extracted using the phase ranges 0.0-0.5 and 0.5-1.0. Each of these were fitted with an absorbed power law, and fixed the column density at the value for the SMC of $6 \times 10^{20}\,\mathrm{cm}^{-2}$ (Dickey & Lockman 1990). The low phase spectrum is well fit with a $\Gamma = 0.34 \pm 0.08$ with a reduced $\chi^2 = 0.85$, and the high phase spectrum is fit with $\Gamma = 0.52 \pm 0.10$ with a reduced $\chi^2 = 1.42$. These values are consistent right at the extremes of their errors. However, they would also seem to indicate that the pulsed emission from the beam is harder than the persistent emission. The pulse fraction has been calculated for both soft (PF_s) and hard (PF_h) energy bands (0.5-2.0 keV and 2.0-8.0 keV respectively). The pulse fraction was determined by fitting a sine function to the folded profiles and defining the pulse fraction as $(F_{max} - F_{min})/(F_{max} + F_{min})$ where F_{max} and F_{min} are the maximum and minimum of the fitted pulse light curves. $PF_S = 28.0 \pm 5.7\,\%$ and $PF_H = 36.5 \pm 4.0\,\%$. The values are both consistent within errors and with the value in McGowan et al. (2007). This is probably due to the lack of soft counts.

3.3 Discussion

3.3.1 SXP101

The identification of the correct counterpart to SXP101 has finally enabled its identification as a Be/X-ray binary. The Hα and Hβ line profiles provide strong evidence that the circumstellar disk is an extremely variable component of the system. The most recent observations, made at the end of 2006, suggest that the circumstellar disk has recently grown in size. Interestingly the Hβ line has shown considerable variation over the course of a few months. Figure 3.2 clearly shows all the Balmer lines to be deep and well defined, including Hβ; 14 days later the Hβ line has considerably changed and is almost totally filled in, with the remaining Balmer lines showing no change (Figure 3.3). This agrees with the Hα observations which show that, over approximately the same time scale, the Hα line has gone from being filled in completely to being slightly in emission. These recent observations provide strong evidence that the circumstellar disk is an extremely variable object. The apparent lag of the Hβ line with respect to Hα could be evidence of the emission originating from a different part of the circumstellar disk than the Hα. This may be the result of temperature or density changes. Further modelling of the circumstellar disk structure would be needed to confirm this.

The classification of B3-B5 is also potentially very interesting, since it would make this Be/X-ray binary one of the latest types to have been found. Comparing the spectral type of SXP101 with the spectral distribution found in the Milky Way (Negueruela 1998), clearly shows that SXP101 would lie on its own. McBride et al. (2008) present a full spectral classification and analysis of all the Be/X-ray binaries in the SMC where the counterparts are known. SXP101 is included in their analysis and is notable as the latest spectral type known in the SMC.

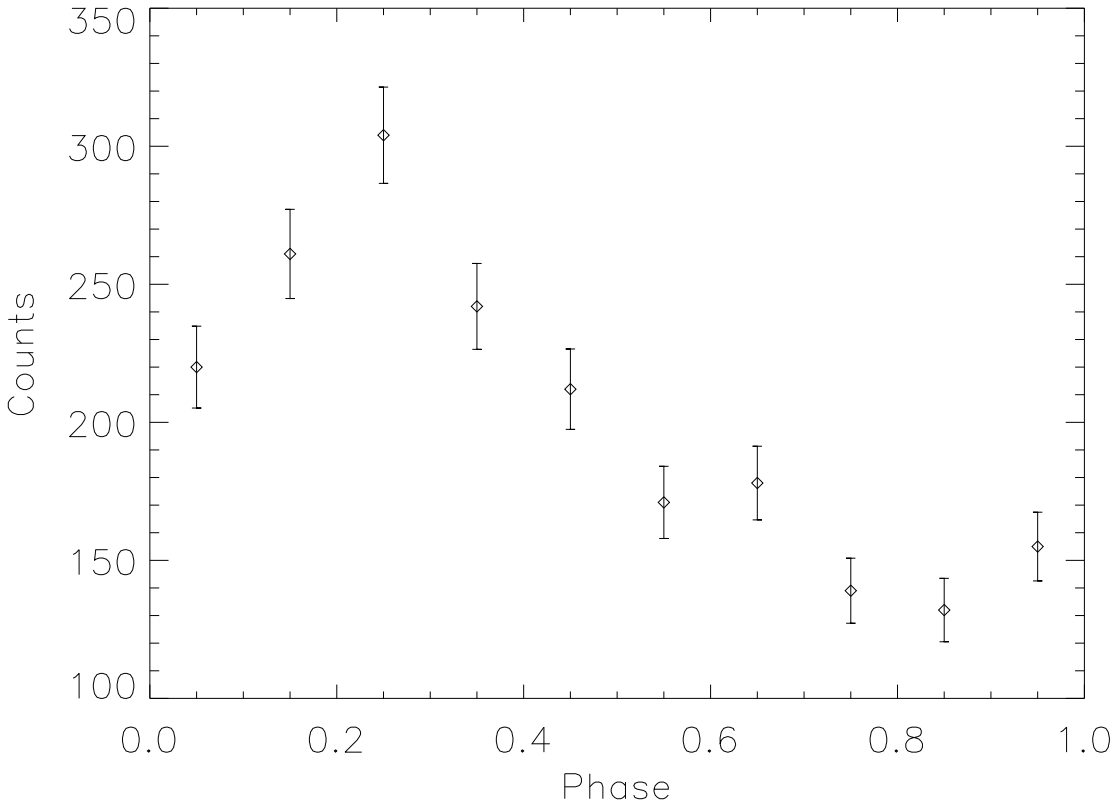

Figure 3.8: Pulse profile for SXP65.8 in the energy range 0.5-8.0 keV.

3.3.2 SXP967

The presence of a strong Hα emission line and a classification of B0-B0.5 clearly places this Be/X-ray binary right in the centre of the Galactic spectral distribution (Negueruela 1998). The unchanging equivalent widths of the Hα line (Table 3.2) suggests that the circumstellar disk was in a fairly stable state. An orbital period of 267.38 ± 15.10 d was found in OGLE III data (McGowan et al. 2007). This period is entirely consistent with that predicted from the Corbet diagram (Corbet 1986) for a 967 s pulsar. Assuming SXP967 only goes into outburst every time the neutron star passes through periastron, then only outbursts approximately every 9 months would be expected. With such long intervals in which no accretion is taking place the circumstellar disk has time to replenish any lost matter. The observations taken during the orbital phase range 0.41-0.68 (see Figure 6. McGowan et al. 2007), show that over approximately one quarter of this orbital period the circumstellar disk has

remained stable. This could be indicative of a stable truncated circumstellar disk at its maximum equivalent width, similar to the stable circumstellar disk observed in GRO J1008-57 (Coe et al. 2007). Reig (2007) presents an up-to-date version of the P_{orb}-EW(Hα) diagram containing all the known Galactic and Magellanic Be/X-ray binaries where the orbital periods are known. The measured Hα value is assumed to be representative of a circumstellar disk at maximum size. The measured values for SXP967 are not consistent with this plot. However, it is noted that the values for GRO J1008-57 (Coe et al. 2007), where the circumstellar disk is in a stable state, are also not consistent with the plot. In order to place SXP967 on this diagram properly, many more observations are required, particularly at varying orbital phases to evaluate the changes that take place in the circumstellar disk.

3.3.3 SXP348

This source was first detected by *BeppoSAX* in 1998 (Israel et al. 1998) with a pulse period of 345.2 ± 0.1 s. After its discovery, a previous *ASCA* observation from 1996 was found to have the same source present at a slightly slower spin period of 348.9 ± 0.3 s (Yokogawa & Koyama 1998). Several later observations reveal that SXP348 has continued its spin up at an almost constant rate These detections were made by *Chandra* in 1999 of 343.5 ± 0.3 s pulsations (Israel et al. 2000) and then *XMM-Newton* in 2000 at 341.21 ± 0.5 s (Haberl & Pietsch 2004). An *XMM-Newton* observation in 2001 showed a slight spin down of the pulsar to 341.7 ± 0.4 s (Sasaki et al. 2003). However, the measurement is consistent within errors to the previously measured period. The recent *Chandra* observation at 339.56 ± 0.58 s supports this trend of continued spin-up. Figure 3.9 shows how SXP348 has been spinning up (McGowan et al. 2007) over the last 10 years. The recent *Chandra* observation suggests that the constant spin up rate has recently slowed.

It appears that SXP348 has transitioned at some point into a different state where the spin period is now changing much more slowly. The observations were divided

into two epochs, with the transition point being the average of the two *XMM-Newton* observations that fall around MJD 52000. Epoch one yields $\dot{P}_1 = (5.1 \pm 0.4) \times 10^{-8}\,\mathrm{ss}^{-1}$, which is consistent with the value found in Haberl & Pietsch (2004), this implies $L_{x1} = (4.5 \pm 0.4) \times 10^{35}\,\mathrm{erg\,s}^{-1}$. Epoch two yields $\dot{P}_2 = (1.2 \pm 0.5) \times 10^{-8}\,\mathrm{ss}^{-1}$, which implies $L_{x2} = (1.1 \pm 0.4) \times 10^{35}\,\mathrm{erg\,s}^{-1}$. An estimate was derived on the magnetic field strength using Eq. (6.24) of Frank et al. (2002). The luminosity value of epoch one yields a field strength of $B_1 = (4.3 \pm 1.6) \times 10^{13}\,\mathrm{G}$. The field strength derived from epoch two is consistent with this value but has significantly larger errors. The change in luminosity is as expected, and would indicate that SXP348 has had significant changes to its accretion rate, possibly implying that the pulsar is nearing a spin period where the accretion flow can be cut off due to the propeller effect caused by the magnetosphere. The estimated value of the magnetic field is higher than expected, which is possibly a reflection of the estimation method used when only a handful of points are known.

The classification of B0-B0.5 agrees with the spectral type of O9-B1 (V-III) determined by Hughes & Smith (1994), and places this source in the middle of the Galactic spectral distribution. The variation of the Hα profile shows that the circumstellar disk is variable on time scales of around a year. This is twice the expected orbital period as predicted from the Corbet diagram (Corbet 1986). Since the state of the circumstellar disk is intricately linked to the spin period changes, many more observations are required before the dynamics of the system are fully understood.

3.3.4 SXP65.8

Observations of a varying Hα emission line and a classification of B1-B1.5 confirm SXP65.8 as a Be/X-ray binary. Since the Hα emission is arising from the circumstellar disk, it is deduced that the reduction in equivalent width is due to the circumstellar disk shrinking in size over the course of a few months.

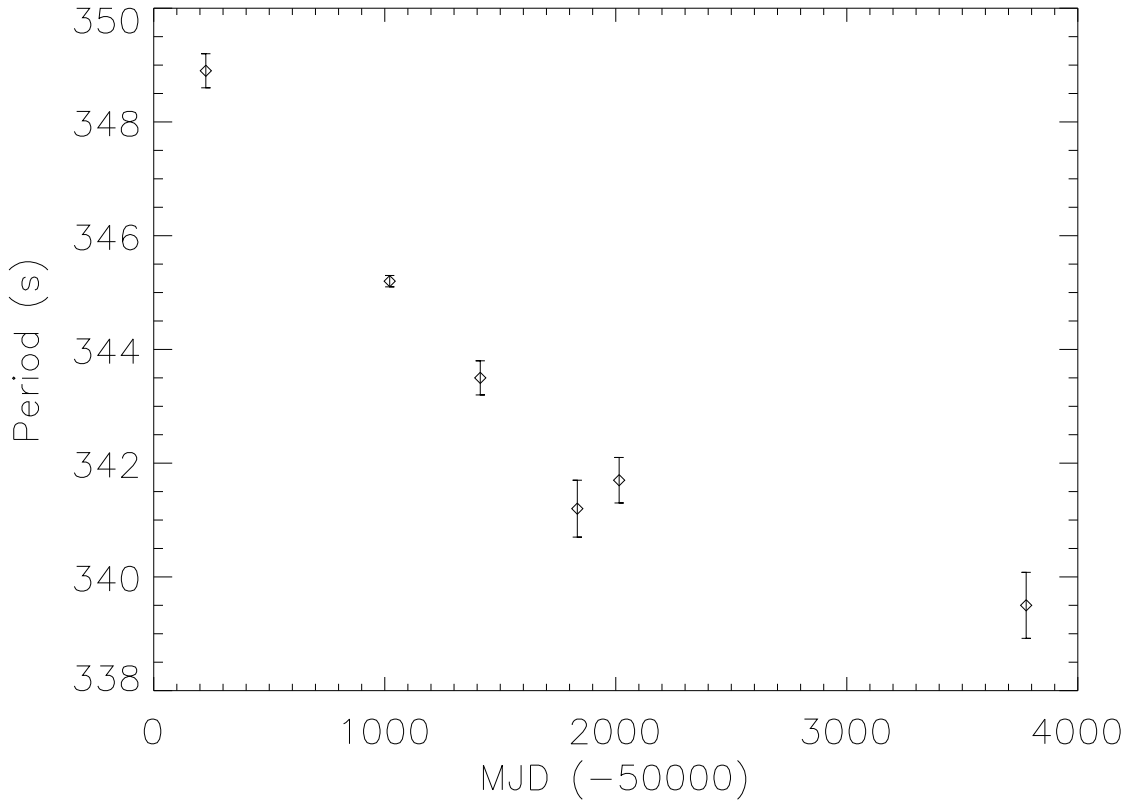

Figure 3.9: Spin period of SXP348 over the past 10 years.

The phase-resolved spectroscopy suggests that as the X-ray beam passes through the line of sight, the X-ray emission becomes harder. This indicates that the soft emission originates in a different location to the magnetically collimated beam and is probably more representative of thermal emission from either the surface of the neutron star or the accretion disk.

3.4 Conclusions

Four pulsars were detected in the SMC *Chandra* Wing survey, SXP101, SXP967, SXP348 and SXP65.8. Follow-up optical observations have enabled spectroscopic classifications of all the counterparts. All the counterparts are classified within the range B0-B5. Red spectra covering the Hα atomic line have revealed that all of the sources have at some point exhibited Hα emission, resulting in their classification as

emission line stars. Three of the Be/X-ray binaries fall within the known Galactic spectral distribution for Be/X-ray binaries (Negueruela 1998). SXP101 falls outside of this distribution and hence becomes the latest spectral type known for a Be/X-ray binary. McBride et al. (2008) have recently analysed the spectral distribution of Be/X-ray binaries in the SMC. They find that the distribution is consistent with the Galactic distribution, with SXP101 being the latest type known. From the Hα monitoring it would appear that SXP967 has a stable circumstellar disk, unlike the three other sources where variations in the profile would suggest a more dynamic circumstellar disk. This is likely to be due to the differences in the length of the orbital periods, and hence the influence of the neutron star on the circumstellar disk's geometry.

McGowan et al. (2007) suggest that the Wing pulsars could be coming from a different population to the Bar pulsars due to the pulsars exhibiting harder X-ray spectra. However, the optical follow-up observations presented here are unable to help clarify this matter further.

Chapter 4

High-mass X-ray binary SXP18.3 undergoes the longest Type II outburst ever seen in the Small Magellanic Cloud

4.1 *RXTE* Monitoring Campaign

The majority of HMXBs are very transient in nature. As was discussed in Chapter 1, there are predominately two types of outburst behaviour, the short Type-I outbursts and the much longer Type-II outbursts. A continuous monitoring campaign studying the X-ray behaviours of the SMC Be/X-ray binaries has been made for the past 11 years. The proportional counter array (PCA) on board *RXTE* made its first observations of the SMC in November 1997 (MJD 50777) after an outburst detected by the All Sky Monitor (ASM) was mistaken for SMC X-3. These early observations found many new pulsars, and it became apparent that the SMC was an extremely interesting place to look for HMXB systems. 1999 marked the corner stone of the

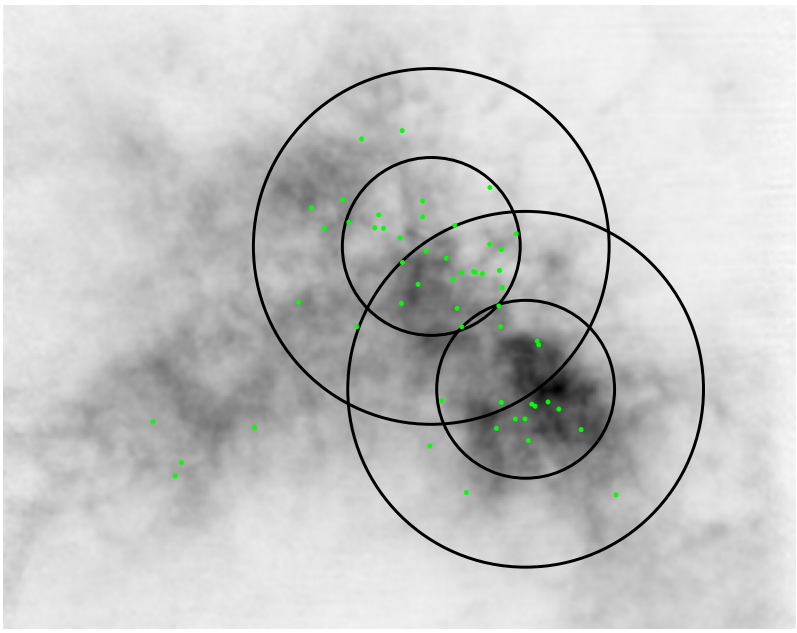

Figure 4.1: HI map (Stanimirovic et al. 1999) of the SMC with the known HMXB sources marked. Over plotted are the two current *RXTE* monitoring positions (E and D to the North and South respectively), the outer and inner circles are 2° and 1°.

exploration into the SMC, when an approved monitoring campaign led by Robin Corbet (40089 – 93076 PI:CORBET) began with the aim of studying these new pulsars. During the past 11 years, this campaign has intensified, resulting in our current state in AO12 where two overlapping positions covering the Bar region are monitored weekly for a total of 15 ks each. Figure 4.1 shows the pulsars that are currently monitored. These two pointing positions cover 93% of the SMC Be/X-ray binaries, with the majority of the sources falling within the inner 1° of the *RXTE* field of view (FoV). However, there are a number of pulsars that fall further out in the lower response regions. Although these pulsars are monitored, only extremely bright outbursts are expected to be seen due to their location within the collimator. A full description of the on-going SMC monitoring campaign and the data processing can be found in Laycock et al. (2005); Galache et al. (2008).

During the AO11 observing period, the *RXTE* SMC monitoring program was focused on the population of Be/X-ray binaries in the Northern SMC. After approximately 6 months of spare detections, it was decided to trial another location. On

12th July 2006 the previously monitored Position D in the South-Western corner was observed. Two pulsars were detected, SXP15.3 and SXP18.3. It was thus decided to move permanently to this location. On 30th August 2006 SXP18.3 was again detected. The source was seen continuously for the following 36 weeks. This is the longest Type II outburst ever seen from a HMXB in the SMC. During the outburst, SXP18.3 was located from serendipitous *XMM-Newton* observations. The identification of the optical counterpart has allowed SXP18.3 to be classified as a Be/X-ray binary. This chapter will report on the analysis of the optical and weekly *RXTE* X-ray data that span the last 10 years. The extreme length of this outburst has, for the first, time enabled an extensive study of the pulse timing of an SMC Be/X-ray binary to be performed. Constraints on the orbital parameters are derived from detailed timing analysis of the detected pulse period. An orbital period of 17.79 d is proposed from the analysis of the OGLE-III light curve, placing SXP18.3 on the boundary of known sources in the Corbet diagram.

4.1.1 SXP18.3 = XTE J0055-727 = XMMU J004911.4-724939

SXP18.3 was discovered in 2003 during routine *RXTE* PCA observations of the SMC (Corbet at al. 2003). They reported detecting pulsations with a period of $18.37 \pm 0.1s$. *RXTE* slew observations were able to narrow the position down to an ellipse with R.A. $= 13.84^\circ \pm 0.1$ and Dec. $= 72.70^\circ \pm 0.06$, but no firm identification of an optical counterpart was possible. Five detections of SXP18.3 were made in 2004. Corbet at al. (2004) noticed that these detections appeared to be occurring on a 34.8 d period and proposed this as the orbital solution. From the full analysis of the X-ray light curve prior to the large outburst, Galache et al. (2008) refined this period to $17.37 \pm 0.01\,d$ (approximately half of the value proposed by Corbet at al. 2004). On 12-13 March 2007 SXP18.3 was identified serendipitously through a 39 ks *XMM-Newton* observation of the emission nebula N19 in the SMC (Eger & Haberl 2008; Haberl et al. 2008a). They reported the presence of a bright X-ray

transient source showing pulsations at $18.3814 \pm 0.0001s$, at R.A. = 00:49:11.4, Dec. = -72:49:39 with a positional uncertainty of $1.18''$. The detection of these pulsations confirms the identification as being SXP18.3 and enabled the optical counterpart to be identified.

4.2 Observations and Data Analysis

4.2.1 Optical Observations

The optical counterpart is clearly identified by the *XMM-Newton* position (Eger & Haberl 2008), as a V=16 mag star (Zaritsky et al. 2002). Figure 4.2 shows the location of the optical counterpart. The source is close ($83''$) to SXP74.4 (also shown). This counterpart is present in a number of optical catalogues of the SMC. These data are summarised in Table 4.1, with the positional offset from the *XMM-Newton* position also quoted. The optical magnitudes, both in the visual range and the infrared, are typical of the many Be star counterparts that are associated with the other Be/X-ray binaries in the SMC (Coe et al. 2005; Schurch et al. 2007).

To compare the Magellanic Cloud Photometric Survey (MCPS) photometry (Table 4.1) with standard stellar models (Kurucz 1979), the data were first corrected for the standard reddening to the SMC of E(B-V)=0.09 (Schwering & Israel 1997). The dereddened MCPS colour (B-V)=-0.04 is typical of the Be star counterparts found in the SMC (McBride et al. 2008; Shtykovskiy & Gilfanov 2005). This colour suggests an optical counterpart in the range $B0 - B2$. Figure 4.3 shows the dereddened MCPS U,B, and V fluxes plotted over possible Kurucz stellar atmosphere models. The U and B fluxes suggest that the counterpart is in fact B2V, whilst the V flux indicates that there is a red excess typical of a circumstellar disk. This classification will need verification from future detailed spectrographic measurements. However, in light of this fit, the proposal by Eger & Haberl (2008) that SXP18.3 is a Be/X-ray

Table 4.1: Optical counterpart matches. "Dist" refers to the offset of the object from the *XMM-Newton* position.

Catalogue	Reference ID	Dist ($''$)	Date (MJD)	U	B	V	I
MCPS[1]	1933826	0.11	-	15.22 ± 0.03	16.01 ± 0.02	15.96 ± 0.03	15.89 ± 0.04
MACHO[2]	208.15911.13	1.31	$48855 - 51527$	-	-	16.0-15.2	16.0-15.4
Catalogue	Reference ID	Dist ($''$)	Date (MJD)	I	J	H	K_s
OGLE-II[3]	smc_sc5 65500	0.45	$50466 - 51871$	16.0-15.2	-	-	-
OGLE-III[4]	SMC101.8 19552	0.45	$52086 - 54487$	15.9-14.8	-	-	-
2MASS[5]	00491147-7249375	0.43	51034	-	15.9 ± 0.1	> 15.119	15.6 ± 0.2
SIRIUS[6,7]	00491143-7249375	0.52	52517	-	16.05 ± 0.02	16.03 ± 0.03	16.13 ± 0.05

[1]Zaritsky et al. (2002), [2]Alcock et al. (1999), [3]Udalski, Kubiak & Szymański (1997); Szymański (2005), [4] Private communication, [5]Skrutskie et al. (2006), [6]Kato et al. (2007), [7]Simultaneous 3-COLOR InfraRed Imager for Unbiased Survey.

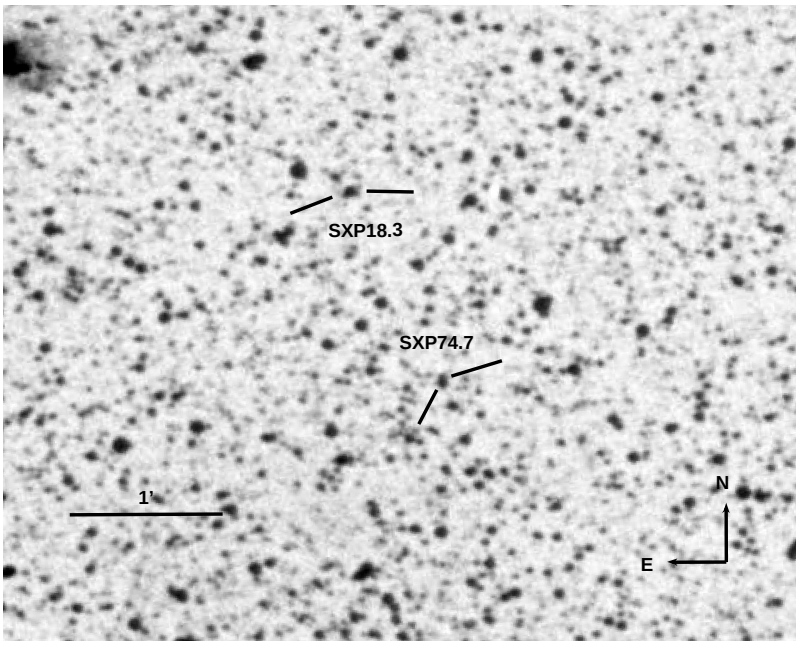

Figure 4.2: Finding chart showing the position of SXP18.3 and the nearby source SXP74.7, (ESO R band image).

binary is strongly supported.

4.2.1.1 Optical light curves

From the combined OGLE-II and III light curves, the instrumental massive compact halo object (MACHO) magnitudes were scaled, so that the continua of both the OGLE-II and MACHO data align. Shifts of +24.81 and +24.55 magnitudes were applied to the blue and red MACHO data respectively. The bottom panel of Figure 4.4 shows the combined light curve from August 1992 to April 2008 (only the overlapping MACHO data are shown). The full MACHO red and blue light curves are shown in Figure 4.5. As is clearly seen, there have been a number of large distinct optical outbursts. The first two lasted for $500 - 600$ d each, and later one giant outburst started around MJD 52800 that lasted for around 1500 d. After each outburst the optical flux has always returned to an approximately steady base value of $\sim 16.0 - 15.9$ mag.

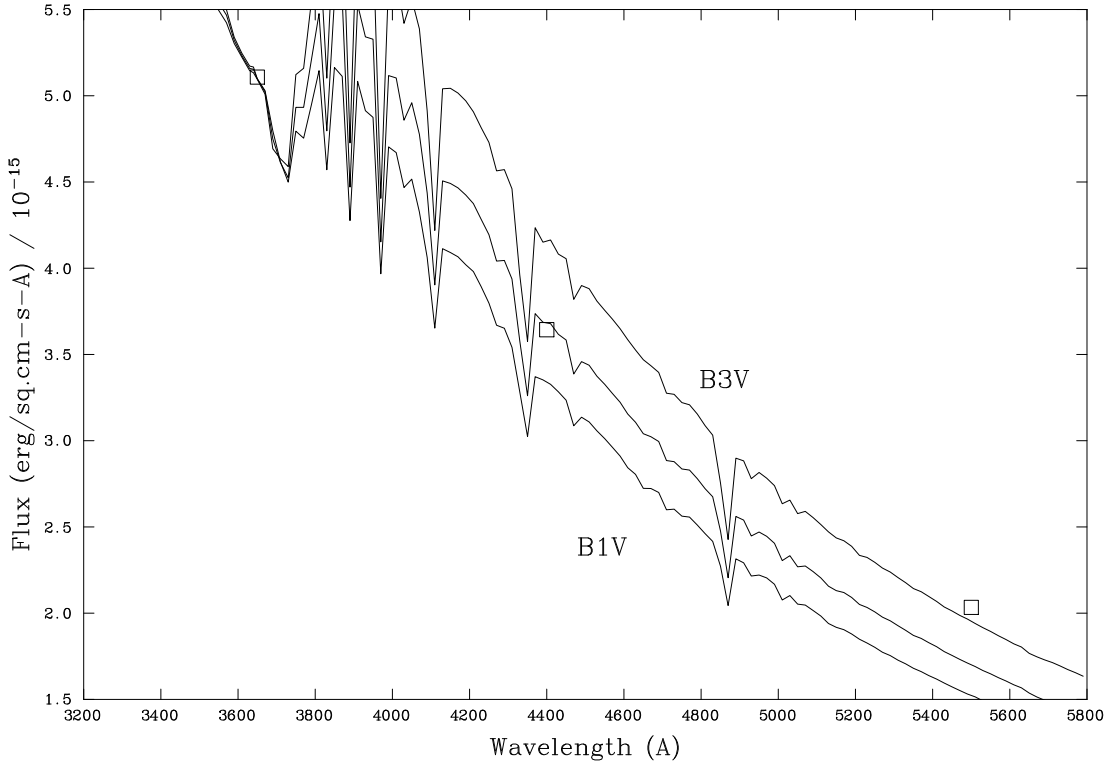

Figure 4.3: Comparison of U,B, and V MCPS fluxes, dereddened by E(B-V)=0.09, with Kurucz stellar atmosphere models.

The simultaneous red and blue MACHO data allows the colour changes throughout the first two optical outbursts to be examined. It is clear that as each of the outbursts proceeds, the source slowly reddens. After the peak of the outburst is reached the colour returns to its baseline configuration. It is worth noting that the colour change is asymmetric. Similar behaviour is also observed in SXP6.85 McGowan et al. (2008). As was suggested in McGowan et al. (2008), the colour variation likely indicates changes in the structure of the circumstellar disk. Either the formation of the disk is increasing the optical brightness by the addition of red light, or the large disk is now masking out part of the surface of the bluer Be star. The latter effect would be dependent on the inclination angle of the system.

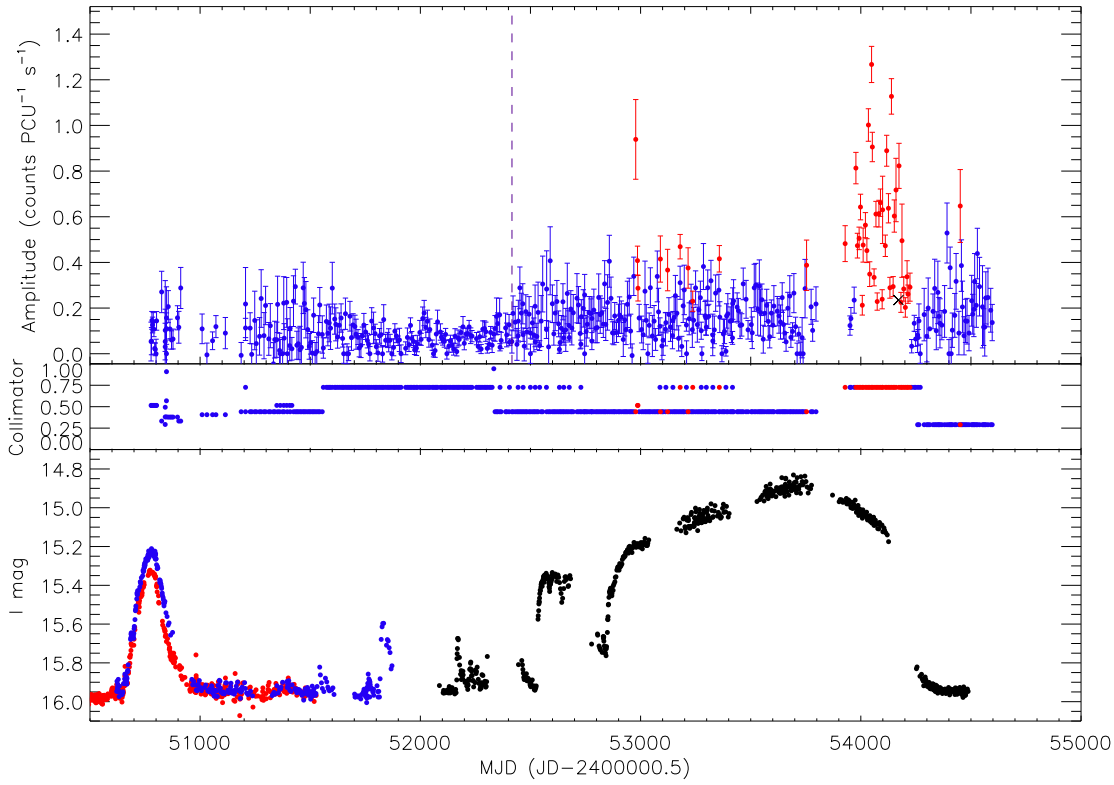

Figure 4.4: SXP18.3 X-ray and optical light curves. Panels are PCA pulsed flux light curve in the energy range $3-10$keV (top), PCA collimator response (middle), combined MACHO (red), OGLE-II (blue) and III (black) light curves (bottom). The black cross represents the *XMM-Newton* detection (MJD 54171) and the dashed line indicates a non detection by *Chandra* ACIS-I, observation 2944 (MJD 52416). The red points in the *RXTE* light curve and collimator response represent detections of the source above a 99% local significance level.

4.2.1.2 Orbital Period

The large optical outbursts seen in the light curve are too bright and occur on vastly longer time scales than would be expected for this source if they were due to the orbital period ($\sim 20-100$ days from the Corbet diagram). These are attributed instead to changes in the size of the circumstellar disk. However, a search for possible binary modulations was carried out on the detrended data. Removing the large variations in magnitude without introducing artificial variations and features proved to be extremely difficult. Periods when the light curve is changing very fast are impossible to detrend meaningfully. Thus, the search was restricted to the last

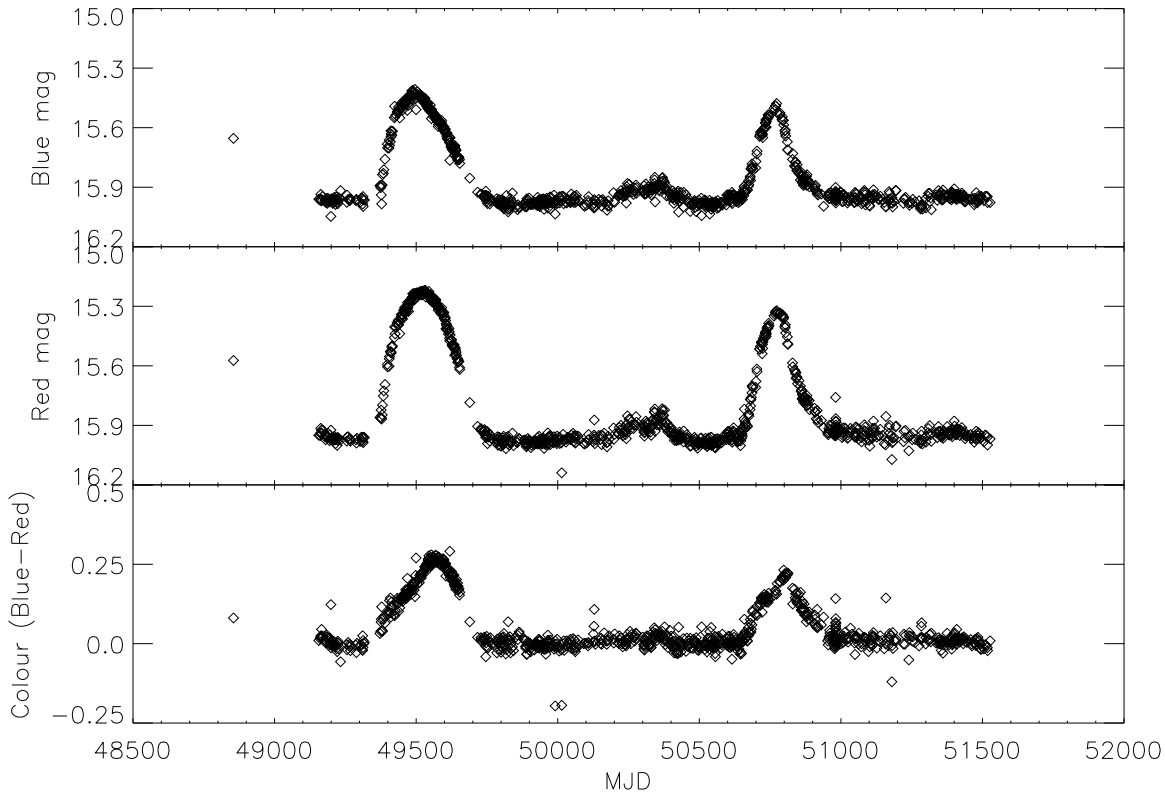

Figure 4.5: MACHO red and blue light curves and colour variations.

4 years of OGLE-III data (MJD 53164.9 to the 54487.6), where it was possible to detrend the data by subtracting linear fits. A single linear fit was used for the first three years. The fourth year of data was first split in half, and then separate linear fits were used for each half. The resultant light curve was searched, both as a whole and as individual years, for periodicities in the range $1 - 100$ d using Lomb-Scargle periodograms (Lomb 1976).

The results of the temporal analysis are shown in Figure 4.6. The statistical analysis of the Lomb-Scargle periodogram follows the perscription of Horne & Baliunas (1986). In this prescription, the probability that a peak above a certain power appears from the analysis of pure noise, follows an exponential distribution, known as the false alarm probability (FAP). The higher the peak the smaller the FAP. The significance of a given peak is simply given by subtracting the FAP from one. This distribution was used to calculate the 99% signifance level for the data. It should be noted through that if there are multiple periods in the data then the distrubu-

tion no longer holds. The error on the detected frequency is given by Equation 14 in Horne & Baliunas (1986). A clear peak well above the 99% significance level occurs at 17.79 ± 0.01d in the first two years of the detrended OGLE-III data, in agreement with Udalski & Coe (2008). This periodicity then disappears completely during the third year, only to reappear, at a much lower significance in the 4th year at a slightly different period. The lobes in the combined year 1 and 2 data are due to the 17.79 d period beating with the one year sampling. The very short period peaks (around 1 d) are due to the one day sampling of the data. The high peaks at 5.87 d in the year 2 data and the peak at 4.40 d in the year 3 data are also noted. These peaks are not the third and fourth harmonics (respectively) of the higher period peak at 17.79 d. As a consequence of its strength the 5.87 d peak appears in the combined data, but its structure has become very double-peaked. No periodic variations were found in the MACHO or OGLE-II data. The 17.79 d optical period, which is interpreted as the orbital period, places this HMXB well within the limits of the proposed Be/X-ray binaries on the Corbet diagram (Coe et al. 2008a; Corbet et al. 1999). The ephemeris of the orbital period is defined by the date of periastron passage prior to the start of the data used in the analysis. The ephemeris of SXP18.3 is MJD $(53178.3 \pm 0.8) + n(17.79 \pm 0.01)$, a phase folded light curve is shown later in Figure 4.9.

4.2.2 *RXTE* Observations

During 2006, a trial observation at Position 5 (12.5°, -73.1°) revealed two pulsars to be in outburst, SXP18.3 and SXP15.3. From 3 August 2006 (MJD 53950) till 19 June 2007, this position was monitored weekly. After three weeks of monitoring on 30 August 2006 (MJD 53977) SXP18.3 switched back on. The source remained in outburst, and was continually detected, every week for the next 36 weeks finally disappearing on 3 May 2007 (MJD 54223). This was the longest uninterrupted outburst ever seen in the SMC. Figure 4.4 shows the full 10 years of *RXTE* monitoring;

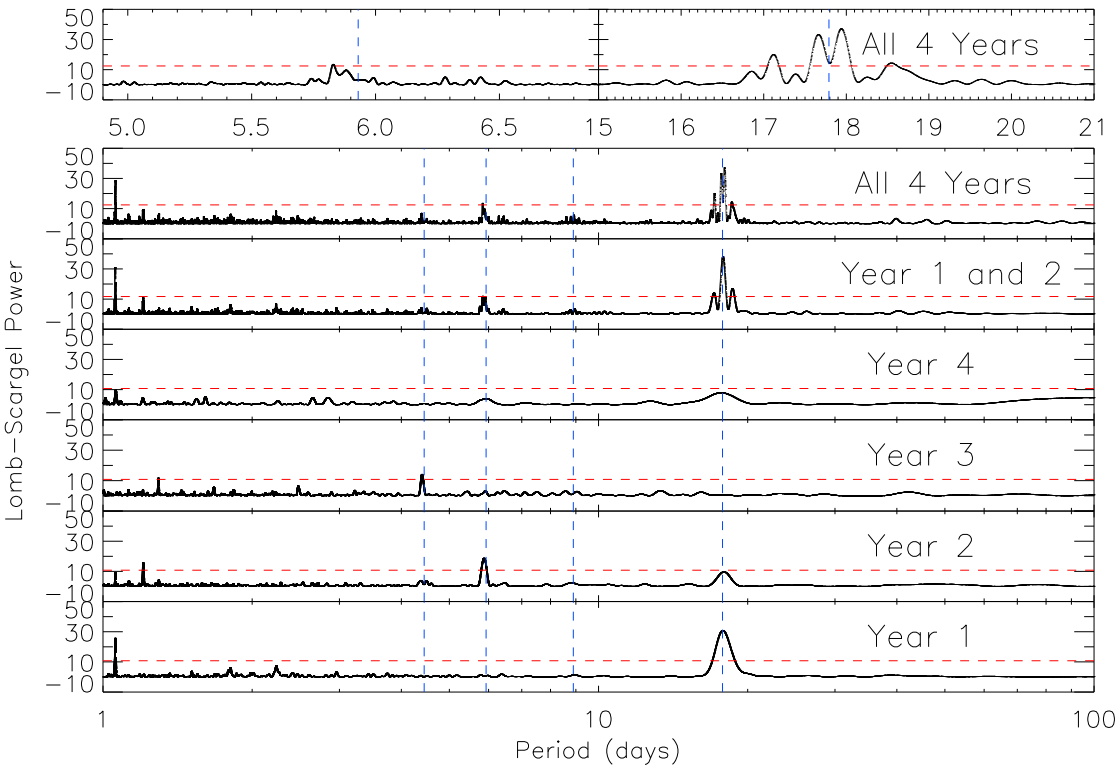

Figure 4.6: Power spectra of the 4 year detrended OGLE-III light curve. The top panel shows two sections of the 4 year search. The dotted horizontal red lines indicate the 99% significance level and the dotted vertical blue line indicates the 17.79 d period and its harmonics at 8.90, 5.93 and 4.45 days.

the collimator response represents the position of the source within the field of view (FoV) of RXTE (1 being at the centre and 0 the edge). The red points represent where 18.3 s pulsations above a 99% local significance level have been detected in the power spectra of *RXTE* light curves. The blue points represent no detection. For specific details of the data processing see Galache et al. (2008). As can be seen, prior to the massive outburst the source was only seen in outburst on seven occasions. These outbursts do not correlate to any particularly interesting features on the optical light curve.

The range of luminosities for this outburst was estimated using PIMMS v3.9f[1] and assuming a distance to the SMC of 60 kpc. The spectral fit found from the *XMM-Newton* observations ($\Gamma = 0.65$, $N_H = 2 \times 10^{22} \mathrm{cm}^{-2}$, Eger & Haberl (2008))

[1](http://heasarc.gsfc.nasa.gov/Tools/w3pimms.html)

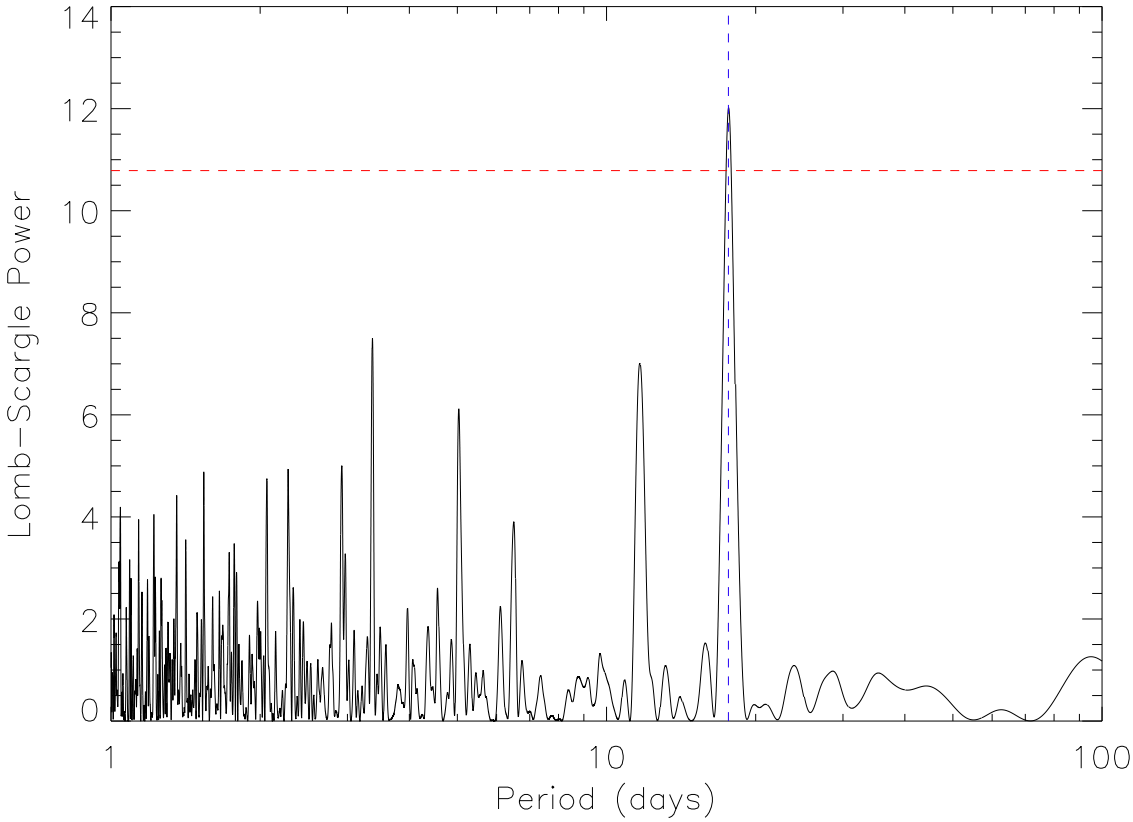

Figure 4.7: Power spectrum of the detected pulse periods of SXP18.3 during the outburst. The dotted horizontal red lines indicate the 99% significance level and the dotted vertical blue line indicates the 17.62 d period.

Table 4.2: Orbital parameters

Parameter	Orbital Solution
$P_{orbital}$ (d)	17.79_{fixed}
$a_x \sin i$ (light-s)	75 ± 3
ω (^{o})	15 ± 6
e	0.43 ± 0.03
$\tau_{periastron}$ (MJD)	53997.6 ± 0.2
P_{spin} (s)	18.3854 ± 0.0004
$\dot{P}_{spin}$ (s/yr)	$[-1.79 \pm 0.11] \times 10^{-2}$
χ^2_ν	8.22

was used. It was also assumed that the *XMM-Newton* measured pulse fraction of $21 \pm 3\%$ remained constant for the entire observation. The *RXTE* luminosity range throughout the outburst is $L_{0.2-10} = (0.51 - 3.2) \times 10^{37}\,\mathrm{erg\,s^{-1}}$. This value is consistent with the *XMM-Newton* value $L_{0.5-10} = 5.5 \times 10^{36}\,\mathrm{erg\,s^{-1}}$. SXP18.3 was observed by *RXTE* two days after *XMM-Newton* (Figure 4.4) with a luminosity of $L_{0.2-10} = 2.1 \times 10^{37}\,\mathrm{erg\,s^{-1}}$.

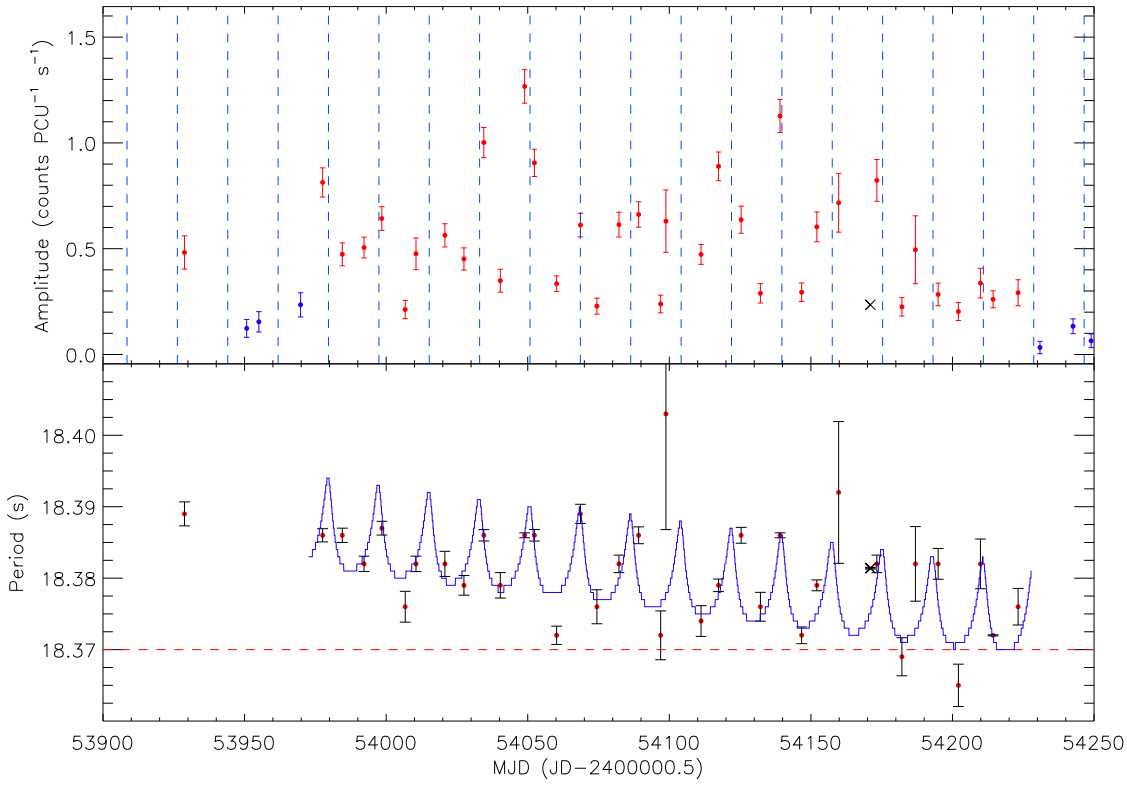

Figure 4.8: SXP18.3 X-ray outburst. Top panel shows the *RXTE* amplitude (red points are above 99% significance) with the vertical dotted lines showing periastron passage as predicted by the optical light curve. The bottom panels shows the detected *RXTE* pulse periods with the orbital solution over plotted. The black crosses are the *XMM-Newton* detected pulse period (orbital phase 0.80) and flux converted to *RXTE* with PIMMS v3.9f.

4.2.2.1 Orbital fitting

Figure 4.8 shows in detail the detected luminosities and pulse periods throughout the 9 month long X-ray outburst. It is evident from the general trend in the detected pulse period (bottom panel) that SXP18.3 was spinning up during the outburst. The neutron star would have had to be continually emitting at a luminosity of $L_{3-10} = 2.67 \times 10^{36}\,\mathrm{erg\,s^{-1}}$(Ghosh & Lamb 1979) to produce the required spin up. The shorter variations occurring throughout the outburst suggest that the detected spin period is being orbitally modulated. The data was detrended and a Lomb-Scargle period search performed, revealing a peak in the power spectrum above the 99% significance level at $17.62 \pm 0.1\,d$ (Figure 4.7). This period would seem to

be consistent to that found in the optical data. Thus, a full orbital solution was fitted to the pulse period values. The orbital fitting is performed by a chi-squared minimisation method (Wilson et al. 1997). The orbital period was fixed at the value determined from the optical analysis because the determination is far more precise than that achieved from the X-ray data. Figure 4.8 shows the orbital fit to the data with the orbital parameters shown in Table 4.2. It is worth noting that the time of periastron passage is consistent with that given by the independent analysis of the optical data. The orbital parameters are typical of those seen in other accreting Be/X-ray binaries (Okazaki & Negueruela 2001); most Be systems have $P_{orbital} \sim 20 - 100\,\mathrm{d}$ with eccentricities in the range $0.3 - 0.5$ (Bildsten et al. 1997).

The first two years of the detrended OGLE-III light curve and the *RXTE* amplitude measurements were folded, so that the orbital solution could be evaluated. The *RXTE* data are folded in 10 bins, and the OGLE-III data have been folded in 20 bins using the orbital period and ephemeris from Table 4.2. Both the X-ray and optical folded light curves (bottom and top respectively of Figure 4.9) have fairly sinusoidal profiles and are well matched with the peaks coinciding. This would suggest that 17.79 d is the orbital period. There is also another probable peak in the optical data at phase 0.7 with some hint of its presence in the X-ray fold.

4.2.2.2 *RXTE* spectra and pulse profiles

Because *RXTE* has such a large field of view, it constantly covers many of the SMC Be/X-ray binaries during the monitoring observations. This makes it extremely difficult to resolve one source from another. Due to the unusually large outburst from SXP18.3 there were several observations where the analysis revealed that it was the only known source to be in outburst. Further restrictions were placed on which observations were suitable for analysis by examining only those observations where the source was detected above the 99% global significance level (for details

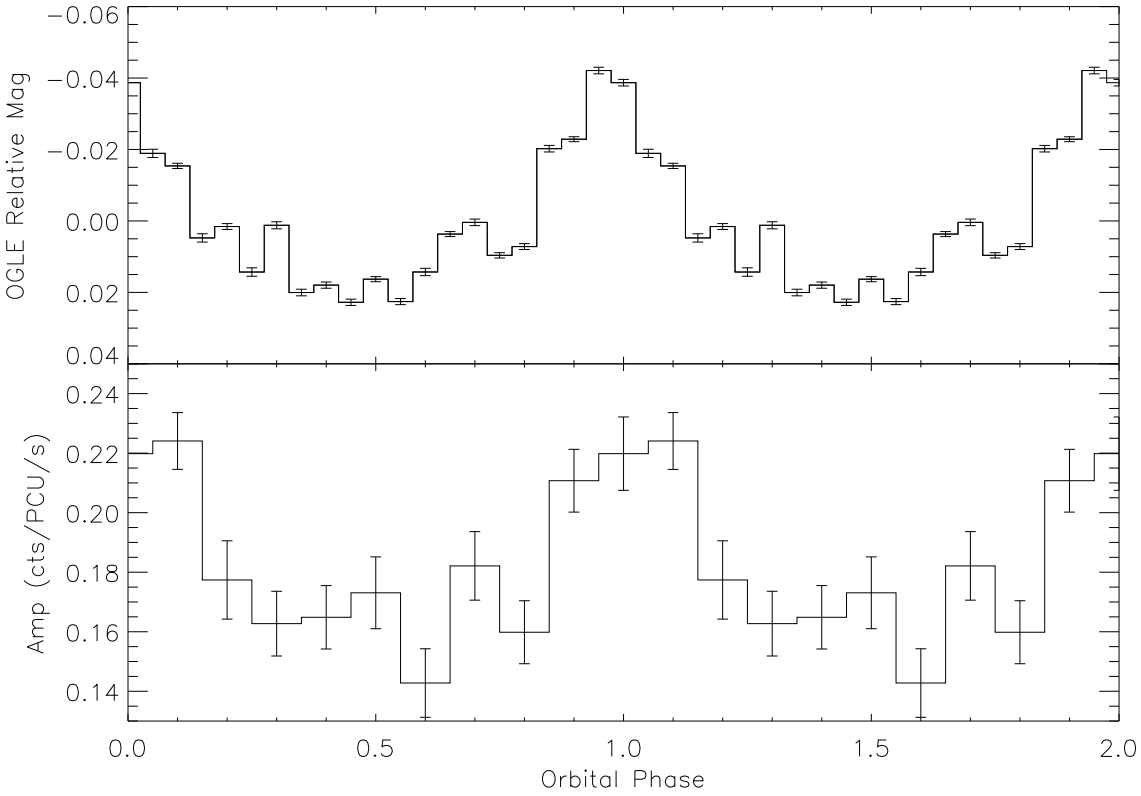

Figure 4.9: *RXTE* (bottom) and OGLE (top) folded light curves.

see Galache et al. 2008). The spectra of 18 out of the 35 observations were examined in the $3 - 10$keV range. Although SXP18.3's outburst was very long, it was never particularly bright, hence the spectra have a low signal to noise ratio. Two absorbed power-law spectral models were fitted to each spectrum; the absorption was both fixed to that of the SMC and allowed to vary. It was not possible to produce any meaningful fits to the spectra. This is most likely due to the unknown contamination from background AGN, and X-ray binaries emitting at a very low luminosity level.

In addition to analysing the spectra, the pulse profiles for each of these observations were examined. The ephemeris and orbital period from Table 4.2 were used to calculate the orbital phase for each observation (shown on each pulse profile), and the observations were then arranged to appear in order of their orbital phase. Duplicated orbital phases were removed (Figure 4.10). In each case an arbitrary pulse phase shift was applied to align the main peak of the profile with phase 0. The majority of the pulse profiles present a very similar sinusoidal shape with a very steep rise

and gradual fall, in good general agreement with those presented in Haberl et al. (2008a). The pulse profiles around periastron passage appear to be fairly stable with small changes to the shape of the fall off. There is some emission that is associated with pulse phase 0.5 with a subsequent steep decline to minimum emission occurring at pulse phase $0.7 - 0.8$. This emission is possibly due to either the X-ray beam fanning out and becoming more conical in shape, allowing emission from the second pole to be seen, or to the accretion stream being preferential to one pole and only occasionally splitting to both poles. When the neutron star is around apastron (orbital phase $0.3 - 0.7$) the pulse profiles become rather more complicated with several additional peaks emerging. The pulse profiles enabled the pulsed fraction to be measured, and it was found to be in the range $22 \pm 10\%$. This is consistent with the value found from the *XMM-Newton* observations.

4.2.3 *Chandra* observation

Chandra observation 2944 (Field 7) was performed on 22 May 2002. The location of SXP18.3 is well within the ACIS-I field of view. The purple line on Figure 4.4 (MJD 52416) shows when the observation was made in relation to the *RXTE* observations. This observation took place at an orbital phase of 0.85. A visual check of the field shows that the source was clearly not detected.

4.3 Discussion

The optical and X-ray data suggest that SXP18.3 is a HMXB transient. From analysis of the MCPS data a tentative classification of the counterpart as B2V has been made, supporting the proposal by Eger & Haberl (2008) that SXP18.3 is a Be/X-ray binary. The optical light curve of SXP18.3 shows periods of extreme brightening occurring over very long time scales. These dramatic outbursts are seen

to occur in many other Be/X-ray binary systems (e.g. SXP46.6, SXP6.85 McGowan et al. 2008) and are most likely due to massive size variations in the circumstellar disk surrounding the Be star. In particular SXP6.85 (McGowan et al. 2008) exhibits similar recurrent optical outbursts of comparable duration and brightness. Complex computer simulations are required to understand the exact nature of these optical outbursts and how they produce the colour variations. The 17.79 d period found in the optical data is interpreted as the orbital period of the binary system. If it is assumed that the equatorial plane of the Be star is approximately coincident with that of the neutron star's orbit, then, as periastron is approached, some distortion of the circumstellar disk is seen due to the larger gravitational attraction between the two objects (Okazaki & Negueruela 2001). These distortions temporarily increase both the size and luminosity of the disk. Such orbital modulation is seen in many Be/X-ray binary systems (Coe et al. 2008a).

It is interesting that the orbital modulation is not always present, only being significantly detected when the I magnitude of the Be star is brighter than 15.2 mag. This suggests that the disk has to be sufficiently large and hence close to the neutron star's orbit for any significant perturbations. However, it is noted that during the massive X-ray outburst there is no modulation in the optical data. This is possibly due to the extreme nature of this outburst. Here it is possible that a situation has developed where the disk has grown to such a size that it is encompassing the entire orbit of the neutron star, allowing continuous accretion. Assuming typical values for the mass of the Be and neutron star and the orbital period found, a semi-major axis of $\sim 85 R_{\odot}$ would be expected. From Hα equivalent width measurements, Grundstrom et al. (2007) have estimated the disk radius in the Be/X-ray binary A0535+26 to reach a maximum size of $90 R_{\odot}$. It is not unreasonable to envisage a disk growing to this size and producing such a massive outburst. If this situation is correct, then the perturbation suffered by the disk may increase the local density of material rather than extend the physical size of the disk, resulting in the orbital signature disappearing. One problem with this interpretation is explaining the orbital signature

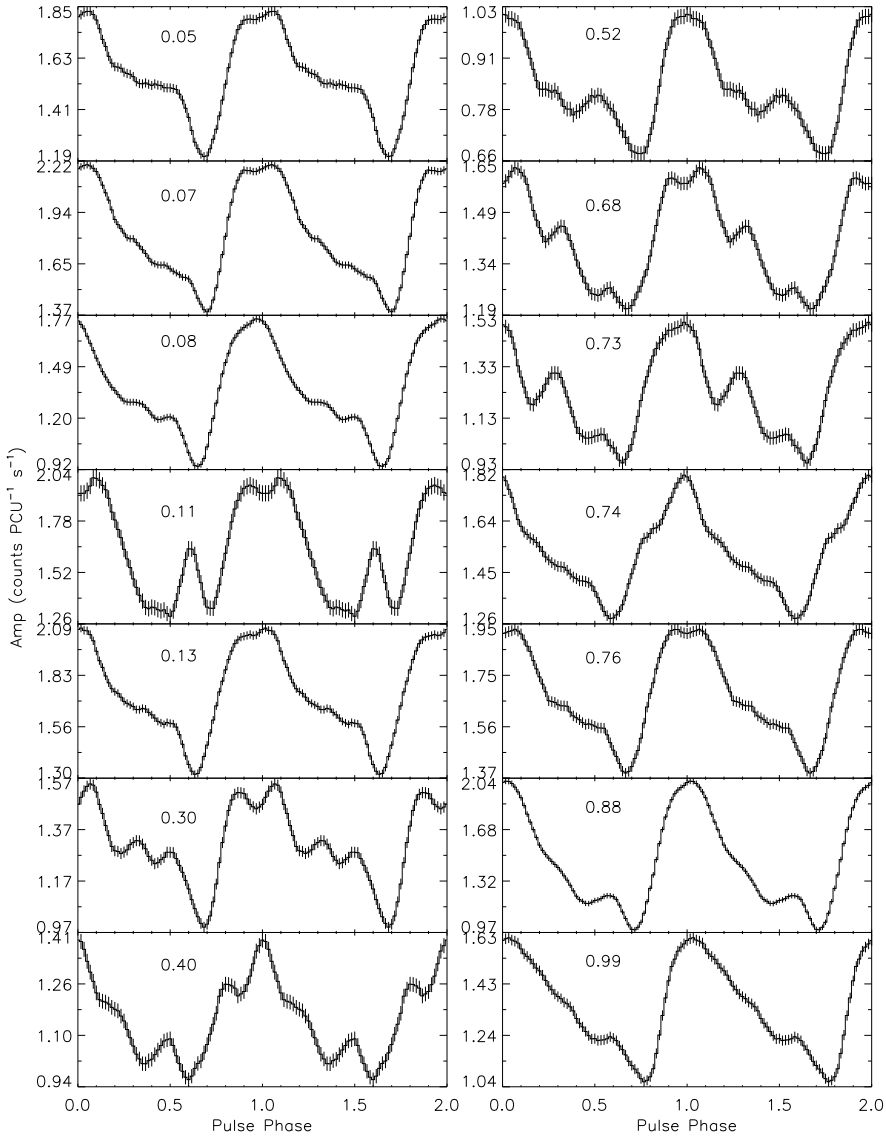

Figure 4.10: Folded pulse profiles of SXP18.3, an arbitrary pulse phase shift was applied to align the peaks since they cannot be phase locked between observations. Arranged in order of orbital phase (given in the label) starting at the top left.

seen in the first two years of detrended OGLE-III data. If the optical outburst is attributed to the disk growing in size then, during these two years the disk is larger or denser than when the X-ray outburst was observed. If the model proposed is correct then the neutron star would have been within the disk for this entire period and no optical signature would be seen, but there would be the possibility of X-ray outbursts. Unfortunately, for the majority of this period SXP18.3 was outside the central 1° of *RXTE's* FoV, thus having a much lower detection sensitivity. SXP18.3 may have dropped below this threshold, and hence it is not clear that SXP18.3 was truly off. It is interesting to note that prior to the massive X-ray outburst SXP18.3 was only detected on a handful of occasions, all during periods when I<15.2mag.

A full orbital solution was fitted to the variations in the observed spin period. The foremost problem with this fit is that the data sampling is too infrequent. As a result, variations in the accretion rate will produce a variable accretion torque. These variations not accounted for, due to the assumption of a constant $\dot{P}_{spin}$, will produce pulse period measurements that deviate from the orbital solution. Even though the data spans many orbital cycles during the outburst, the fact that there are only two or three data points per orbital cycle is simply insufficient to constrain the orbital parameters properly. However, the close match between the X-ray and optical folded light curves clearly suggests that 17.79 d is the true orbital period.

SXP18.3 lies in the bottom left corner in the low orbital and spin period regime of the Corbet diagram. It is right on the edge of the distribution of Be/X-ray binaries. If this source was to move slightly further to the left (shorter orbital period) it would start to fall into the Roche lobe overflow group. When the types of outbursts exhibited by SXP18.3 are examined, it is clear that there are a number of short lived typical Type I outbursts just above our detection threshold, and then the massive 36 week Type II outburst. Outbursts of this length are extremely rare for Be/X-ray binaries, since for the duration of this period the neutron star must be accreting constantly. SAX J2103.5+4545 is a Be/X-ray binary where similar X-ray behaviour is seen (Baykal et al. 2002). It is a pulsar with a long spin period of ∼359 s but a

very short orbital period of 12.7 d (comparable with SXP18.3). This would place it at the top left of the distribution of Be/X-ray binaries in the Corbet diagram. SAX J2103.5+4545 has exhibited several bright X-ray phases lasting hundreds of days, with luminosities $\sim 10^{36}\,\mathrm{erg\,s^{-1}}$. It is only during these bright phases that the orbital period has been detected. Blay et al. (2004) suggest that this could be due to the density/size of the circumstellar disk being large enough to temporarily fill its Roche lobe during periastron, and hence allow accretion to take place. It could be that the moderately bright outburst seen in SXP18.3 is due to a very similar mechanism to that which produces the outbursts seen in SAX J2103.5+4545. It could be imagined that these short orbital period systems possibly flip between states of Roche lobe overflow and quiescence. Monitoring the state of the Hα line before, during and after an outburst would help shed some light on the accretion mechanisms at work in these systems. Be/X-ray binary systems like these may well be indicative of a lower limit for Be/X-ray binaries on the Corbet diagram.

4.4 Conclusions

In light of the optical and X-ray data, SXP18.3 becomes the newest member of the group of transient Be/X-ray binaries in the SMC. The proposed orbital model requires intensive observations and detailed computer simulations to fully reveal the orbital parameters and help explain the possible presence of the second optical peak. The limits of the Corbet diagram are beginning to be explored. Sources like SXP18.3 are key to this study as they exhibit a mixture of behaviours.

Chapter 5

OGLE and *RXTE* Light curves

There are 56 known X-ray pulsars in the SMC. The study of these pulsars is done in two principal ways, either through the X-ray emission, the optical emission or both. The majority of these pulsars have well-identified optical counterparts from precise X-ray localisations. Only through the combined study of both their X-ray and optical activity will the most interesting features of these systems be revealed. McBride et al. (2008) have recently performed optical classification of all the pulsars with known counterparts in order to study the overall distribution of spectral counterparts. All but one of these (SMC X-1) has a Be star counterpart with a main sequence luminosity classification. The distribution of spectral classes is entirely consistent with that of the Milky Way Be/X-ray binaries. The classification of the counterpart as a Be star implies that at some point the star has shown emission in one or more of the Balmer lines, as discussed in Chapter 1. The strength of this emission is related to the size of the circumstellar disk around the Be star and these systems can appear highly variable over both short and long time scales. Not only does the cooler circumstellar disk give rise to the Balmer line emission, it also contributes heavily to the general continuum emission of the star. This contribution is most noticeable at infrared wavelengths due to the relatively cool disk temperature. As a result, the OGLE I band data is perfect for studying the changes that take

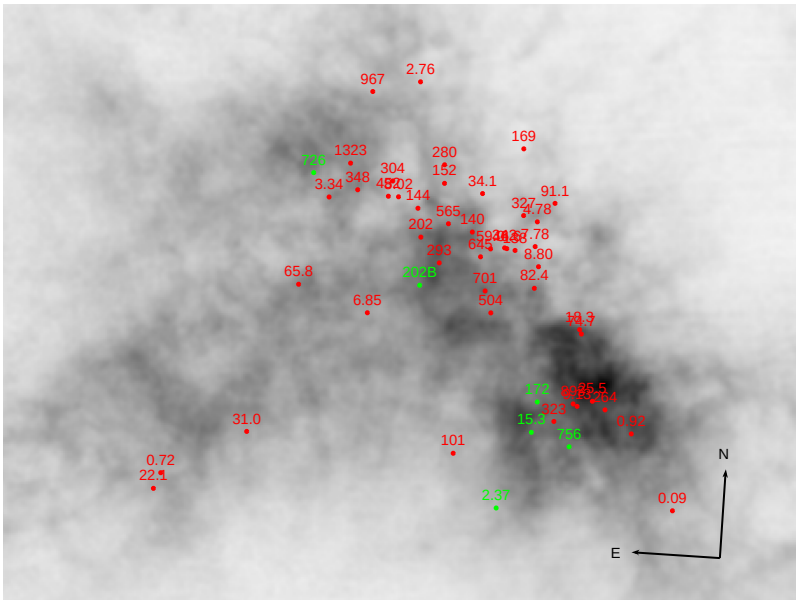

Figure 5.1: HI map of the SMC with the known sources marked (Stanimirovic et al. 1999). Plotted in green are the six pulsars discussed in this chapter.

Table 5.1: Optical counterpart identifications.

Name	R.A.	Dec.	MACHO	OGLE-II	OGLE-III
SXP2.37	00:54:34	-73:41:03	-	-	SMC107.5 25
SXP15.3	00:52:14	-73:19:19	212.16075.13	SMC-SC6-99923	SMC100.1 48026
SXP172	00:51:52	-73:10:35	212.16077.13	SMC-SC6-22749	SMC100.2 44100
SXP202B	00:59:29	-72:37:03	207.16541.15	SMC-SC8-139407	SMC105.3 29894
SXP726	01:05:55	-72:03:50	-	SMC-SC10-137851	SMC113.3 10946
SXP756	00:49:42	-73:23:16	212.15960.12	SMC-SC5-90506	SMC100.8 22903

place in Be stars' circumstellar disks. The OGLE data primarily comprise two data sets, OGLE-II and OGLE-III, together covering the range MJD 50600-present. The OGLE data are sampled daily, but, due to the positions of the OGLE telescope at the Las Campanas astronomical site in Chile, the SMC is only visible for approximately two thirds of the year. Hence the combined OGLE light curve (which will be referred to as the OGLE light curve) has large periodic gaps. The MACHO light curves have been used to supplement this study when optical data are required prior to the OGLE light curves. The MACHO observations provided continuous monitoring with approximately daily sampling during the period MJD 49150 – 51550.

The OGLE data are extremely well-matched to the X-ray monitoring of the SMC

with the *RXTE* space observatory. As was previously mentioned in Chapter 4, *RXTE* has been observing the SMC in one way or another since 1997. This has provided a unique data set of X-ray activity for a population of X-ray binary sources, all located at a similar distance. Timing analysis of the observations identifies both new and previously known pulsars. Identification of the previously unknown pulsars is tricky, due to the X-ray signals either having to be detected extremely strongly or regularly within the same pointing. Even after a pulsar is established as real, narrowing its position down to a small enough area to enable the identification of an optical counterpart is almost impossible. The FoV of *RXTE* is simply too large (2° FWZI diameter), and the SMC is too crowded. As was shown for SXP18.3 in Chapter 4, even with multiple follow-up observations using a variety of methods, the resultant error circle was not sufficient to identify an exact optical counterpart. However, the resultant long term light curves can be used to probe the outbursting nature of the SMC binaries revealing orbital periods and recurrence rates. Through comparisons of the *RXTE* and OGLE light curves, the observed X-ray outbursts can be put into context with the optical behaviours and often the suspected orbital periods can be confirmed. Sources like SXP756 (Coe & Edge 2004; Schmidtke et al. 2004) and SXP46.6 (McGowan et al. 2007) have shown outbursts that are often seen in both data sets. This chapter will present a thorough study of the X-ray and optical light curves of a number of SMC Be/X-ray binaries. Table 5.1 lists the sources studied and their optical identifications, their positions within the SMC are marked in Figure 5.1.

5.1 SXP2.37

SXP2.37, otherwise known as SMC X-2, was discovered in the SMC by SAS 3 observations in 1977 (Li et al. 1977). Early X-ray observations showed the source to be highly variable (Li & Clark 1977). Soon after the X-ray source was found, Murdin et al. (1979) revealed that the suspected optical counterpart was in fact

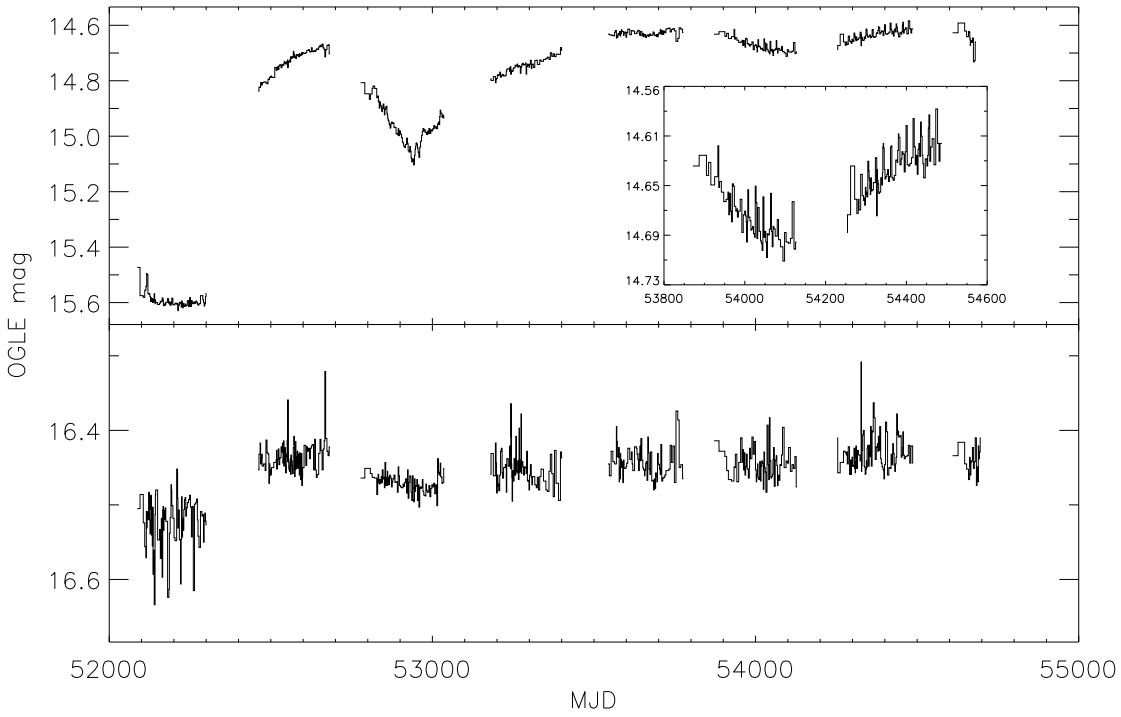

Figure 5.2: OGLE-III light curves for both the North (top) and South (bottom) candidates to SXP2.37. The insert in the top panel shows the 6th and 7th year of OGLE-III data.

a close North-South double; they classified the two stars as O (northern) and Be (southern). It has been impossible to identify clearly which of these two stars is the true counterpart due to the large X-ray error circle. 2.37 s pulsations were first discovered during a giant outburst from January to May 2000 (Corbet et al. 2001).

5.1.1 OGLE

The two possible counterparts are not present in either the MACHO or OGLE-II catalogues. Schmidtke, Cowley, & Udalski (2006) presented a thorough analysis of the first 5 years of OGLE-III data for both stars. They found no significant periodicities in either star and proposed the brighter more northern star to be the true counterpart due to the large variations in its light curve. McBride et al. (2008)

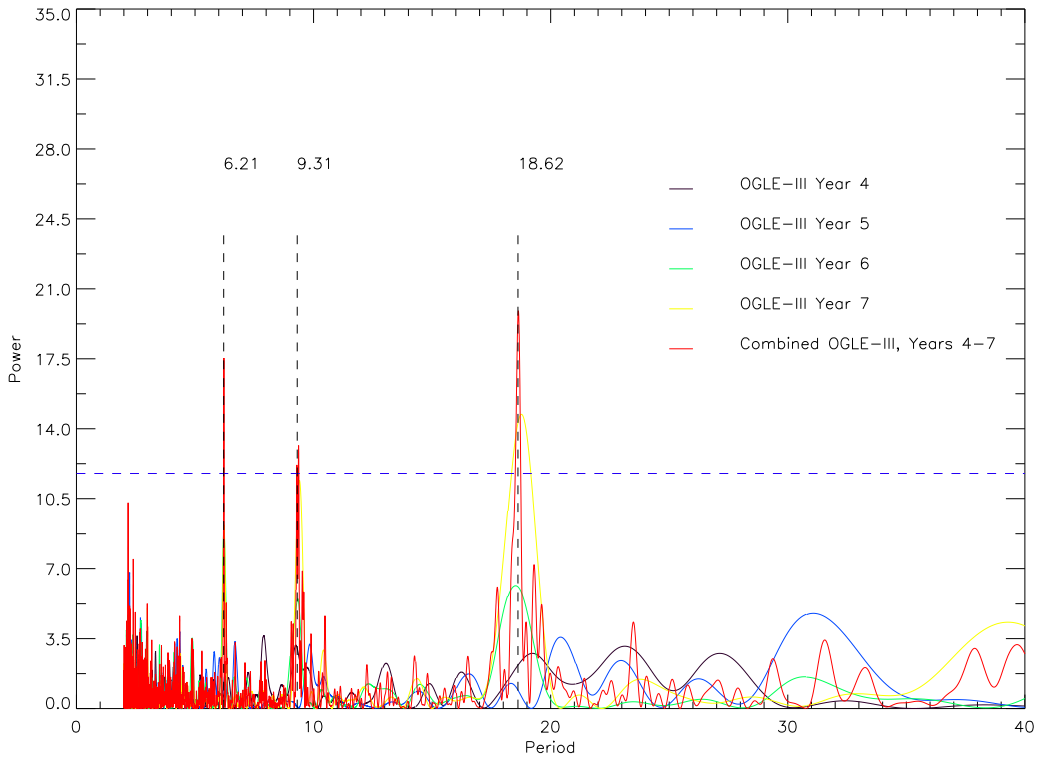

Figure 5.3: Periodogram of the OGLE-III data (4 years) for the northern counterpart. The coloured lines represent the individual years. The red line is the analysis of the entire 4 years of data. The detected periodicity at 18.62 d and its harmonics are marked. The horizontal blue line represents the 99% significance level.

classified the northern star as O9.5 III-V.

Two further years of OGLE-III data for both stars are now available providing a total coverage of 7 years. The total OGLE-III light curve for both the northern and southern objects is presented in Figure 5.2. It is clear to see that the northern object is highly variable varying by up to 1 mag. The insert in Figure 5.2 clearly shows that there is a periodicity in the 7th year of data. By comparison, the photometry of the southern star is fairly flat, with the variation in magnitude between the first and second year of data highly suggestive of contamination from the northern star.

In order to search for periodicities in this data, it is essential first to detrend the data. However, it was decided to exclude the first three years of data for the northern

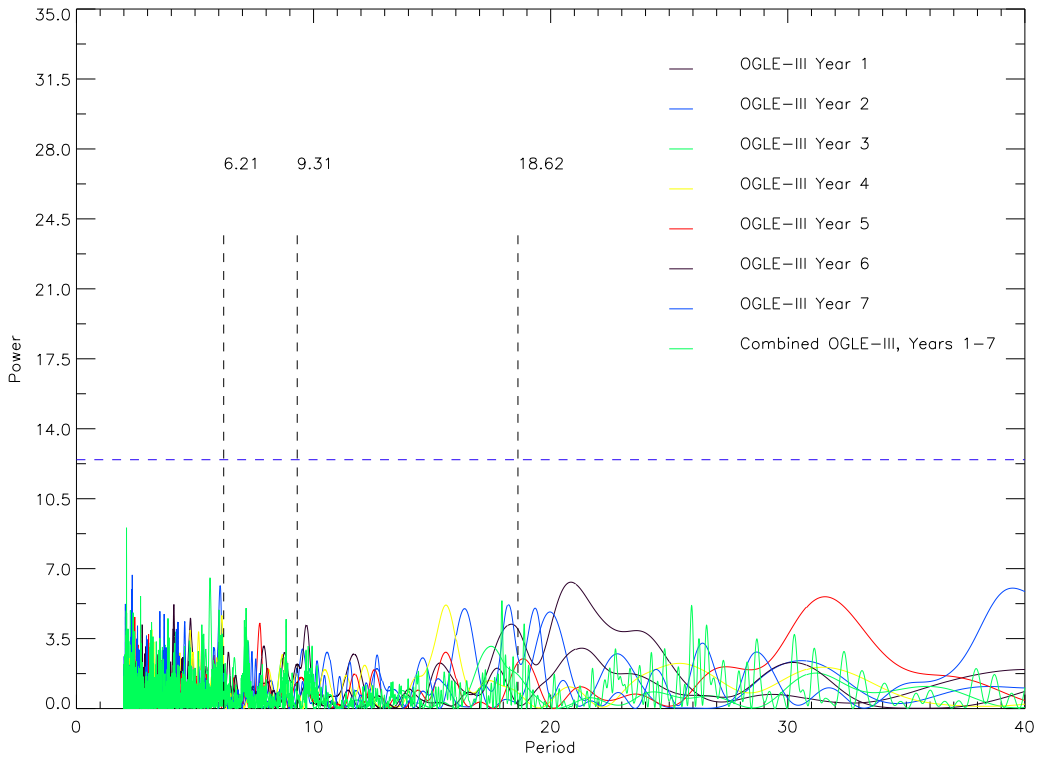

Figure 5.4: Periodogram of the OGLE-III data (7 years) for the southern counterpart. The detected periodicity in the northern star at 18.62 d and its harmonics are marked for reference. The horizontal blue line represents the 99% significance level.

star because the changes were too rapid to remove satisfactorily. The detrending was performed by fitting a straight line to each individual year of data. The two remaining light curves were then searched, both as a whole and in individual years, using Lomb-Scargle analysis. Figure 5.3 shows the analysis of the northern star. It is clear that in the 7th year of data a strong periodicity is present above the 99% significance level. The 2nd and 3rd harmonics are also identifiable, at a slightly lower level. In the analysis of the entire 4 years worth of data, the primary peak and both harmonics have increased in strength. The periodicity is at 18.62 ± 0.02 d with harmonics at 9.31 and 6.21 d.

The same analysis was performed on the light curve of the southern star. Figure 5.4 shows the Lomb-Scargle results. There is no periodicity seen in any of the individual 7 years of data, and none when the light curve is taken as a whole. This indicates

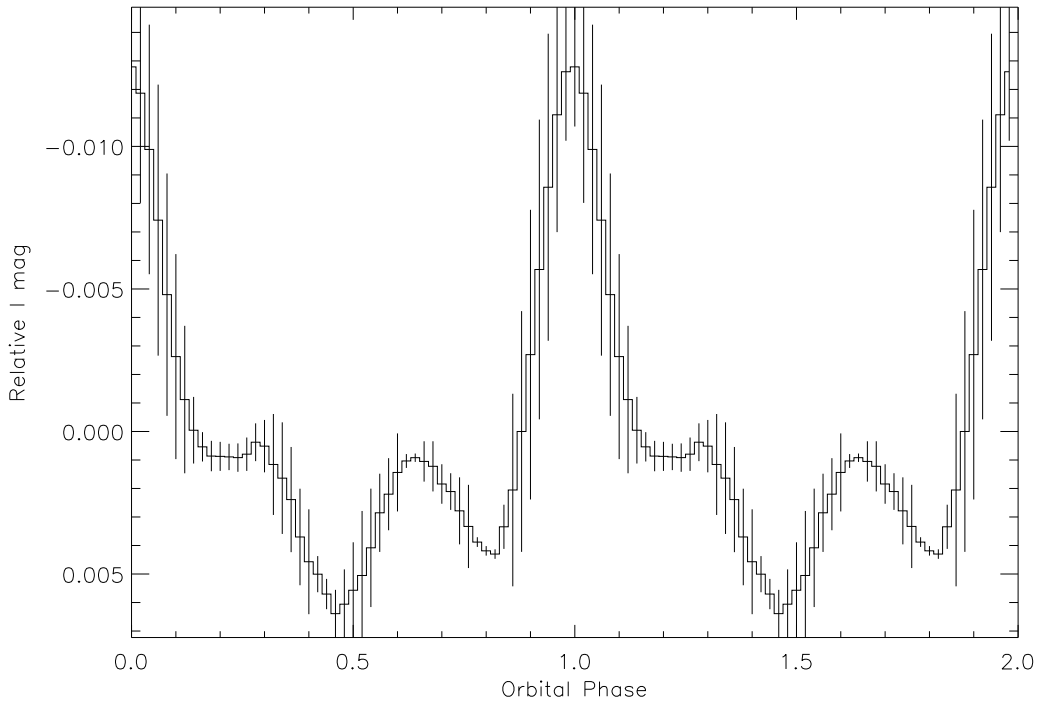

Figure 5.5: Optical orbital profile for the northern star counterpart to SXP2.37. Detrended OGLE-III data for years 4 to 7 were folded on 18.62 d.

that the observed periodicity in the northern star is real and not an artefact of the close proximity of the stars, or of the data extraction process.

Combining this period with the well known pulse period of 2.37 s places SMC X-2 on the edge of the distribution of Be/X-ray binaries in the Corbet diagram. This supports the proposal by Schmidtke, Cowley, & Udalski (2006) that the counterpart is the northern star, and suggests that 18.6 d is the binary period of the Be/X-ray binary system (Schurch, Udalski, & Coe 2008). Figure 5.5 shows the orbital profile for SXP2.37. Only the portion of the optical light curve that was used in the period search was folded. The orbital profile reveals a very steep rise and fall in optical brightness as the neutron star passes through periastron. The ephemeris derived is MJD $(53170.56 \pm 0.18) + n(18.62 \pm 0.02)$ d.

Table 5.2: X-ray Error positions for SXP15.3

Reference	Detector	R.A.	Dec.	r_{90} ($''$)	Name
Kahabka & Pietsch (1996)	*PSPC*	00:52:11.30	-73:19:13.0	11.0	K96
Kahabka (2000)	*HRI*	00:52:15.60	-73:19:13.0	6.0	K00
Haberl & Sasaki (2000)	*PSPC* & *HRI*	00:52:13.90	-73:19:13.0	7.3	H00
Covino et al. (2001)	*HRI*	00:52:13.27	-73:19:19.5	3.3	C01
Finger et al. (2001)	*HRI*	00:52:13.65	-73:19:19.5	7.1	F01
Haberl et al. (2008a)	*XMM-Newton*	00:52:15.30	-73:19:14.6	1.7	H08

5.1.2 *RXTE*

SXP2.37 is located at the South-West corner of the SMC (see Figure 5.1). Due to this position it has been poorly studied by *RXTE* (see Galache et al. 2008, for details). The only X-ray detection to overlap with the OGLE-III coverage was recorded on MJD 52228. There is no noticeable correlation between this X-ray detection and any optical feature of either star that would aid in identifying the correct counterpart. Full analysis of the X-ray light curve is presented in Galache et al. (2008). There is no supporting orbital period from the X-ray data.

5.2 SXP15.3

As part of an analysis of recent *XMM-Newton* data, Haberl et al. (2008a) reported a source at the position R.A.=00:52:15.3, Dec.=-73:19:14.6 and identified it as RX J0052.1-7319 (otherwise known as SXP15.3). The position of this source has now raised issues over the correct optical counterpart for SXP15.3. Here the refinements made to the X-ray positions since the discovery of the source in 1996 are described, including the history behind the identification of an optical counterpart. Table 5.2 contains the precise X-ray positions and errors, these are also plotted over the ESO MAMA U-band image in Figure 5.6.

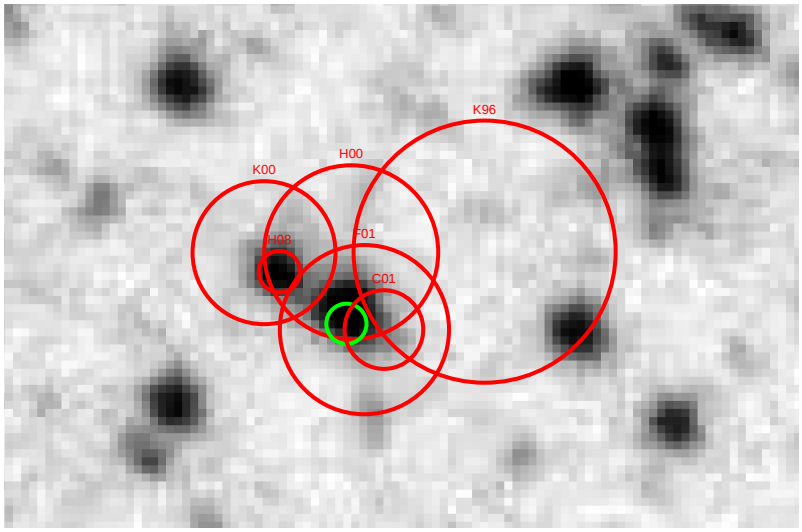

Figure 5.6: ESO MAMA U-band image of SXP15.3. The red circles refer to the X-ray positions and errors in Table 5.2. The green circle is the location of [MA93]552.

Lamb et al. (1999) reported detecting pulsations at 15.3 s from the X-ray source RX J0052.1-7319 in both *ROSAT HRI* and *BATSE* observations taken in 1996. The likely optical counterpart was then subsequently identified by Israel et al. (1999) as a Be star with R=14.54 that was within the current 11″ *ROSAT PSPC* X-ray error circle (Kahabka & Pietsch 1996). However, they also reported the presence of an R=16.1 star within the error circle. The identified optical counterpart is found in the optical catalogues of Meyssonnier & Azzopardi (1993) as [MA93]552. Kahabka (2000) refined the *ROSAT* error through careful analysis of several *ROSAT HRI* observations. This new position is incompatible with their previously reported position, as can be seen in Figure 5.6. Unfortunately this reduction was still insufficient to distinguish between the two potential counterparts. They analysed early OGLE-II data revealing that both stars were variables. The authors also reported that no Hα emission has been detected from the fainter object. In light of this, they supported the identification of the brighter Be type star as the counterpart. At the same time as these data were published, Haberl & Sasaki (2000) analysed both *ROSAT PSPC* and *HRI* data. Their position is consistent with the previously identified optical counterpart and so they supported the identification. Covino et al. (2001) then presented a detailed analysis of the *ROSAT HRI* data using a sliding

cell and wavelet transform based algorithm. After a subsequent boresight correction, their final position had an error of 3.3″, providing the most accurate position. The error circle now clearly selects [MA93]552 as the only possible optical counterpart. They performed spectroscopic and photometric analysis of [MA93]552, finding a classification of either O9.5IIIe or B0Ve depending on how much of the reddening can be attributed to the circumstellar disk. They also noted that the other candidate previously mentioned shows no sign of emission lines at Hα or Hβ, and has a spectral class that is later than [MA93]552. Finger et al. (2001) presented the timing analysis of the original data taken in 1996 when the source was at its brightest. They supported the position and identification of the counterpart made by Covino et al. (2001) and suggested that the earlier positions quoted by Kahabka (2000) were less accurate due to the low count rate of the data they analysed.

The *XMM-Newton* detection is the first observation of this region by a telescope with a positional accuracy that is small enough to distinguish clearly between the two possible counterpart stars. It is clear from Figure 5.6 that the *XMM-Newton* source is not associated with the previously identified optical counterpart to SXP15.3. Unfortunately, the observation by *XMM-Newton* occurred while the source was in a low-state $\sim L_{0.2-10} = 4.0 \times 10^{34}\,\mathrm{erg\,s^{-1}}$. The ∼300 counts were insufficient to detect any X-ray periodicities and hence the association with SXP15.3 is not certain. Two possible outcomes remain:

- That the detected *XMM-Newton* source is the same source that *ROSAT* detected 15.3 s pulsations from, and that the previous attempts to reduce the systematic errors in the *ROSAT* observations were incorrect. The counterpart is the more northern star, with a spectral classification later than B0Ve.
- That there are two distinct X-ray sources associated with two separate optical counterparts. The 15.3 s pulsations are associated with the Be star [MA93]552.

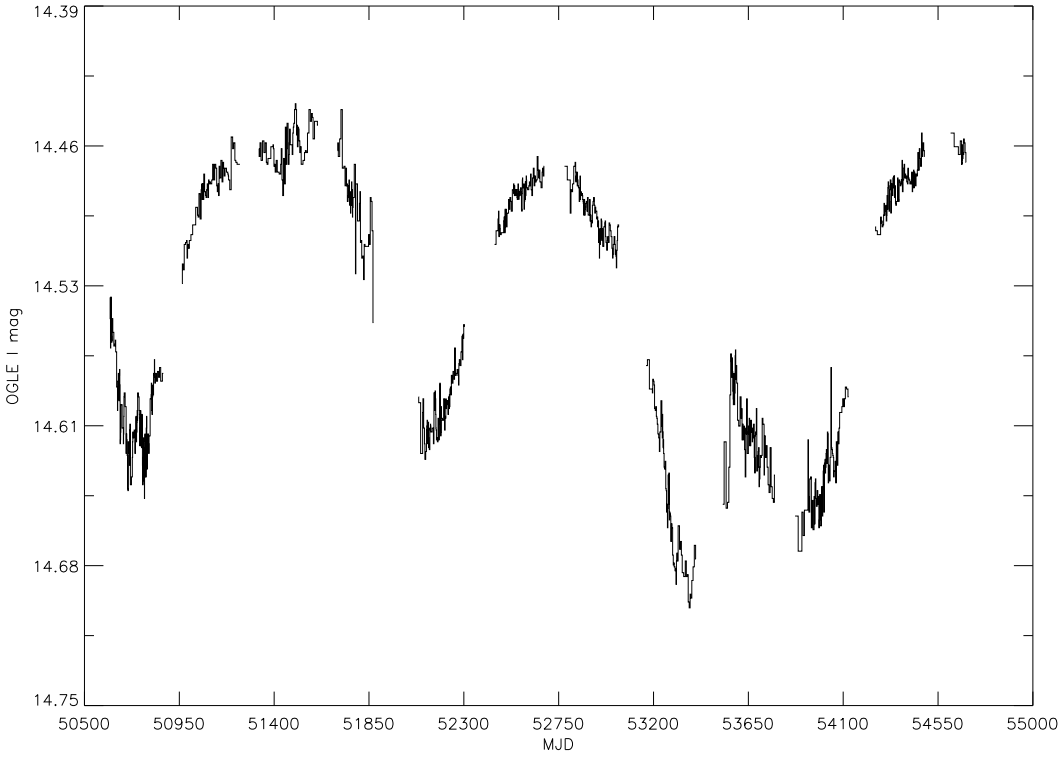

Figure 5.7: OGLE light curve of [MA93]552. A proposed counterpart to the source RX J0052.1-7319 as identified by *ROSAT*.

5.2.1 OGLE

Edge (2005) and Coe et al. (2005) have extensively analysed a total of 11 years of MACHO and OGLE data for [MA93]552. They identified a possible orbital period of 75 d. The subsequent 4 years of OGLE data continue to show the large optical variability of this source (Figure 5.7). It was decided not to re-analyse this data; firstly, due to the difficulty in removing this variability and secondly, because the previous analysis and findings are not doubted. This section will present the optical analysis of the second star that is associated with the *XMM-Newton* source. OGLE-II and III data have been merged into a single light curve for this star.

Figure 5.8 shows the extreme optical variations in the OGLE light curve. The $\sim$0.5 mag outbursts are semi-periodic, recurring on timescales of $1000 - 1400$ d and lasting for up to 600 d. These timescales are far too large and too variable to be

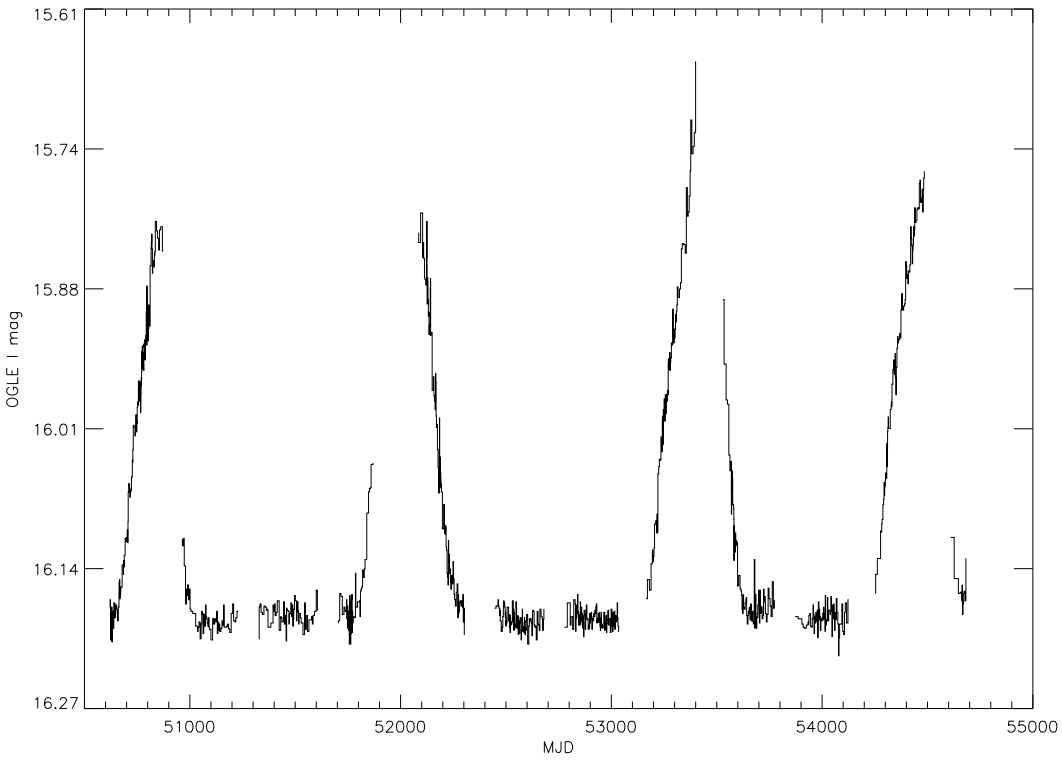

Figure 5.8: OGLE light curve of the potential northern counterpart to the source RX J0052.1-7319 as identified by *XMM-Newton*.

attributed to the orbital period of the system. Similar outbursts are seen in other sources such as SXP18.3 (Haberl et al. 2008a, and Chapter 4). The variations are most likely due to changes in the structure of the circumstellar disk. Although there are long periods in-between the outbursts where the light curve is fairly constant, it was still decided to try and detrend the outbursts. The primary reason for detrending is that small blips are noticeable on top of the outburst profiles. Similar blips are seen in other SMC Be/X-ray binaries (for example, SXP46.6 McGowan et al. 2007) and are often characteristic of an orbital signature. Due to the extremely linear rise and fall of the outbursts, the light curve was fully detrended using only linear fits. The fifth year of data was removed from the final detrended light curve, due to the poor linear fit, producing an artificial wiggle in the light curve.

The periodogram shown in Figure 5.9 clearly shows a significant peak well above the 99% significance level in the data at 21.68 ± 0.01 d. If it is assumed that the correct

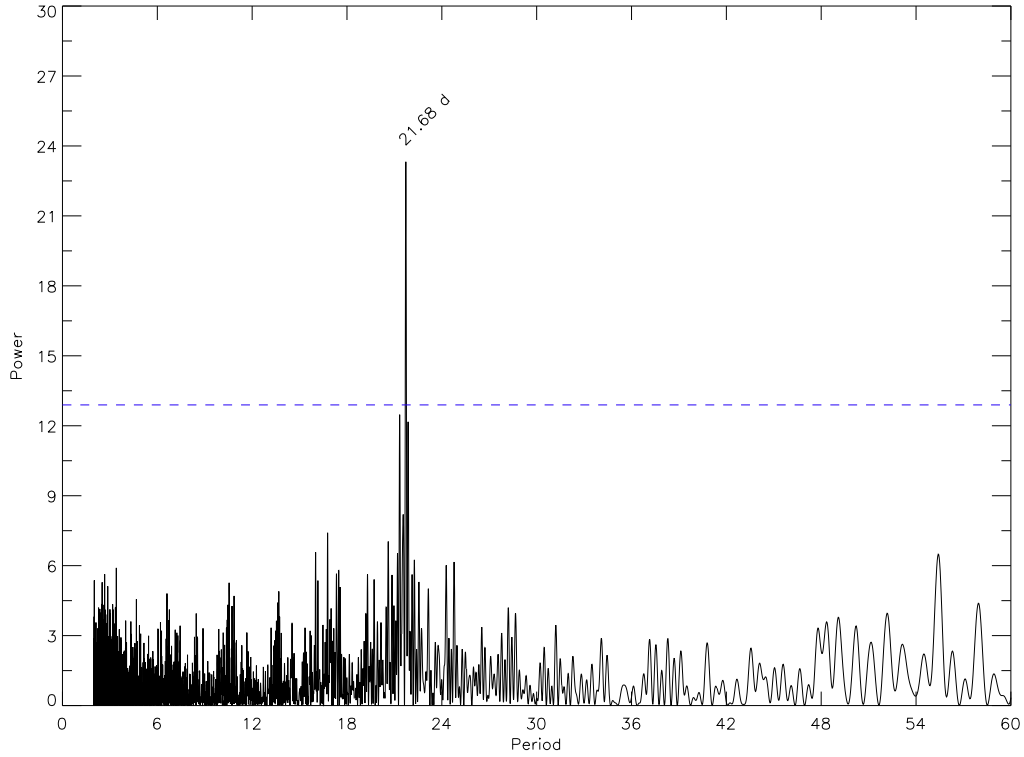

Figure 5.9: Periodogram of the detrended OGLE light curve of the potential northern counterpart to the source RX J0052.1-7319. The horizontal blue line represents the 99% significance level.

scenario is that this star is the real counterpart to the 15.3 s pulsating X-ray source, then the period found in the OGLE light curve would be entirely consistent with the expected orbital period from the Corbet diagram. The source would occupy a position at the lower end of the distribution of Be/X-ray binaries on the Corbet diagram. However, the previously identified counterpart to the south also exhibits an optical period that is consistent with the expected range of orbital periods. An orbital period of 75 d would place the system in the middle of the distribution of Be/X-ray binaries on the Corbet diagram. Both stars seem to exhibit orbital periods and behavioural variations that are consistent with other counterparts to Be/X-ray binaries. The magnitude ranges are also consistent with other counterparts in the SMC. The only major difference between the two sources is the spectral classification. The southern star ([MA93]552) has been well classified as a Be star as would be expected from a HMXB counterpart. From spectra taken on 19^{th}

and 20^{th} January 1999 by the Danish 1.5 m telescope at La Silla, Covino et al. (2001) noted that the northern star shows no emission features and has a much later type spectrum. However, this does not rule out the possibility it is a mid or even late B type star. Through independent photometry taken on 20^{th} January 1999 by the 1.0 m SAAO telescope, Finger et al. (2001) also noted that the northern source shows no Hα excess when compared to the surrounding stars, unlike the southern star. These spectral and photometric characteristics are inconsistent with other HXMB counterparts. However, these observations were taken during the period MJD 51197 − 8; Figure 5.8 indicates that the source was in its base state at the time of these observations. If this state is indicative of a B star without a circumstellar disk, then no Hα emission would be expected. Accurate spectral classification particularly during a period of outburst would enable this object to be placed within or possibly outside the distribution of SMC Be/X-ray binaries.

5.2.2 *RXTE*

The *RXTE* light curve for SXP15.3 is shown in Figure 5.10. During the course of the monitoring program, detections of SXP15.3 have been rare. However, for a period of about 100 days SXP15.3 did enter into a giant Type-II outburst phase (beginning on MJD 53564). This outburst was particularly interesting since it showed signs of being orbitally modulated. Unsuccessful attempts to fit an orbital solution to the data were performed by Galache et al. (2008); however, they note that variations in the detected period during the Type-II outburst suggest an orbital period of ∼28 d. Possible correlations were examined between the observed X-ray activity and the two possible optical light curves, in an attempt to distinguish the correct counterpart. There are no obvious features in the optical light curves that seem to correspond with any of the X-ray activity. Edge (2005) noted that an earlier X-ray detection by the *ROSAT HRI* occurred simultaneously with a large peak in the MACHO data for the southern star. An independent Lomb-Scargle analysis of

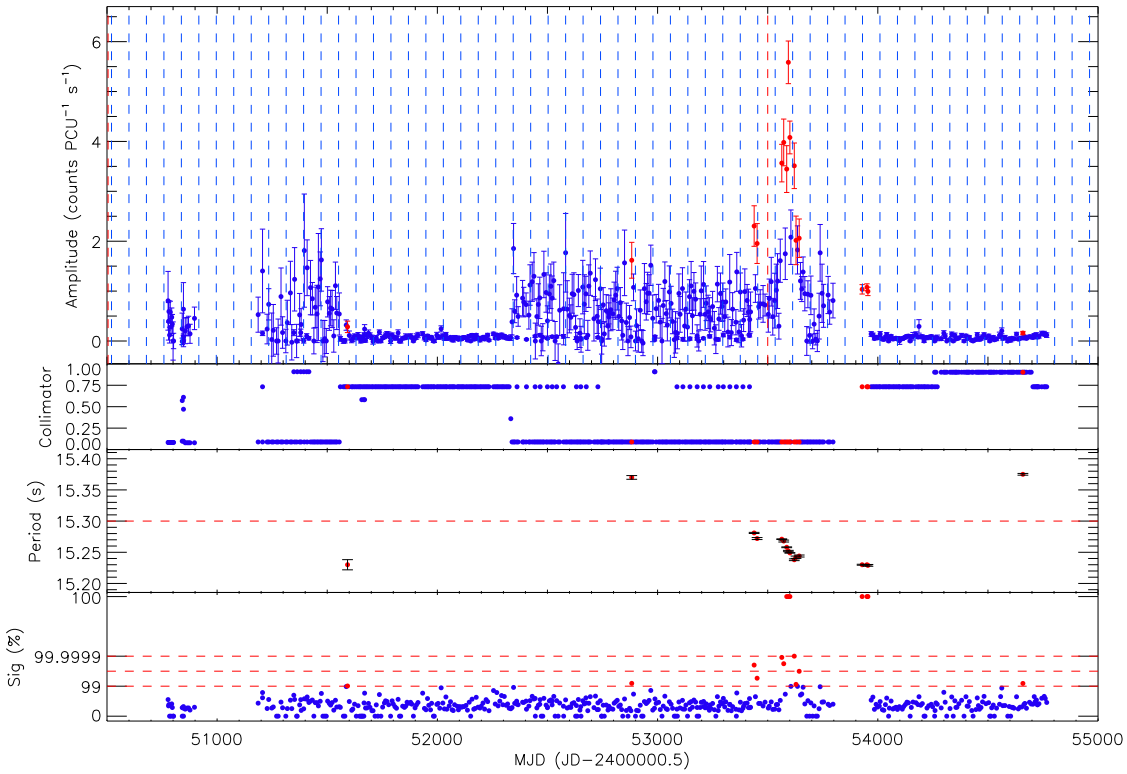

Figure 5.10: *RXTE* light curve of SXP15.3.

the *RXTE* light curve was performed. No significant periodicities were found in the data. Galache et al. (2008) suggested a period of ∼28 d from orbitally fitting the large Type-II outburst, and this period is neither confirmed nor ruled out by our analysis of the *RXTE* data.

The analysis of the optical light curves has been unable to clarify the identity of the true optical counterpart to SXP15.3. Through the *XMM-Newton* X-ray observation it is known that there is an X-ray source associated with the northern star. This northern star is suspected to be a binary system with a 21.7 d orbital period. However, from the earlier spectra presented in Covino et al. (2001) the counterpart does not resemble a Be star. This is extremely interesting since it is potentially the first X-ray binary system in the SMC where the counterpart is not a Be or super giant star. In fact, if the later classification is believed, it would be the first XRB system to have an A type counterpart. The association of this source with SXP15.3 is still unclear, and so it cannot be identified as a pulsating neutron star system.

The uncertainty over this source will remain until such a time that further X-ray observations are made during a period when SXP15.3 is in outburst. Such observations require simultaneous positional and timing capabilities so that the localisation and identification of the source can be made. Optical observations of both these systems are required, but in particular of the northern counterpart during the next period of maximum optical flux, so that a precise optical classification can be made. Measurements of the Hα during this period will provide us with an indication as to whether the optical flux variations seen in the OGLE-III are related to some sort of circumstellar disk.

5.3 SXP172

SXP172 is a member of the group of pulsars in the South Westerly region of the SMC. Pulsed X-ray emission at 172.4 s was discovered in *ASCA* data of the *ROSAT* source RX J0051.9-7311 Yokogawa et al. (2000). This X-ray source was previously identified with the Be star [MA93]504 by Cowley et al. (1997). These identifications were confirmed when a source exhibiting 172.21 s was detected in a *XMM-Newton* observation at the position of the optical counterpart suggested by Haberl & Pietsch (2004). McBride et al. (2008) have recently classified the counterpart to be an O9.5-B0 V star, confirming its Be/X-ray binary classification. The MACHO and OGLE-II data have been well studied by Schmidtke & Cowley (2006). They proposed an orbital period of 69.9 d from the first two years of OGLE-II data.

5.3.1 *RXTE*

Through the extensive monitoring campaign with *RXTE*, SXP172 was recently observed to go through several outbursts. This is the second time in the history of SXP172 that a succession of X-ray outbursts has been seen. The *RXTE* light curve

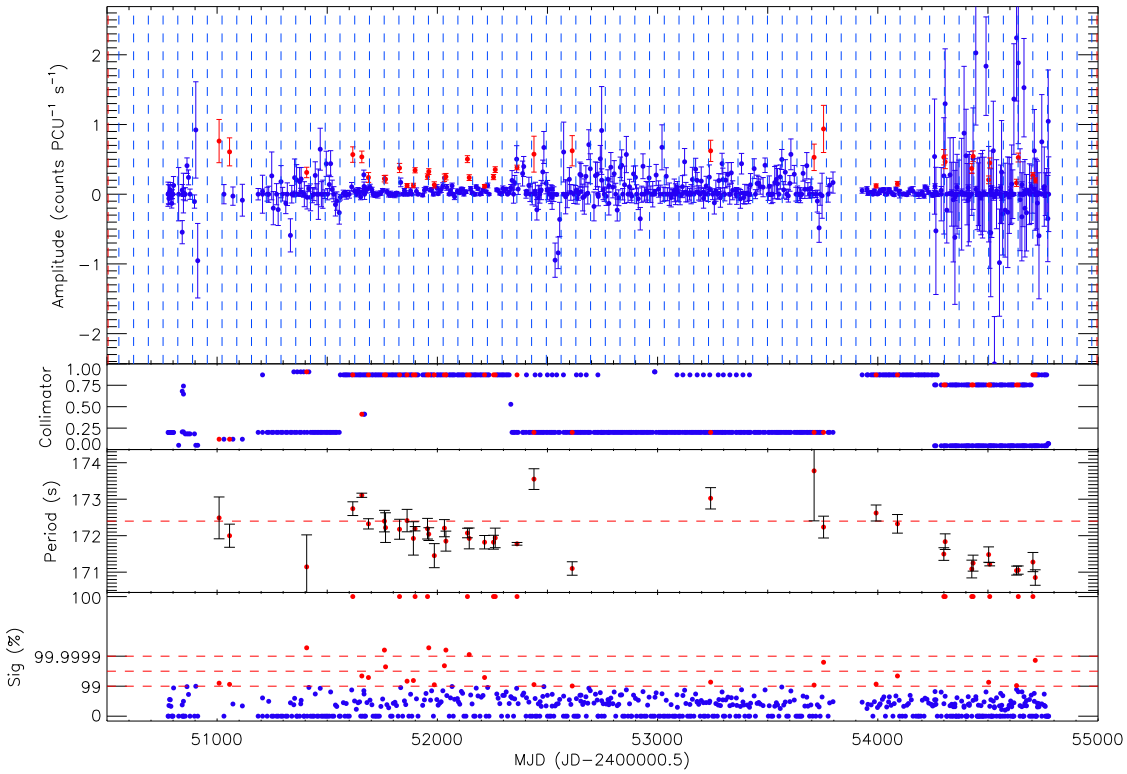

Figure 5.11: *RXTE* light curve of SXP172.

for SXP172 is shown in Figure 5.11. The two periods of outbursting behaviour are clearly visible. The outbursts occurring around MJD 52000 have previously been studied by Laycock et al. (2005) and Galache et al. (2008). Analysis of these outbursts has suggested several possible orbital periods, none of which were conclusive (Galache et al. 2008). Since this light curve was last analysed, two further years of data have been collected, and the second set of outbursts was observed. This longer light curve was also analysed in order to confirm the true orbital period of this Be/X-ray binary.

Due to the observing strategy employed in our *RXTE* monitoring program, there have been periods when SXP172 has fallen very close to the edge of the FoV of *RXTE* (see the collimator response in Figure 5.11). The effect of this is that possible outbursts are missed unless they are extremely bright. As a result, including these periods of low collimator response has the effect of "muddying the water" when searching for orbital periods using Lomb-Scargle analysis. It was decided only to

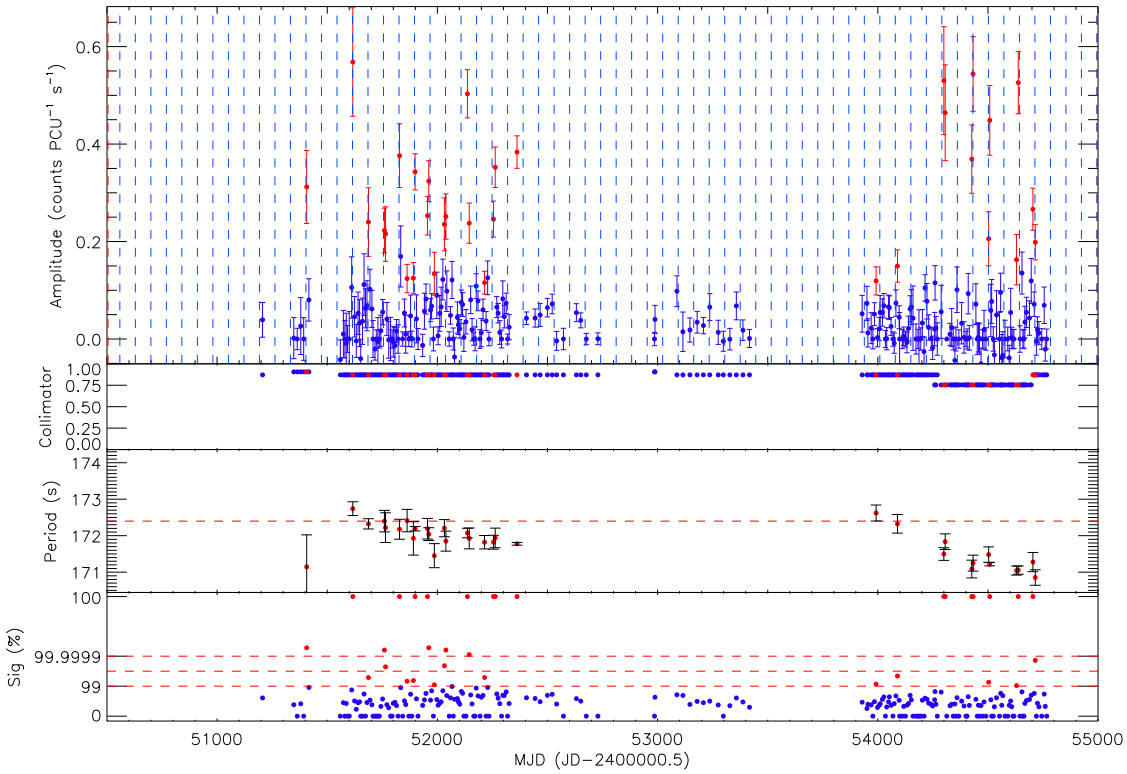

Figure 5.12: *RXTE* light curve of SXP172 where the source position was within 0.5′of the pointing position.

analyse data which were taken with SXP172 extremely close to the centre of the FoV, thus producing a data set with the maximum data quality. A collimator response limit of 0.75 was chosen. The resultant X-ray light curve is shown in Figure 5.12. Analysis of this light curve produces a number of significant peaks above the 99% significance level as shown in Figure 5.13. The highest of these peaks is at 70.42 ± 0.15 d, which is consistent with the orbital period suggested by Galache et al. (2008) from the first period of outbursts, and with the optical period of Schmidtke & Cowley (2006).

5.3.2 OGLE

Schmidtke & Cowley (2006) found an orbital period of 69.9 ± 0.6 d from analysing the first 2 years of OGLE-II data. No reported periodicities were found in the

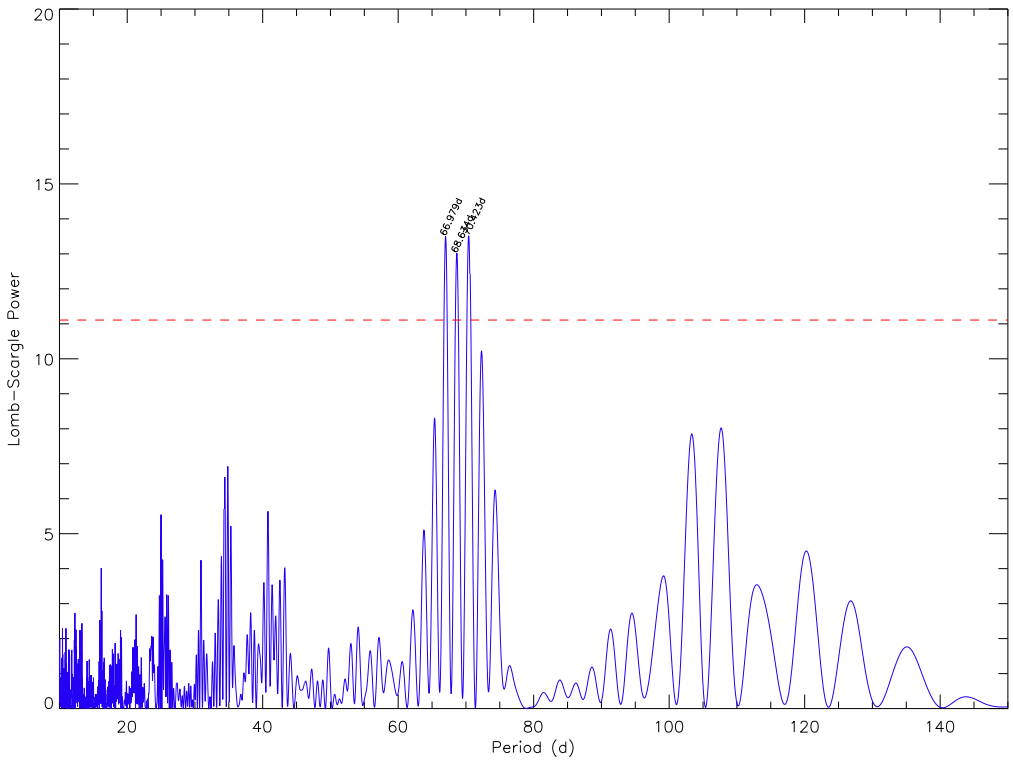

Figure 5.13: Lomb-Scargle analysis of *RXTE* light curve of SXP172. The horizontal dashed red line represents the 99% significance level.

corresponding MACHO or OGLE-III data. They reported the period of 69.9 d due to finding peaks in their Lomb-Scargle and PDM analysis at 23.4 d and 34.9 d, these are the second and third harmonics of a 69.9 d period. A re-analysis of the OGLE-II data is presented including the most recent OGLE-III data in order to try and establish the orbital period. The source is extremely variable with many magnitude changes up to 0.5 mag, as seen in Figure 5.14. Any possible link between these periods of optical flaring and the observed X-ray outbursts will be investigated later.

Figure 5.15 shows the periodogram for each single year of data and for the combined light curve. The analysis of the year two data clearly produces two peaks both below the 99% significance level. These can be identified with the peaks identified by Schmidtke & Cowley (2006). When each subsequent year of data is analysed singly, they all show a distinct lack of variability at any of the previously seen

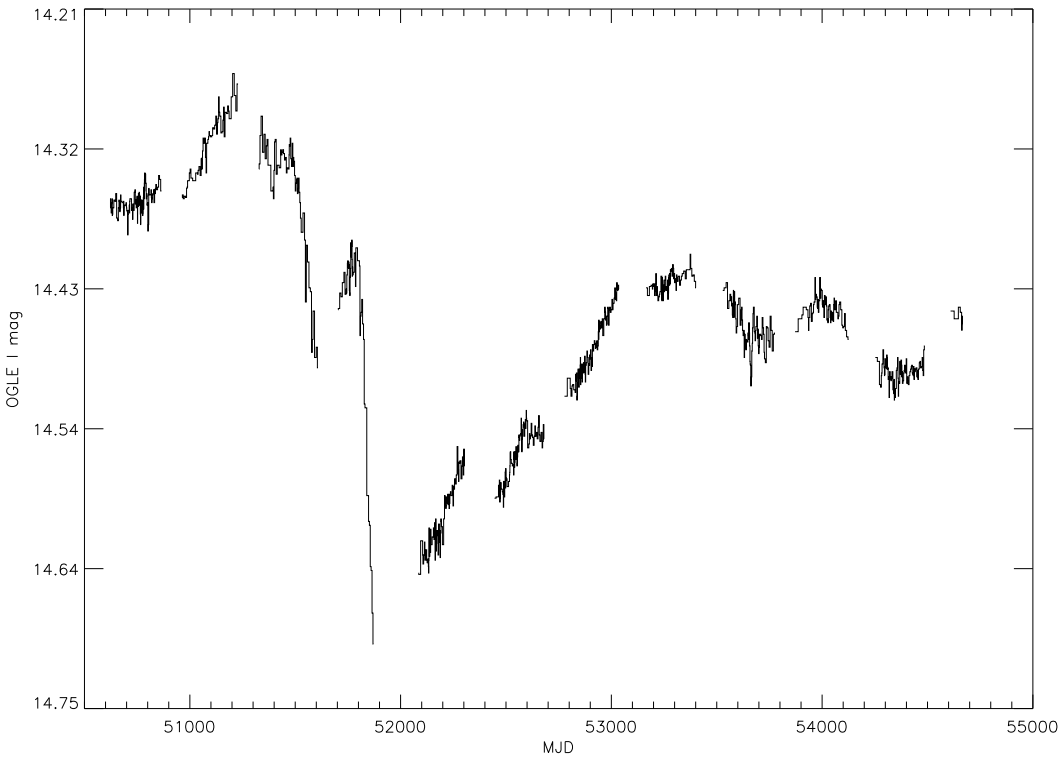

Figure 5.14: OGLE light curve of SXP172.

periods or the suspected orbital period of 69.9 d. Since the light curve is highly variable no periodicities were seen in the search of the combined data, thus the data was detrended so that the entire light curve could be searched for the orbital period. Detrending was performed using the method described is §5.2 and §5.1. The resulting detrended light curve is shown in Figure 5.16. This light curve was then put through exactly the same period analysis. The results shown in Figure 5.17 show that the previous peak at 34.9 d is lost in the detrended year two data, but the peak at 23.4 d gets slightly stronger and is now above the 99% threshold. When the entire light curve is searched as one (the red over-plotted line) it can be seen that there is a significant peak around 23 d but it has shifted to a slightly shorter period of 22.9 ± 0.1 d. The next peak also above the 99% significance threshold occurs at 17.16 d. There is also a hint of the return of a peak at 34.4 d slightly below the threshold. These three values would form the first, second and third harmonics of a 68.9 d period. There is a slight peak around this value in the Lomb-Scargle

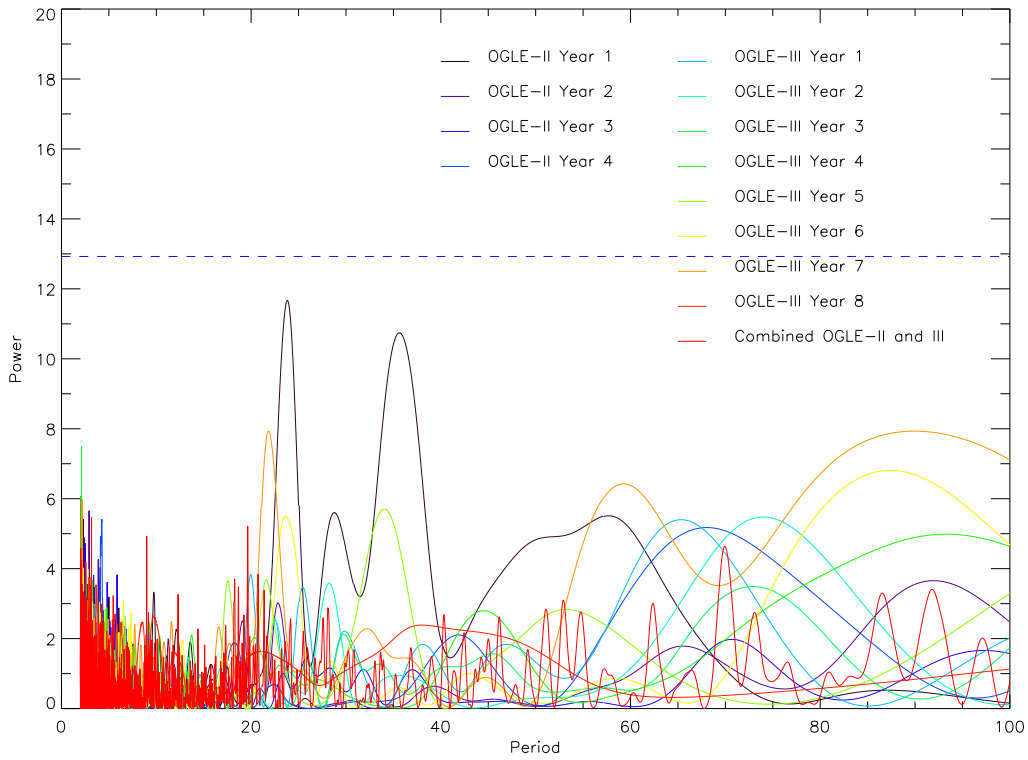

Figure 5.15: Lomb-Scargle analysis of OGLE light curve of SXP172. The horizontal blue line represents the 99% significance level.

periodogram. However, it is extremely weak and not would not be identifiable on its own. A break down of each year shows no further signs of any periodicities.

In light of the close agreement between the derived periods from the independent analysis of both the X-ray and optical light curves, and the agreement of these values with the findings of Schmidtke & Cowley (2006), it is proposed that the orbital period of the system is 68.9 d. Although the X-ray period differs slightly it is noted that one of the several peaks with a significance above 99% in Figure 5.13 sits at 68.7 d, it is likely that these peaks are actually caused by the two separate datasets being separated by a four year period.

Both the detrended optical and X-ray light curves for SXP172 were folded to compare the shape of the orbital profile. The ephemeris found through the analysis of the optical data is MJD $(50581.24 \pm 0.68) + n(68.9 \pm 0.17)$ d.

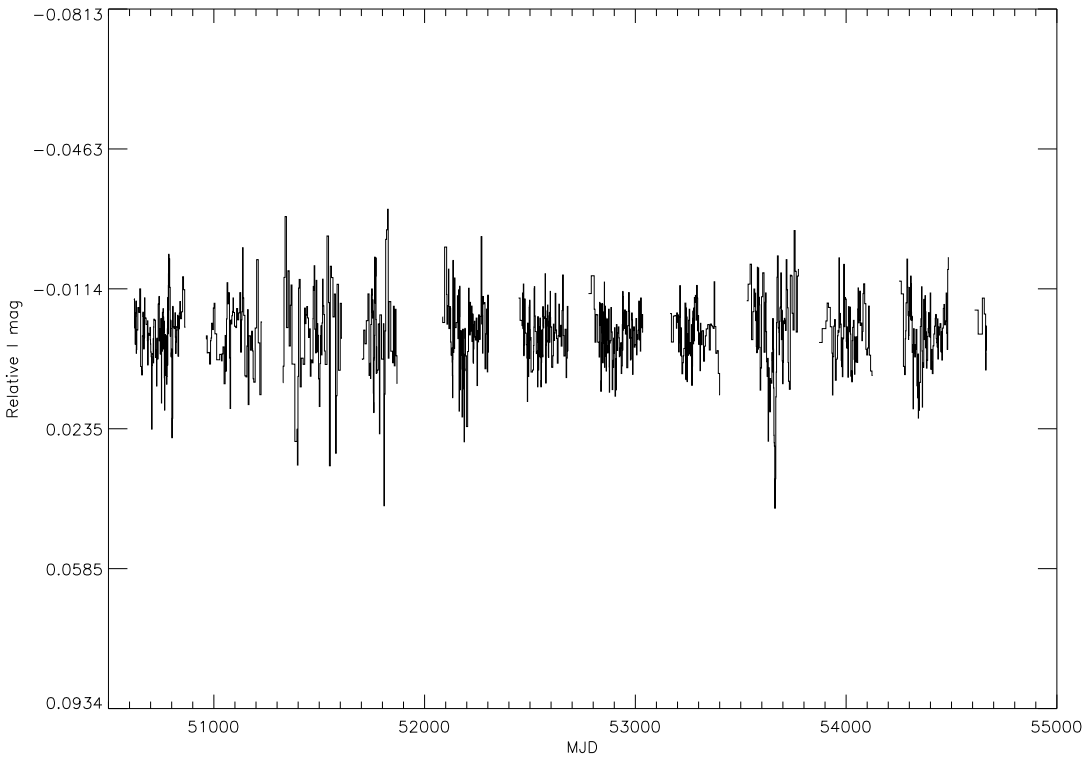

Figure 5.16: Detrended OGLE light curve of SXP172.

The shape of the profile shown in Figure 5.18 is unusual in that the optical emission seems to have one main peak and then a broad plateau lasting for approximately one third of the orbit. This feature may be linked to the fact that the orbital period is detected through the presence of a strong second harmonic. There is also the the possible presence of two further peaks during the plateau stage. For a direct comparison, the X-ray light curve data used earlier was folded at the detected optical period. Figure 5.19 reveals that the X-ray is well matched to the optical. The main X-ray outburst is narrow and very symmetric. This type of X-ray profile is typical of those seen in the other SMC Be/X-ray binaries (Galache et al. 2008). The comparison with the optical reveals that the X-ray outburst begins 0.1 orbital cycles before the optical outburst, but they both peak in phase. The presence of the two smaller optical peaks is confirmed by the corresponding peaks in the X-ray profile. The optical emission again appears to be delayed. However, this time they peak at different slightly different orbital phases. These apparent delays would suggest

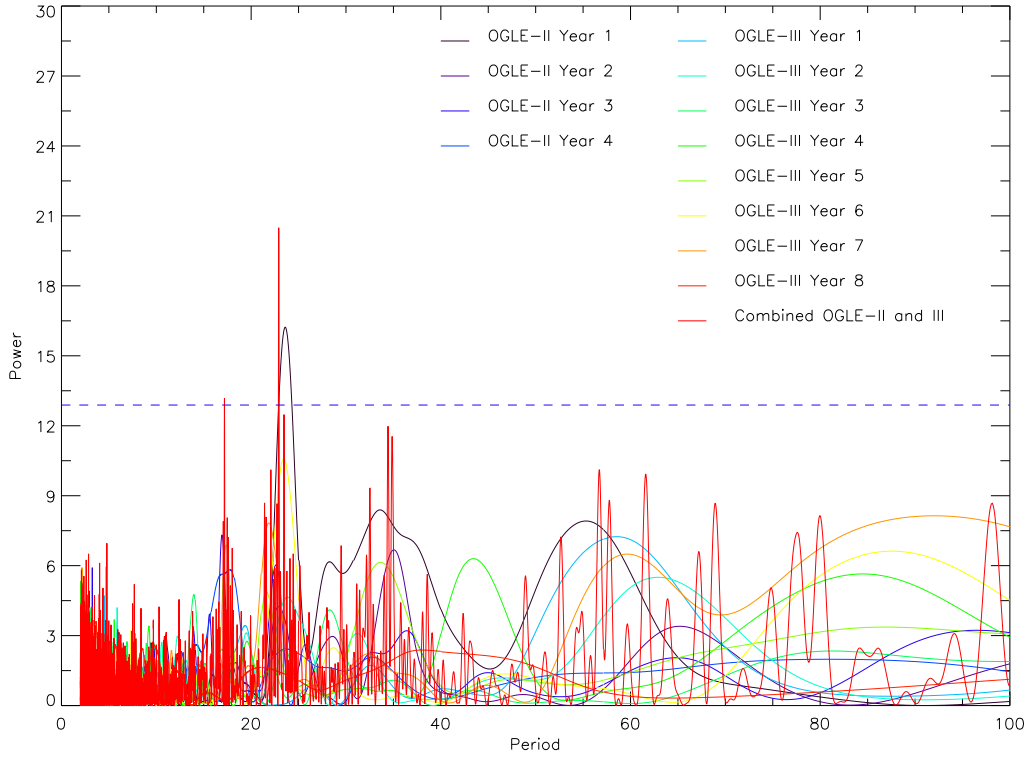

Figure 5.17: Lomb-Scargle analysis of detrended OGLE light curve of SXP172. The horizontal blue line represents the 99% significance level.

that the X-ray emission is the cause of the optical emission, possibly through X-ray heating of the circumstellar disk.

5.4 SXP202B

SXP202B, or XMMU J005929.0-723703, was recently discovered during a series of *XMM-Newton* observations of the SMC by Haberl et al. (2008a). *XMM-Newton's* positional accuracy allowed the identification of [MA93]1147 as the optical counterpart. The counterpart was previously classified as B0-5(III)e in the 2dF survey of the SMC by Evans et al. (2004). Haberl et al. (2008a) performed a thorough analysis of the MACHO and OGLE-II data revealing possible periodicities at 334 d and 220 d from broad peaks in the power spectra. These were attributed to quasi-periodic

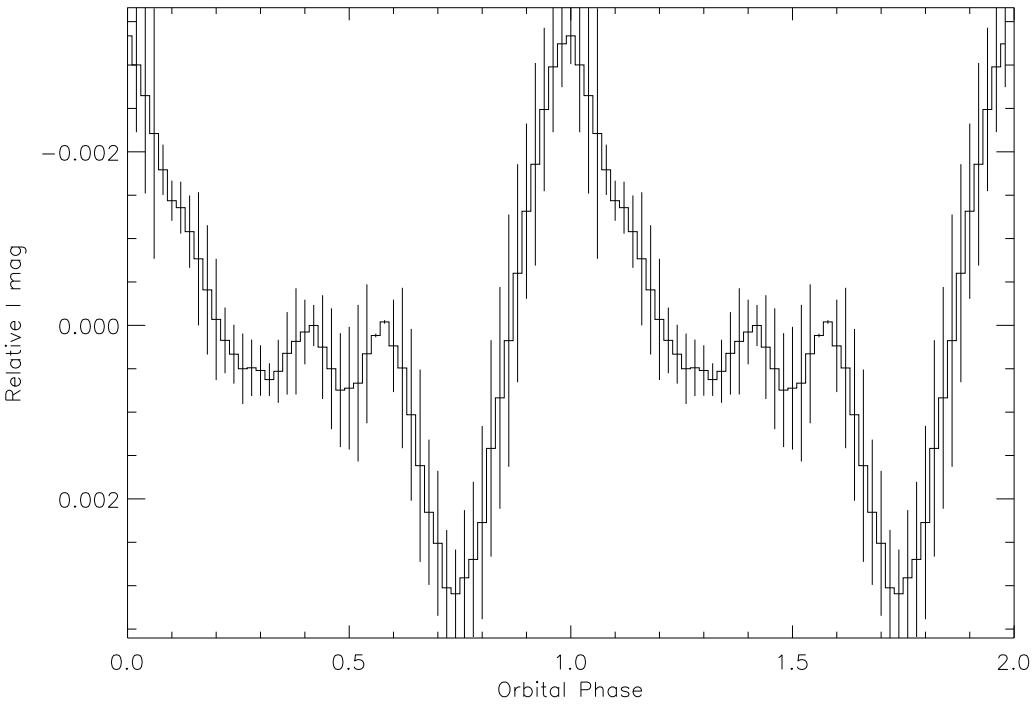

Figure 5.18: Optical orbital profile for the counterpart for SXP172 folded on 68.9 d.

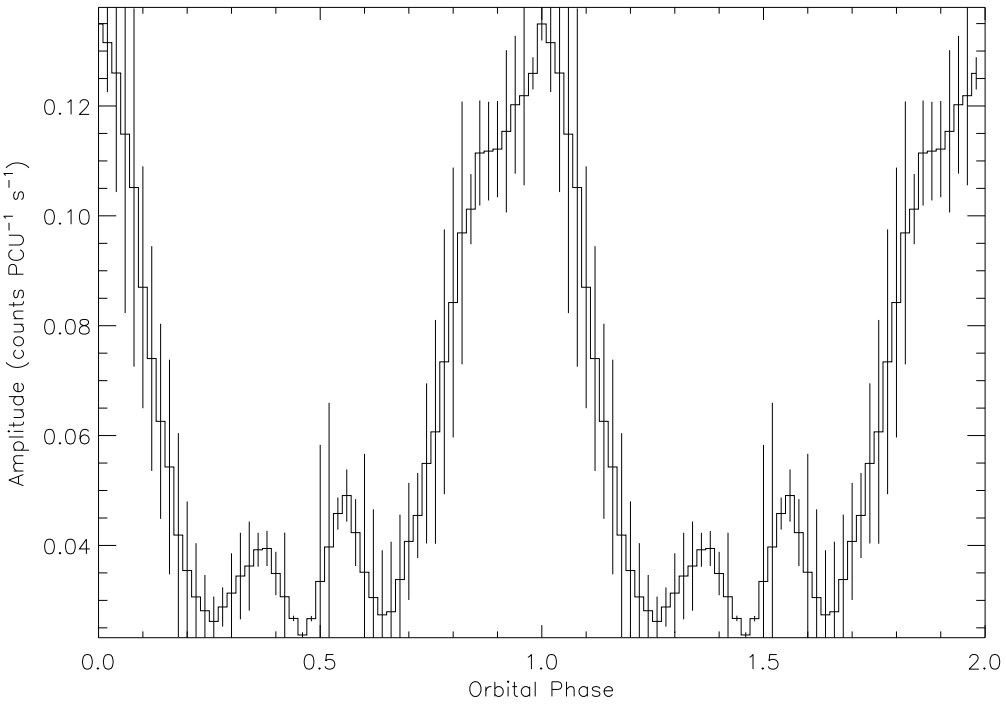

Figure 5.19: X-ray orbital profile for the counterpart for SXP172 folded on 68.9 d.

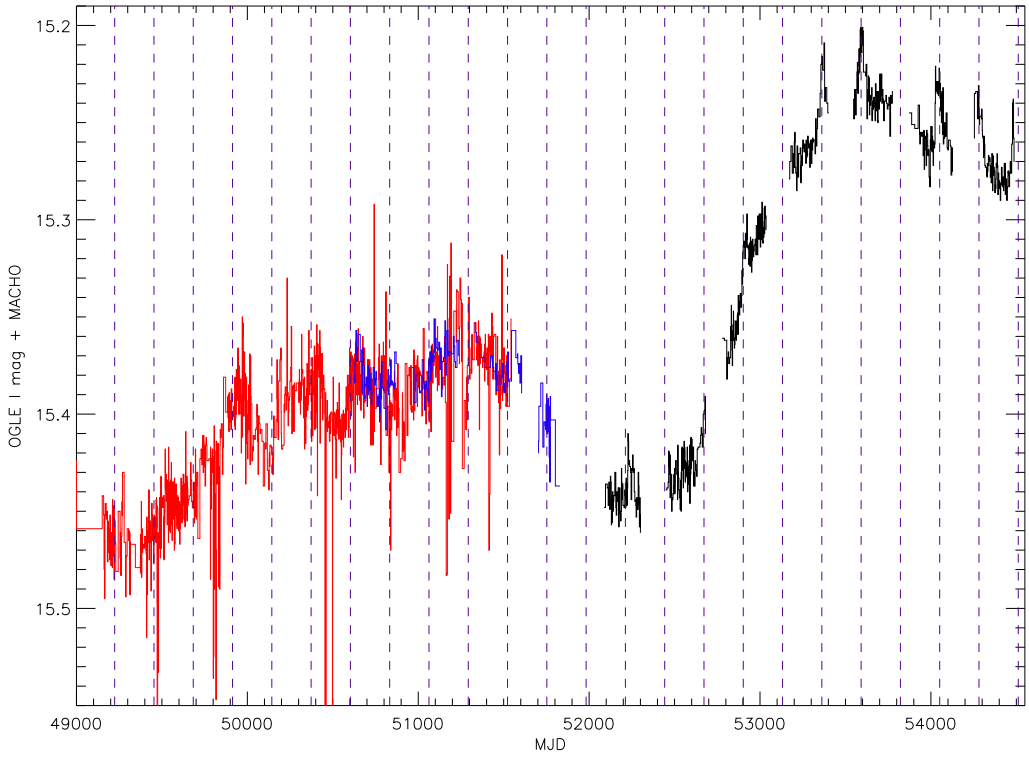

Figure 5.20: Optical light curve of SXP202B, MACHO (red) OGLE-II (blue) and OGLE-III (black). Vertical dotted lines show periods of predicted periastron passage.

variations (QPVs) in the Be disk.

5.4.1 OGLE

The optical counterpart to SXP202B is contained within the MACHO, OGLE-II and OGLE-III data sets. The counterpart is an extremely variable source (Figure 5.20) showing dips and rises of the order 0.3 mag. On top of this underlying variation, there are 8 clear optical outbursts of ∼0.04 mag in the OGLE-III light curve each lasting for around 100 d. From a visual check they appear to occur periodically. The MACHO data also hints at these outbursts but, due to the general data quality and the underlying variations, they are hard to see. It was decided to restrict the data analysis to the two OGLE data sets only. Detrending the light curve was

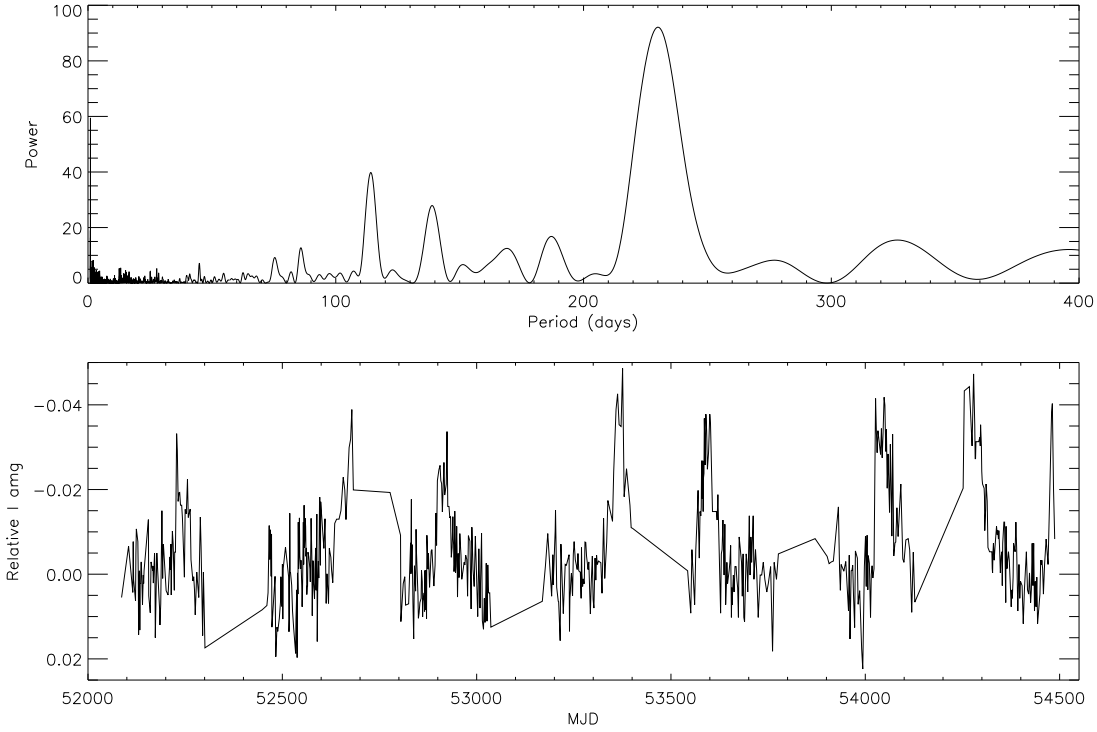

Figure 5.21: Detrended OGLE light curve of SXP202B (bottom). The top panel shows the Lomb-Scargle analysis.

slightly trickier than described for the previous sources in this section because the length of the outbursts are approximately one third of the length of the observable year for OGLE, and so significantly effect the detrending line. Thus the data were detrended by just using a fit to the intervals between outbursts. The resultant OGLE light curve showing the prominent outbursts can be seen at the bottom of Figure 5.21. The Lomb-Scargle periodogram analysis shown in the top panel of Figure 5.21 reveals a strong periodicity at 229.9 ± 0.9 d (Schurch & Udalski 2008). Also identifiable are the 1st and 2nd harmonics. The two peaks at 140 days and 85 days are due to beating of both the fundamental and the 1st harmonic with the one year sampling. Haberl et al. (2008a) find a broad signal in the analysis of MACHO R-band data at 220 d. Combining the 229.9 d period with the pulse period (202 s) places the source directly in the centre of the distribution of Be/X-ray binaries on the Corbet diagram.

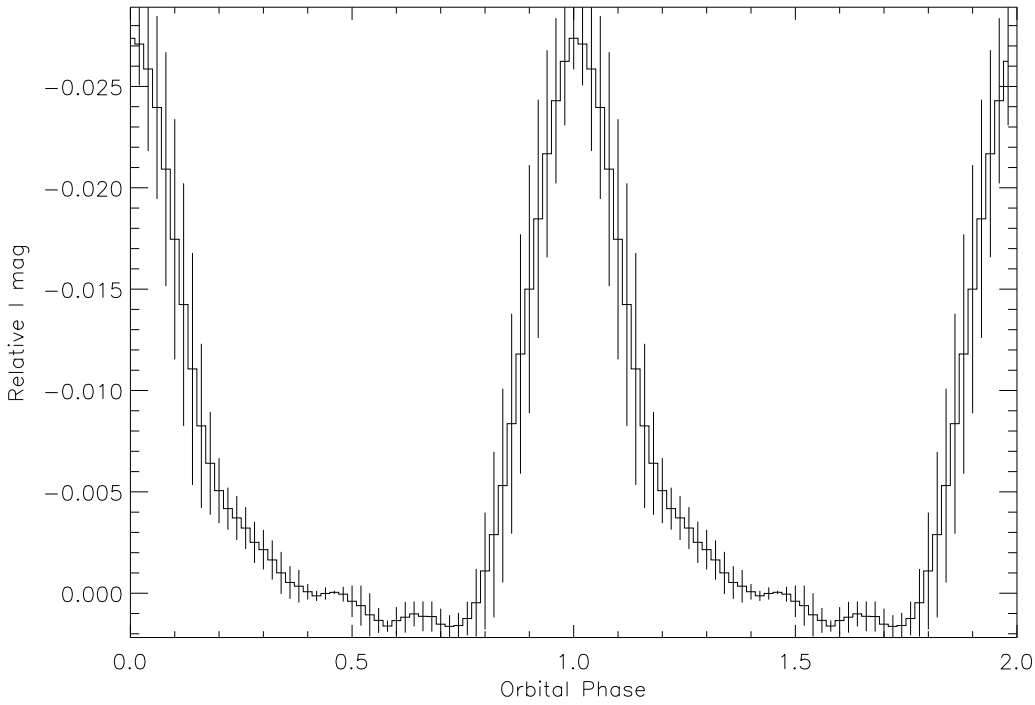

Figure 5.22: Optical orbital profile for SXP202B. The detrended OGLE-III light curve was folded on 229.9 d.

The orbital profile for SXP202B (Figure 5.22) is typical of many of the SMC Be/X-ray binaries. The profile is very symmetric with a steep rise and fall. There is an extra tail in the decay of the outburst, which may suggest that the cause of the optical emission, possibly an over-density or hot spot in the circumstellar disk, slightly outlives the passage of the neutron star. The ephemeris derived is MJD $(52672 \pm 2) + n(229.9 \pm 0.9)$ d.

5.4.2 *RXTE*

This source was added to the *RXTE* database so that the entire ten years worth of data could be searched. The location of SXP202B (approximately in the centre of the SMC) is extremely close to SXP202 originally discovered by Majid, Lamb, & Macomb (2004) in *XMM-Newton* observations. The two sources were each identified and localised by *XMM-Newton* and are sufficiently distant from each other that there

is no possibility that they are the same object. This presents major difficulties when searching for either source in the *RXTE* data, since only temporal searches can be performed. The resultant light curve when the *RXTE* data is searched for significant peaks in the range $199 - 205$ s will be a merger of the two individual light curves. Comparing the X-ray light curve with the known orbital period for either source does not result in a number of X-ray outbursts being attributed to either pulsar. Unfortunately, it is impossible to disentangle the X-ray histories of these two objects, and, without time consuming follow-up observations with satellites such as *SWIFT* or *XMM-Newton*, it will remain impossible to disentangle any future outbursts unless they happen to start appearing on one of the known orbital periods. There are a number of observations where only one pulsar fell within the FoV; however, the respective pulsar was always at the edge of the FoV with a very low collimator response. No detections of either source were made during these observations. Many other complicated effects could be possible through a combination of both pulsars being in an outburst. If they were in anti-phase then a peak at 101 s would be seen, or they could be in phase, effectively increasing the strength of the outburst providing misleading information in either system. The only X-ray detections that can be attributed to either pulsar must be made by a telescope with both imaging and timing capabilities. Follow-up observations of either pulsar could be triggered after *RXTE* outbursts are detected. Using a few ks of *SWIFT* time would be sufficient to distinguish between the two pulsars, but there is always the danger that the source may have switched off by the time the observations are made. Currently our only possible discriminating tool is the comparison to the optical light curves when periods of periastron passage can be predicted.

5.5 SXP726

SXP726 is located in the far North-Eastern area of the SMC near the supernova remnant SNR 1E0102.2-7218. A recent study of the 22 *XMM-Newton* observations

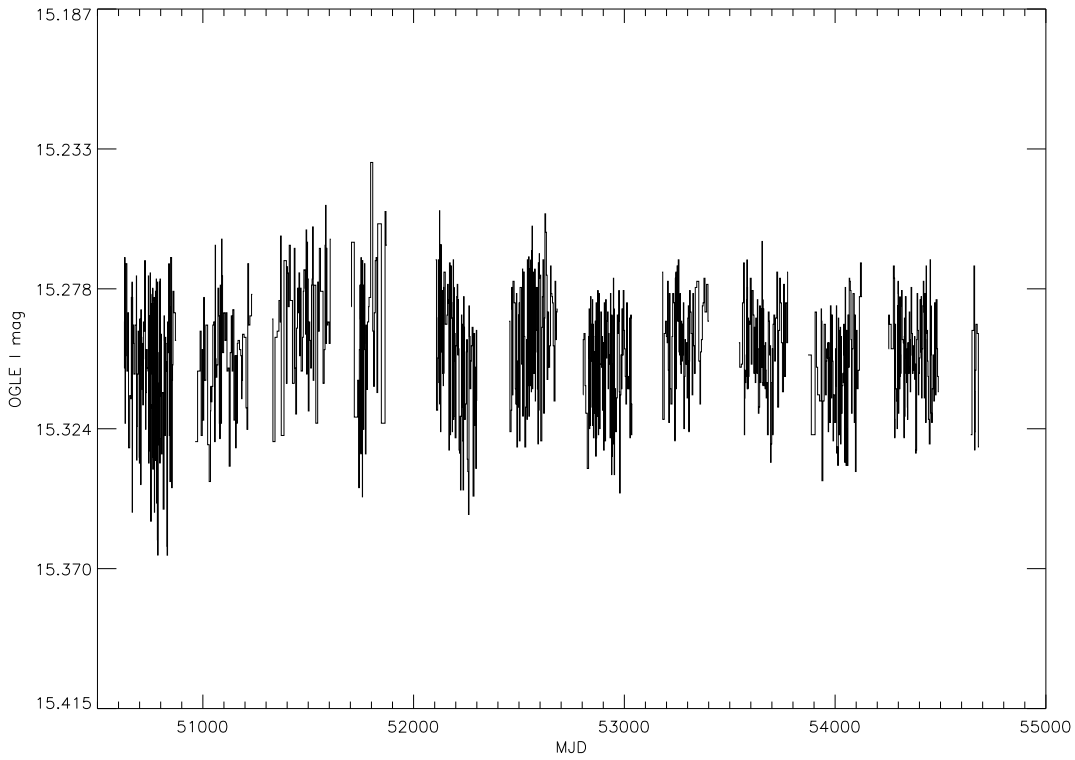

Figure 5.23: Optical light curve of SXP726, showing the full 11 years of OGLE monitoring.

pointed at this region by Eger & Haberl (2008) has revealed 726 s pulsations being emitted from a previously identified *ROSAT* source (RX J0105.9-7203). In addition to studying the X-ray emission, Eger & Haberl (2008) have also analysed some of the optical data. They performed timing analysis on the OGLE-II data, finding possible quasi-periodic variations (QPVs) at 2.35 and 3.2 days. Following the method of Coe et al. (2005), they estimated a spectral class of B0.5-B3 from its B-V colour index, typical of the many Be/X-ray binary systems in the SMC. Schmidtke & Cowley (2008) subsequently re-analysed the OGLE-II data and have proposed that the light curve shows QPVs at 0.30 and 0.67 days, which are possibly caused by non-radial pulsations of the Be star. They attribute the longer period QPVs found by Eger & Haberl (2008) to aliasing due to the more prominent shorter period QPVs.

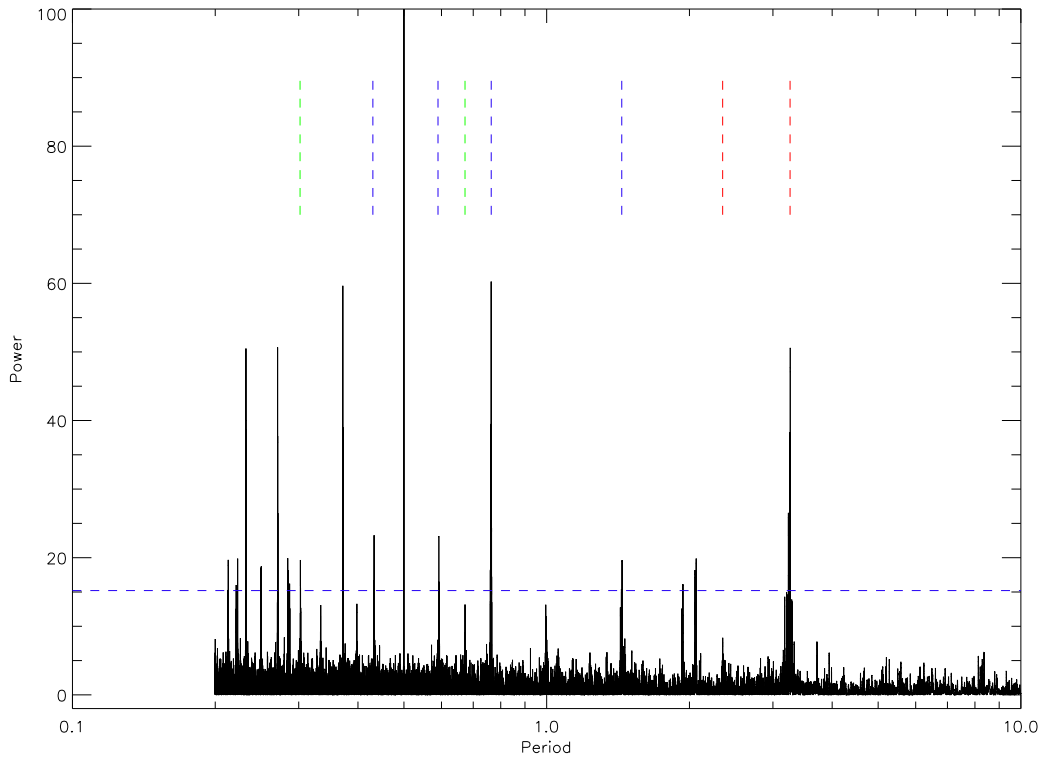

Figure 5.24: Periodogram analysis of SXP726s OGLE light curve. The power scale has been restricted so that the smaller peaks are visible. Marked by the dashed green and red lines are the QPVs identified by Schmidtke & Cowley (2008) and Eger & Haberl (2008) respectively. The blue dashed lines refer to the beats of the 3.26 d peak. The horizontal blue line represents the 99% significance level.

5.5.1 OGLE

No MACHO data exists for this source due to its location in the SMC. The combined OGLE-II and OGLE-III data were analysed in order to study which of these possible QPVs are present in the data. A small magnitude correction (0.19mag) was made to the OGLE-II data so that the average value of the two light curves matched up. Figure 5.23 shows the full OGLE light curve.

The data did not require any prior detrending. A Lomb-Scargle analysis was applied to the entire light curve. It is restricted to the search range, 0.2 to 100 days. This search range extends well above the Nyquist frequency for the data. However, this

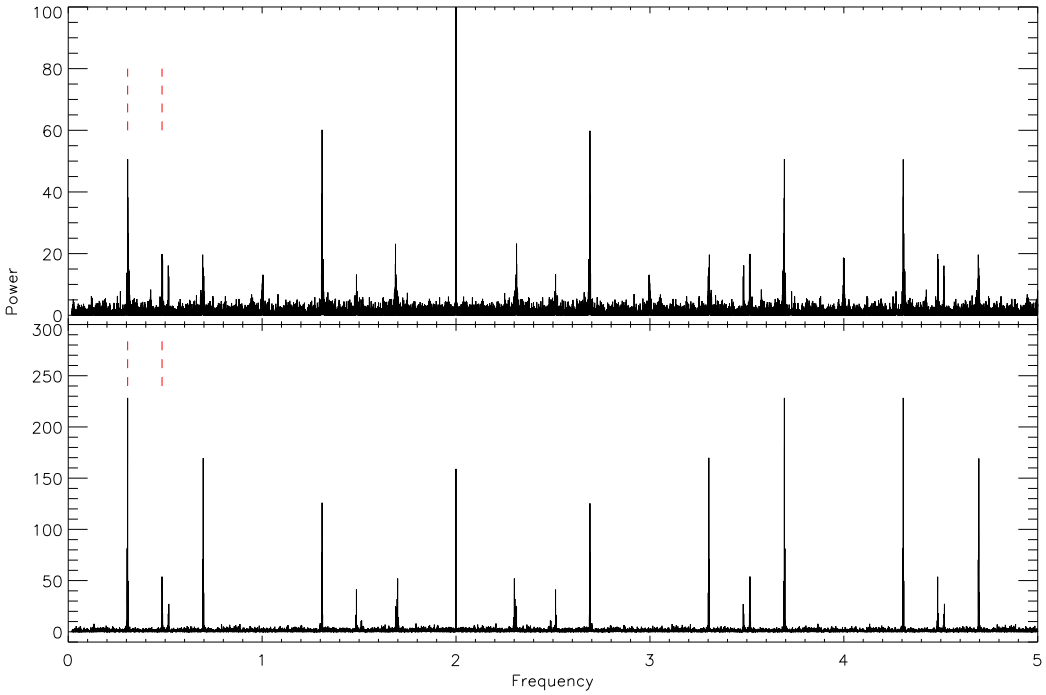

Figure 5.25: Periodogram analysis of SXP726s OGLE light curve (top) and a simulated light curve (bottom) based on two QPV periods, 3.26 d and 2.06 d. The two periods used for the simulated light curve are marked by the red vertical dashed lines.

is acceptable due to the unevenly sampled data and the necessity to check the previously reported periods. There are no significant features above 10 d, so Figure 5.24 has been restricted to the search range $0.2 - 10$ d. There are a number of low period peaks, including the exceptionally strong peak at 0.5 d. In order to attribute this peak to the sampling, the data were randomised 100 times and then the same Lomb-Scargle search was performed. The only peak to appear in these 100 trials was the very strong peak at 0.5 d. Examination of the data sampling revealed that the minimum period between observations was 0.25 d. Thus the traditional Nyquist frequency would be at $2\,d^{-1}$. The peak seen at 0.5 d is due to Nyquist frequency and will be used as the lower bound for periodicity searching, although, there may be real periods present below this cut-off. The next step in the analysis was to compare the periodogram against the previously suggested QPV values.

The lower bound immediately throws out the 0.302 d peak suggested by Schmidtke & Cowley (2008), and their second peak at 0.673 d has now become significantly weaker and is no longer a prominent peak (both of these are marked on Figure 5.24 by the green dashed line). The 2.35 d peak suggested by Eger & Haberl (2008) has remained at a similar power but is now being dwarfed by the peak at 3.26 d (power $\sim$50) (marked by one of the red dashed lines). Also identifiable are three beat periods at 0.764, 1.44 and 0.592 days (marked by blue dashed lines). The first two of these are the beats of 3.26 d with the average $\sim$1 d sampling and the last is the beat with the Nyquist frequency. Two peaks are also present in the data around 2 d. The top panel in Figure 5.25 shows the same periodogram analysis as in Figure 5.24, but this time plotted in frequency space. The symmetrical nature of the periodogram about the Nyquist frequency is clearly evident. The light curve was randomised and a fake signal was added based on the 3.26 d period. Analysis of this simulated light curve failed to recreate all the visible peaks in the original analysis, in particular the two peaks around 2 d. A second period was introduced into the simulated light curve with a period of 2.06 d. The periodogram analysis of this simulated light curve is shown in the bottom panel of Figure 5.25. All the peaks in the original data analysis are now reproduced by the simulated light curve. The remaining period peaks in the original periodogram were investigated in this manner. However, the analysis of these simulated light curves did not reproduce the original results.

The necessity of two periods to successfully recreate the original analysis indicates that there is a minimum of two QPVs in the Be star. The broadened structure of the 3.26 d peak in the periodogram would suggest that the QPV is varying throughout the light curve. A moving search for the QPV was performed throughout the 11 years of data using an 80 day search window. This was performed using the routines developed for the analysis of SXP756 in §5.7. The period range searched was limited to $1-25$ d. The results of this search are shown in Figure 5.26 where the red points refer to detections of the QPV above 99% significance. It is immediately clear that

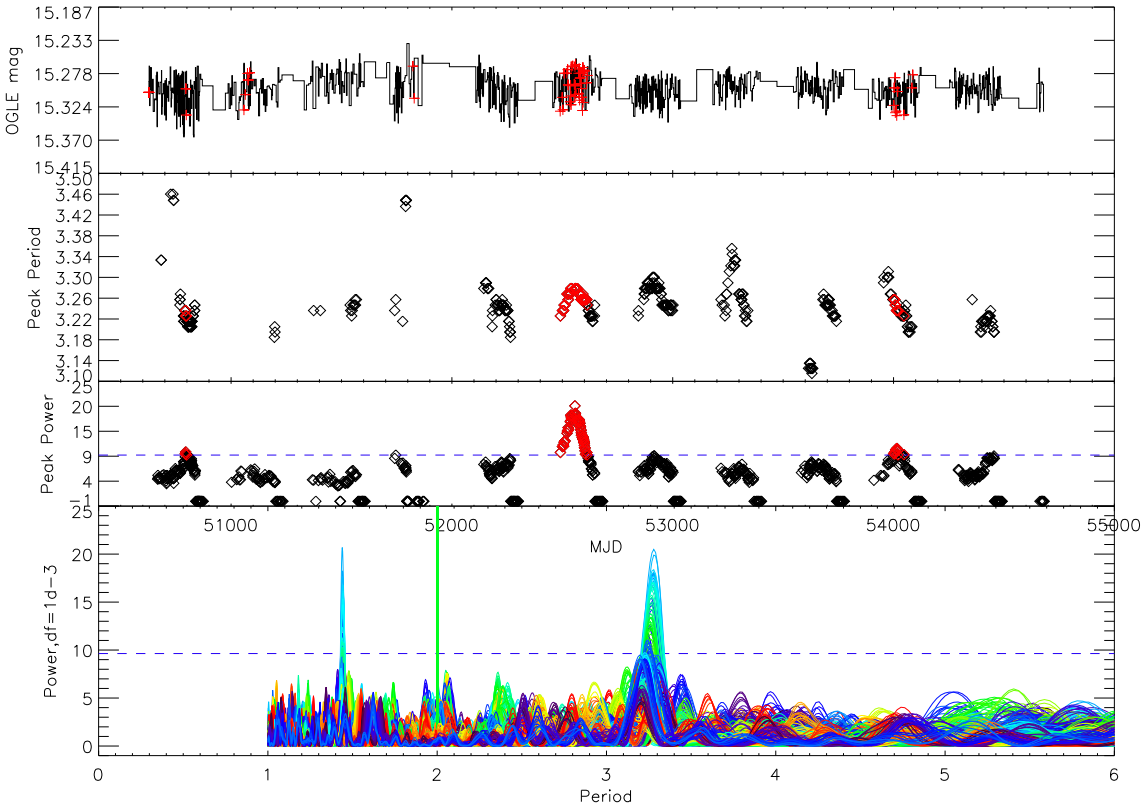

Figure 5.26: Analysis of the 3.26 d QPV throughout the OGLE light curve. First panel (top): OGLE light curve. Second panel: QPV peak period (restricted range to show detail). Third panel: Power of the QPV (restricted range). Fourth panel (bottom): All the periodograms over plotted (colour is not directly linked to a particular period in the light curve). The horizontal blue dashed line represents the 99% significance level. The red points throughout the panels correspond to these significant detections.

the QPV is not always significantly detected within all the 80 d windows. However, it tends to be the largest peak throughout the majority of search windows. Other noticeable features are the beat peaks at 1.44 d, that occur when the 3.26 d peak is strongest and the extremely large narrow spike at 2 days. This spike appears strongly (with a power >500) in several periodograms. The extreme strength and the precise value of 2 suggest that it is due to the data sampling during the particular search window, and this is confirmed when the data set is randomised and the analysis is run again.

During the 6th year of OGLE data the QPV is seen strongly and appears to vary

slightly around the 3.26 d period. As the search window progresses the QPV moves to longer periods reaching a maximum period of ∼3.30 d. It then returns back towards the starting point. This type of behaviour is seen during several other periods of the OGLE data, but the significance falls just below 99% level. If this variation of the QPV is due to some kind of modulation, then the time scale that it is occurring on is around $200-300$ d. The Corbet diagram predicts an orbital period for this systems somewhere in the range $100-400$ d, consistent with the possible modulation time scale. The detected QPV periods were analysed for this orbital modulation. Figure 5.27 shows the results of the period search. The highest peak at 362.3 d and its two harmonics at, 181.2 and 120.3 days are most likely a result of the yearly sampeling. These strong peaks and side lobes make it impossible to identify any peak that can be atributed to the possible orbital modulation. However, this is not to say that it is not present or possibly very close to one year. In this scenario, a hot spot in the circumstellar disk or an over density is created during periastron passage, and this feature of the disk then orbits around the star creating the QPV. Eventually the QPV either moves inwards and slows down, becoming totally absorbed by the disk at some critical orbit, or it simply disperses leaving a flat uniform disk. This interaction could manifest itself during each periastron passage and hence give a suggestion of the orbital period. It is possible that SPH simulations such as those carried out by Okazaki & Negueruela (2001) could be used to investigate such a possible phenomena.

5.6 *RXTE*

This new pulsar was added to the *RXTE* search lists for SMC pulsars, the entire 10 year SMC *RXTE* data archive being searched for pulsations. A search range for pulsations was defined to be $720-735$ s, this range being chosen due to the range of detected pulsations from the *XMM-Newton* observations (Eger & Haberl 2008). This search range allows SXP726 to be clearly separated from the other 700 s sources.

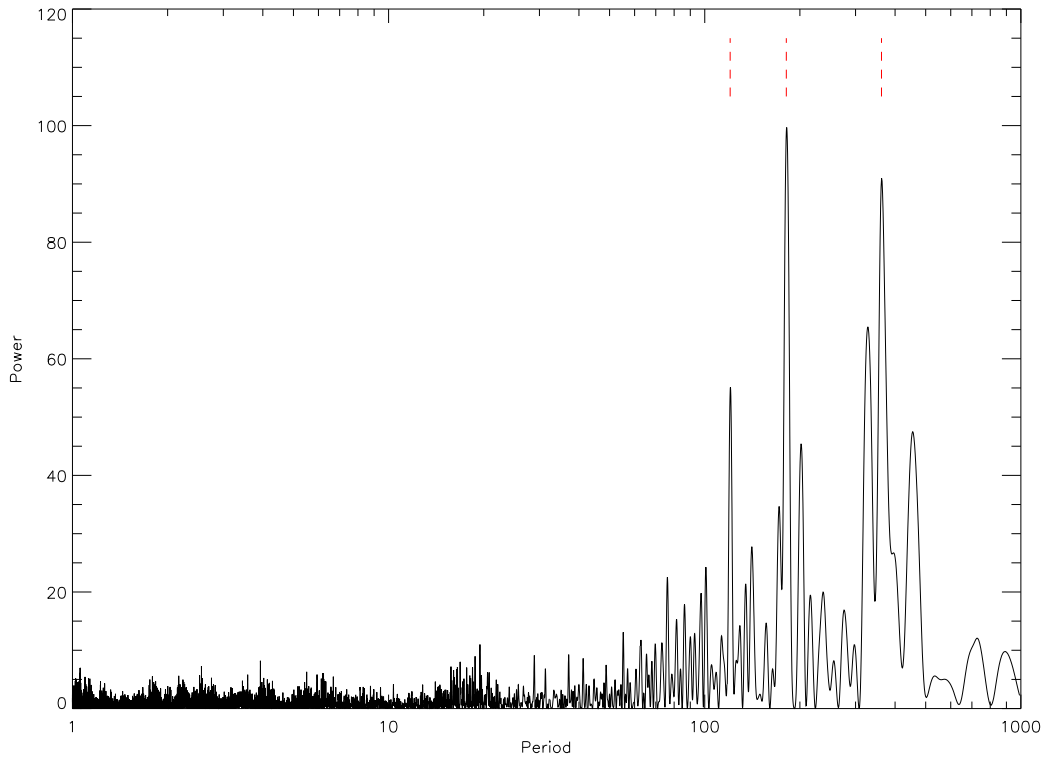

Figure 5.27: Periodogram of the detected 3.26 d QPV. Marked by the dashed red lines are the peaks at 362.3, 181.2 and 120.3 days.

Figure 5.28 shows the results of the search. It is clear that SXP726 has rarely fallen within the monitoring positions, due to its location in the North-Eastern area of the SMC. SXP726 has only been detected by *RXTE* on three occasions (MJD 53839, 54381 and 54597). There are not sufficient data to allow an orbital period search of the X-ray light curve.

5.7 SXP756

In April 2000 *ASCA* detected pulsations at 755.5 s during a long 177 ks observation Yokogawa et al. (2000). Since then the source has been well studied at both X-ray and optical wavelengths. Edge & Coe (2003) identified the optical counterpart to be a Be star, and subsequently McBride et al. (2008) have spectrally classified it to be

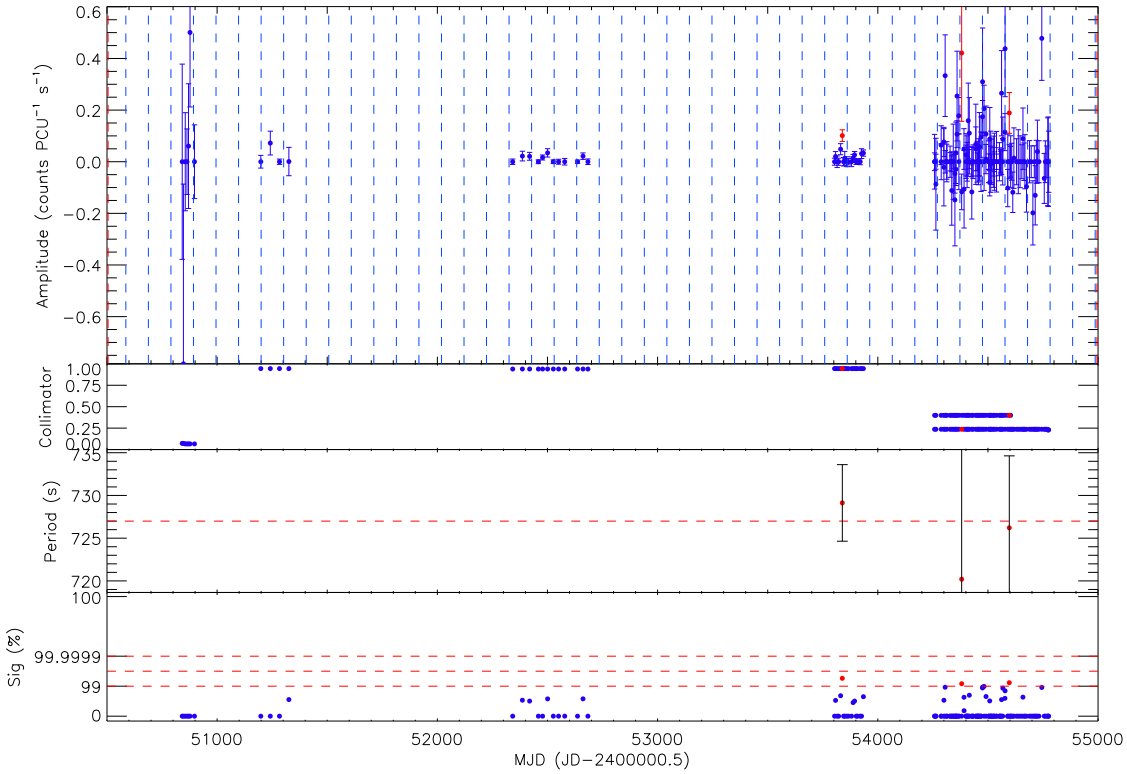

Figure 5.28: *RXTE* light curve of SXP726.

O9.5-B0.5 III-V. The optical light curve is one of the most dramatic of all the SMC X-ray binaries. Figure 5.29 shows the combined OGLE data. Cowley & Schmidtke (2003) have performed a thorough analysis of the OGLE-II and MACHO data, and they found that the optical spikes occur with a period of ∼394 d. They identified this with the orbital period. They also noted the presence of a QPV occurring on a ∼11 d cycle. Subsequently Coe & Edge (2004) studied this QPV behaviour through analysis of the MACHO data using a moving 80 d window. They reported that the QPV varied over time in the approximate range $5 - 15$ d. They also noted that the modulation amplitude of the QPV increased dramatically during the periods of optical outburst, which in turn suggested that the outburst is either creating the QPV or causing the modulation. The previous studies of the optical emission from SXP756 are all based on the older MACHO and OGLE-II data. There is now a further 10 years of OGLE-III data which can be used to evaluate the prior claims about the QPV. The older data was also re-examined in order to confirm and

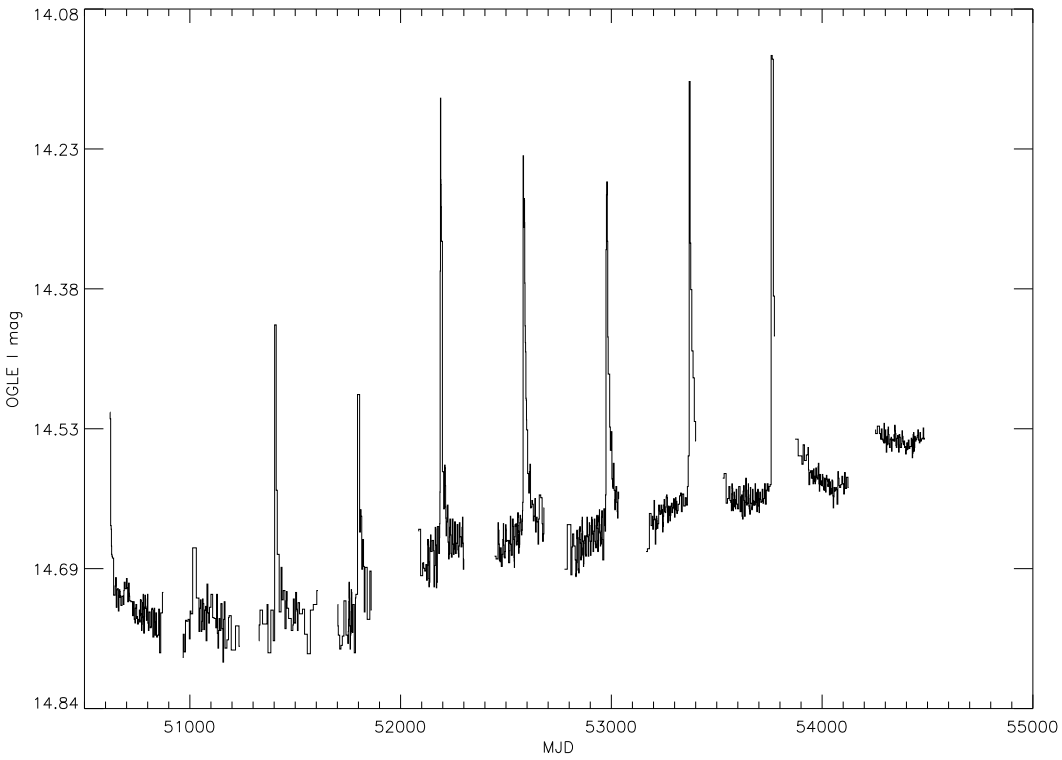

Figure 5.29: OGLE light curve of SXP756 .

compare the results.

5.7.1 OGLE

Initially, the raw light curve was searched for periodicities so that a fundamental power density spectrum could be used as a comparison for all subsequent trials. The main problem with this power spectrum is the many peaks due to the orbital period outbursts. This system is peculiar in that the orbital motion of the neutron star produces extremely spiky optical outbursts, which are extremely hard for a Lomb-Scargle analysis to pick out since they are not sinusoidal in nature. Hence there are a number of high power peaks at various periods throughout the search range that can all be attributed to these spiky outbursts. The spikes were removed in order to search for the QPV over the entire 10 years. The spikes were removed from the data by hand. The light curve was then detrended following the previ-

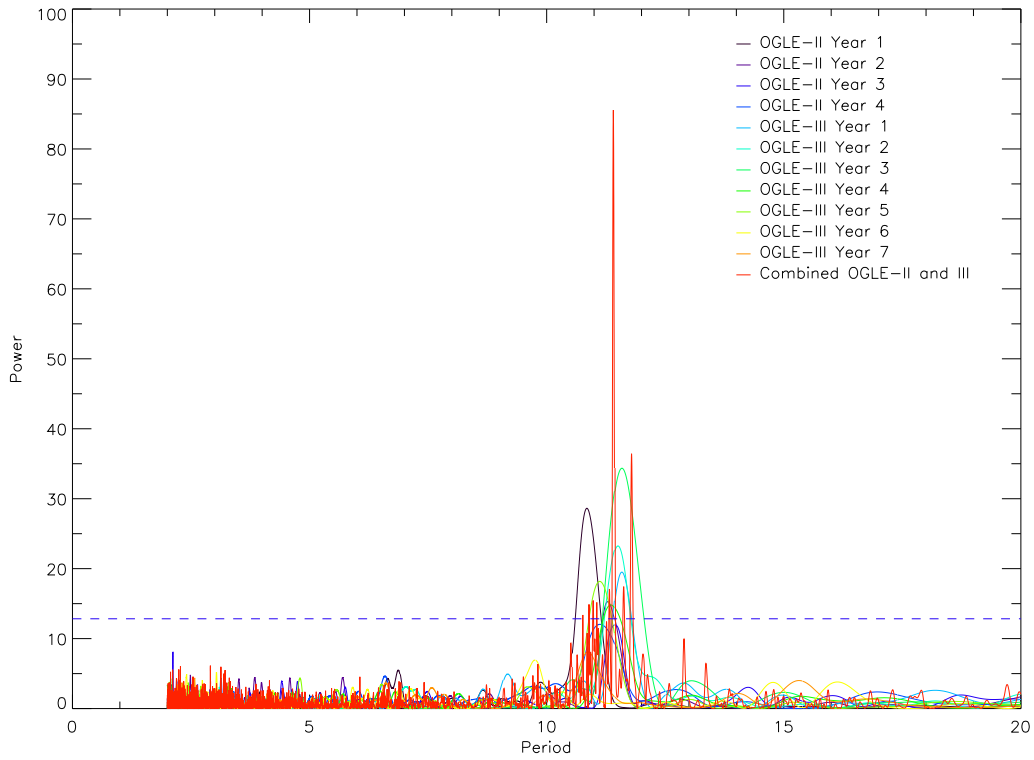

Figure 5.30: Periodograms of the edited and detrended OGLE light curve of SXP756. The years are represented by the different colours as indicated by the legend. The horizontal blue line represents the 99% significance level.

ously described methods in this chapter. Lomb-Scargle analysis was performed on both the individual years and the entire light curve. The resultant Lomb-Scargle periodograms are show in Figure 5.30. The power spectra for the individual years clearly reveal the presence of the QPV above the 99% significance level at ∼11 d. It is also clear that, as was previously seen in the MACHO data, the QPV is moving around. In the first year it is seen at 10.83 d, then by the 7th year it has moved to 11.58 d. The full light curve search (shown by the red line) identifies the QPV with an even greater significance at approximately the average value of 11.40 d.

In the light of these results, it was decided to analysis the newer OGLE data using the same approach as Coe & Edge (2004), i.e. an 80 d moving search window. The large gaps in the OGLE data made applying this method difficult. The analysis was performed as follows:

- The start point of the portion of the light curve to be searched was taken from the first data point. The last data point within 80 days of this point was taken as the end of the range. If no data points were within 80 days then the analysis would proceeded to the next data point.
- A minimum search range length of 70 days was set. If the search range is under 70 days then the analysis would proceeded to the next data point.
- Periodicities were searched for in the period range $3 - 25\,\mathrm{d}$, with a frequency sampling of $df = 1 \times 10^{-3}\,\mathrm{s}^{-1}$.
- The maximum power and its corresponding period were recorded.
- The middle of the search range was taken as the date corresponding to the search.
- This process was repeated moving along the light curve.

This search was performed on the entire OGLE light curve, including the optical outbursts since it had been proposed that they were affecting the observed QPV behaviour. Figure 5.31 shows the results of the analysis.

As the earlier analysis of the yearly data has shown, the QPV period varies throughout the 10 years of data. What is immediately obvious is that the only significant detections occur in-between the optical outbursts. It is clear from the years when an optical outburst is present that, as soon as the search range includes the outburst, the power in the QPV drops and the highest peak in the power spectrum is found well below the 99% significance threshold and can occur at many frequencies. When the search range is less than 70 days long no Lomb-Scargle analysis is performed, and the power and period values are set to 0 and -1 respectively. Contrary to Coe & Edge (2004) the OGLE data provides no evidence that the optical outbursts increase the QPV, so it was decided to apply this analysis to the older MACHO data to check the result.

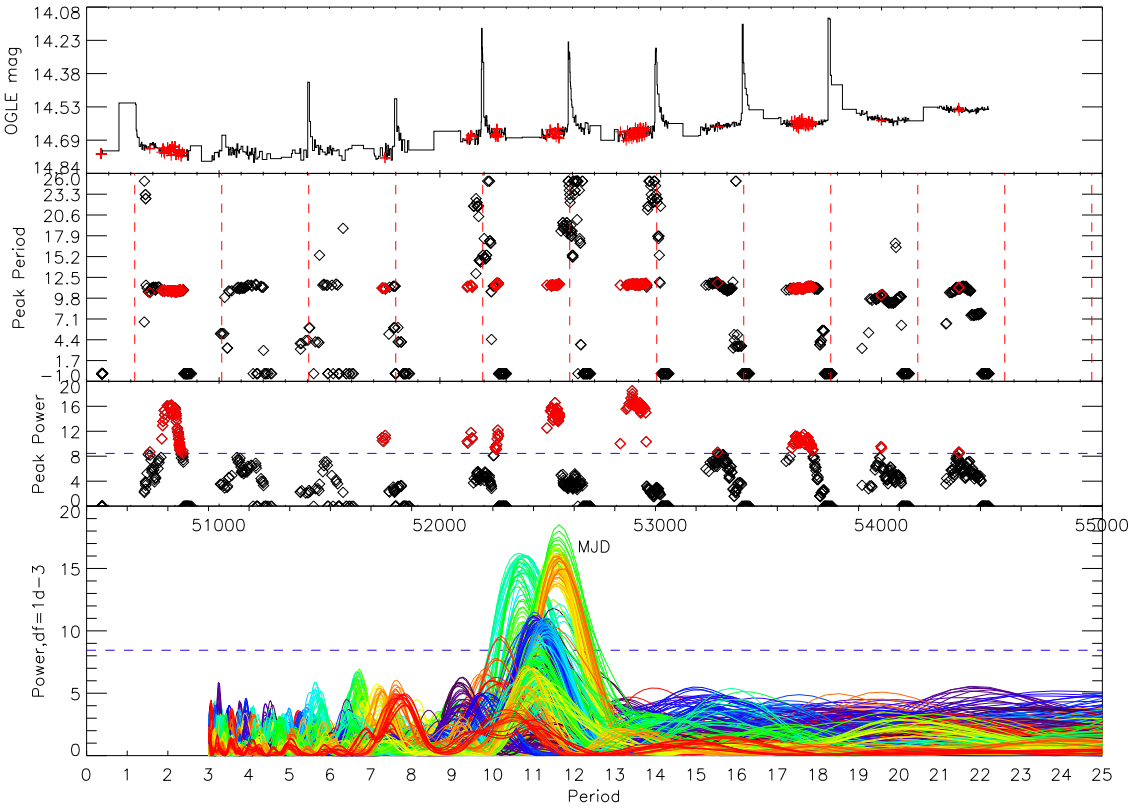

Figure 5.31: Analysis of the QPV throughout the OGLE light curve. First panel (top): OGLE light curve. Second panel: QPV peak period, values of -1 indicate where the search window was less that 70 days. The red dashed vertical lines represent the points when the large optical outbursts take place. Third panel: Power of the QPV. Fourth panel (bottom): All the periodograms over plotted (colour is not directly linked to a particular period in the light curve). The horizontal blue dashed line represents the 99% significance level. The red points throughout the panels correspond to these significant detections.

Figure 5.32 shows the results of the MACHO search. The results agree with the OGLE data. As the search window passes over the optical outbursts the power of the QPV drops and the search method picks up random peaks, usually towards long periods. It is obvious to see from the power spectra that none of these peaks are significant. What is also clear is that the QPV initially started at a lower value ∼9 days and slowly moved its way up to ∼11 days. This is in agreement with the findings of Coe & Edge (2004). If the detected QPV values are compared to those of Coe & Edge (2004) then it is found they follow approximately the same course. The main difference between the two results is that they noted that the semi-amplitude

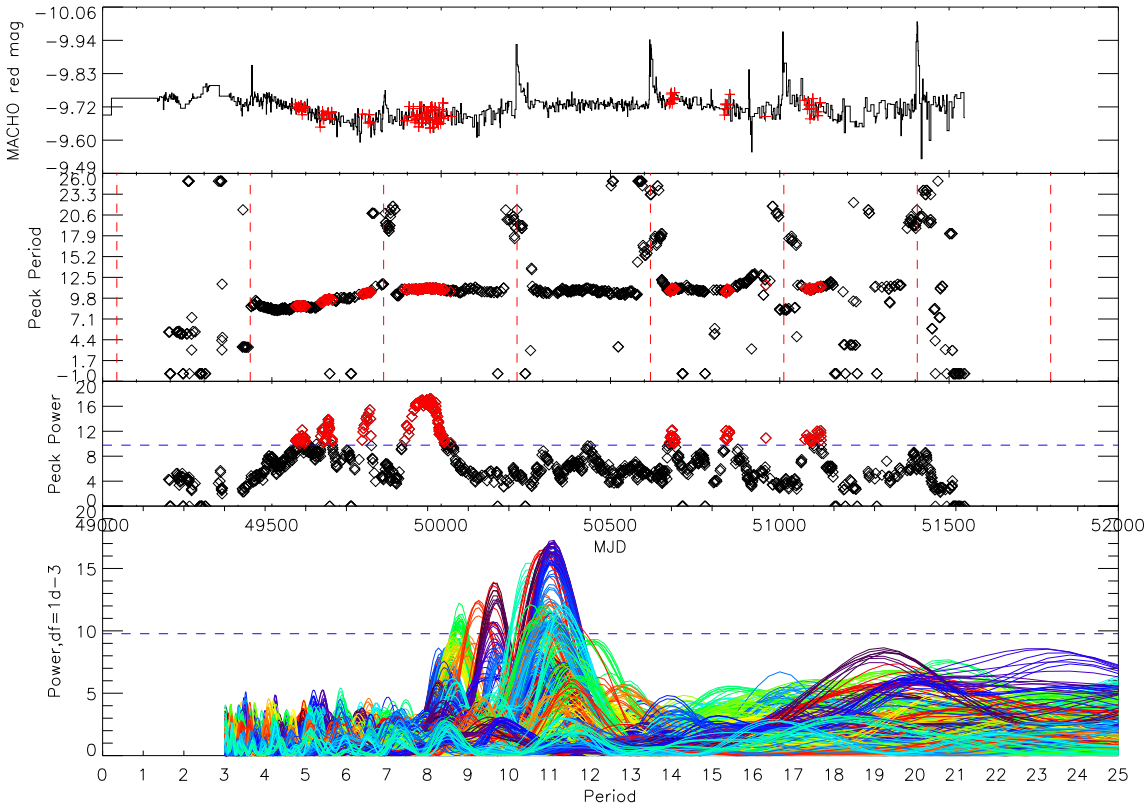

Figure 5.32: Analysis of the QPV throughout the MACHO light curve. First panel (top): MACHO light curve. Second panel: QPV peak period, values of -1 indicate where the search window was less that 70 days. The red dashed vertical lines represent the points when the large optical outbursts take place. Third panel: Power of the QPV. Fourth panel (bottom): All the periodograms over plotted (colour is not directly linked to a particular period in the light curve). The horizontal blue dashed line represents the 99% significance level. The red points throughout the panels correspond to these significant detections.

of the QPV increases as they include the optical outburst, whereas the findings presented here show the power decreasing. This difference is due to the process, used by Coe & Edge (2004), of calculating the semi-amplitude from the power, the following equation is used:

$$Semi - amplitude = \frac{2 \times \sqrt{Power \times Variance}}{Num} \tag{5.1}$$

where Num is the number of data points. It is the variance of the analysed section

of the light curve that is causing the discrepancy. When the outbursts are included the variance increases, sometimes by a factor of 10 or more. This has the knock-on effect of increasing the semi-amplitude artificially by a factor of 3 or more, producing the misleading result that the QPV has increased in strength. Coe & Edge (2004) failed to realise that this equation is only valid under the assumption that the light curve is dominated by a sine wave. This assumption is violated here due to the extreme nature of the optical outbursts. The results from the OGLE data and the reanalysis of the MACHO data show that there is a low period QPV present in the data between the outbursts. However, due to the nature of the outbursts it is not possible to detect the presence of the QPV during the outbursts. Removing the optical outbursts from the data does not initially help, since they cause large $\sim$100 d gaps in the data. If the search window size is increased so that when the gaps are reached the window can cross the gap and still have a sufficient number of data points, then the QPV is detected throughout the entire light curve. In order to achieve this the search window was increased to 300 days, in doing so it is not surprising that the QPV is detected, this is because a search centred on the removed outburst contains a significant proportion of data in-between the outbursts where the QPV was previously detected.

Cowley & Schmidtke (2003) studied the variations in the QPV behaviour by analysing only the data in the periods between the outbursts. They measured the QPV value at 4 points throughout the light curve. Their measured values are consistent with the findings from the moving window analysis. They suggested that the QPV is linked to the circumstellar disk surrounding the Be star. It is clearly seen from the light curve that the passage of the neutron star through periastron is severely affecting the optical emission. This excess emission is believed to be due to changes in the circumstellar disk. It is possible that the disk is locally heated by the X-ray emission thus generating a 'hot spot'. The disk could be perturbed such that an over density of matter is formed at the interaction point, or that the disk shape is changed in such a way as to increase the optical brightness. If one of these is the

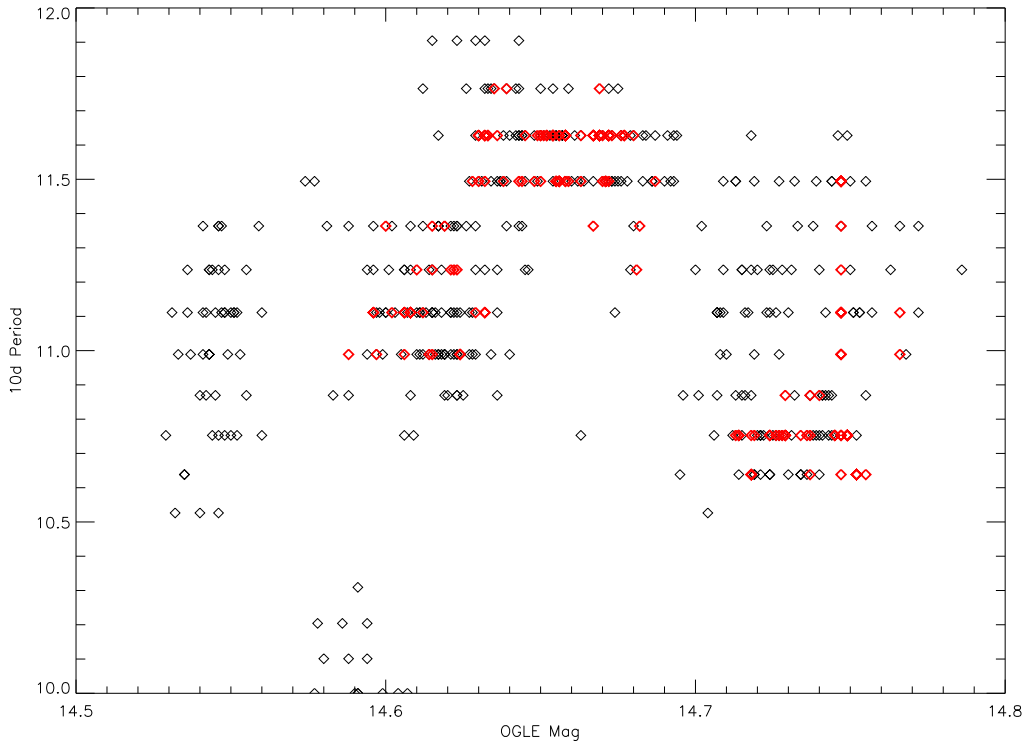

Figure 5.33: Variations of the detected QPV period as a function of the OGLE optical brightness. The red points correspond to detections where the significance was above 99%.

cause, then it is reasonable to expect the effected area to maintain its orbit after the neutron star has left its vicinity and ceased its interaction. This would manifest itself as a rotating hot spot or bulge. Given a high enough orbital inclination to the line of sight, this would result in a QPV signature in the optical light curve, with the variations in detected period indicating the size of the disk. Attempts to correlate the observed QPV period with the observed optical brightness of the system were made. Figure 5.33 shows the comparisons of both the MACHO and OGLE data. A +24.45 shift was applied to the MACHO data to align it with the OGLE-II data. There is no apparent correlation with optical brightness.

5.7.2 *RXTE*

The *RXTE* light curve for SXP756 is extremely well matched to the optical emission. Figure 5.34 shows both the observed X-ray and optical emission. It is clear to see that the X-ray outbursts are correlated with the optical outbursts. As suggested by Coe & Edge (2004), this confirms the 394 d period as the orbital period. Both the missed X-ray and optical outbursts are due to a lack of coverage. There have also been three sets of detections that do not appear at periastron. The first two of these detections around MJD 51625 and 52360 (phase 0.53 and 0.42 respectively) are roughly consistent with the neutron star being at apastron, however, the third at MJD 54020 (phase 0.69) is not (Galache et al. 2008). Unfortunately, the optical coverage for the first two of these is non-existent, and so no comment can be made on changes in the state of the disk. For the third detection though it is clear that there is no additional optical emission, suggesting that the neutron star is able to continue accreting from the stellar wind. Interestingly there is no X-ray emission during the subsequent periastron passage. Explaining this lack of X-ray emission is particularly tricky since it is not known whether there was a corresponding optical outburst. In all the prior cases where there is an optical outburst there has always been some corresponding X-ray emission detectable.

5.8 Discussion

The careful analysis of the optical light curves for a number of SMC Be/X-ray binaries is now revealing a variety of behaviours. The MACHO and, in particular, OGLE light curves are providing an extremely good optical history for these sources. This history is revealing orbital periods and sometimes short period QPVs. Understanding how these behavioural patterns relate to the creation and evolution of the disk is key if the complex nature of these highly interacting systems is to be fully understood.

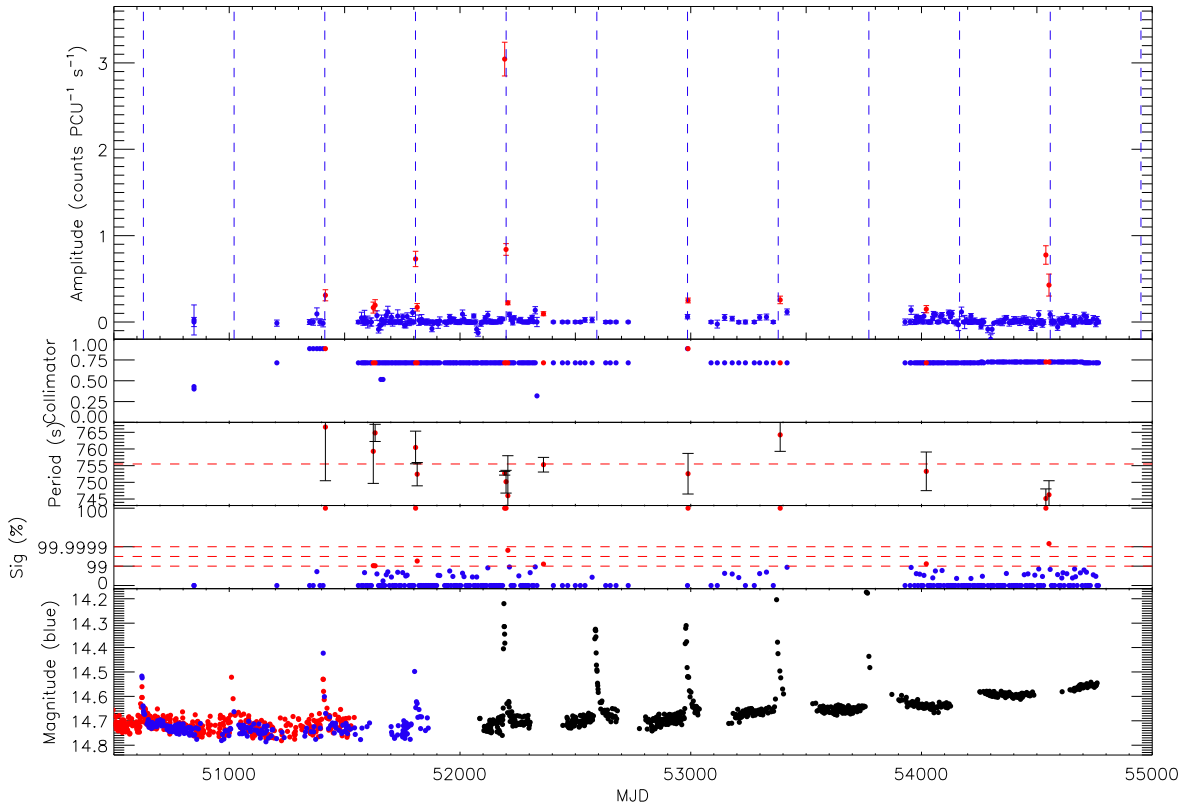

Figure 5.34: *RXTE* and optical data for SXP756, panels from top to bottom: *RXTE* light curve, collimator response, detected pulse period, local significance and optical light curve.

Extensive analysis has been performed on the behaviour of the short-period QPVs in two of the SMC Be/X-ray systems. Although the two systems analysed here both had relatively long X-ray pulse periods (726 and 756 s), QPVs are seen in a large number of the SMC systems.

These QPVs are also seen in other SMC Be/X-ray binaries, such as SXP3.34 and SXP323 (Schmidtke & Cowley 2006; Coe & Edge 2004). The OGLE light curves for all these Be/X-ray binaries are relatively similar in that their average magnitudes remain fairly constant, unlike the large magnitude variations seen in other systems like SXP46.6 and SXP6.85 (McGowan et al. 2007). The exception is SXP756, where large optical outbursts are present; however, these are orbitally modulated and are not due to random changes in the size of the circumstellar disk. If the outbursts are removed from the light curve, then it closely resembles the light curves of the other

two sources showing QPVs.

Interpreting the changes in the light curve is crucial in understanding the binary system and the observed X-ray activity.

The variations in these light curves may be attributed to a variety of effects. Primarily these effects are seen in the circumstellar disk, but this is not always clear when dealing with the short period QPVs. The types of characteristic signatures that are seen in the optical light curves of Be/X-ray binaries are summarised below. Sometimes one or more of these features are present.

- Steady systems: Periods in the light curves when the average magnitude of the system is approximately constant. In some systems this behaviour is seen throughout the entire light curve (for example SXP726, see §5.5), whereas in others it can appear as a fundamental base level.

- Highly variable systems: The light curve shows large magnitude changes seemingly unrelated to the orbital parameters of the binary system. These can either brighten or dim the system by anything from $0.1-1$ mag. The changes are not necessarily repetitive and can often change direction suddenly, for example SXP18.3 (see Chapter 4).

- Orbitally modulated outbursts: These outbursts are the results of the orbit of the neutron star. Their profile is strongly dependent on the orbital parameters of the system: in some systems they appear spiky (e.g. SXP756 see §5.7) and in others they can appear to vary smoothly (e.g. SXP202B see §5.4). The size of the outbursts is controlled by the orbital parameters, but can range from $0.05-0.5$ mag. Typical orbital periods are from $10-300$ days.

- Short period QPVs: Only ever seen in sections of the light curve when the system is in the steady state, due to the effect being washed out during the large changes in magnitude. Typically they cause variations in the light curve

of < 0.1 mag. They can be found in the range of periods $0.5 - 10$ days (for example SXP726, see §5.5).

Okazaki & Negueruela (2001) have shown that the circumstellar disks truncate at resonant radii. However, if the truncation radius switches between resonant states then this would allow the disk to move either outwards or inwards. These large changes in the size of the disk are responsible for the large variations seen in the highly variable systems. The orbitally modulated outbursts are analogous to the Type-I X-ray outbursts seen in almost all Be/X-ray binary systems. They are the result of the neutron star interacting with the circumstellar disk as it passes through periastron. The X-ray emission is due to matter that is transferred from the circumstellar disk into an accretion disk around the neutron star, and is eventually accreted. The optical emission is probably caused by the disk swelling at the point where the matter is transferred to the neutron star. The swelling could be in the form of a localised over-density or a hot spot where the material is heated by locally increased frictional forces. In both these cases the interaction point is linked to the position of the neutron star. The outburst dies down once the neutron star is sufficiently far away. This type of disk variability is also know as the one arm instability (Okazaki 1991).

One of the most interesting features that are starting to be found in these optical light curves is the short period QPVs. These are now being found in ever increasing numbers, but are still extremely poorly understood. The mechanisms that potentially cause these QPVs are very unclear. As proposed earlier, one possible cause could be the orbital period of a hot spot or one-armed oscillation. If this was the primary mechanism, then this type of signature would only be expected from systems where the circumstellar disk plane is inclined to our line of sight. Thus the Hα emission from these systems would be expected to exhibit a double peaked structure. It is also possible that the QPVs are the result of non-radial pulsations (NRPs) originating in the Be star. NRPs are a form of travelling-wave known to exist in

early-type stars (Osaki 1986). They are revealed through line profile variations in high resolution spectroscopy, and as a result are often seen as short period variations in optical light curves. One key property of NRPs is their ability to transfer angular momentum around the star. In this manner they have been linked as a possible mechanism for providing the extra angular momentum to the outer stellar surface layers allowing B type stars to form circumstellar disks (Osaki 1986). Generally, NRPs observed in HMXBs have periods less than a day (Schmidtke, Cowley, & Udalski 2006; Schmidtke & Cowley 2006). However, it is also possible that the NRP can leak out into the circumstellar disk causing longer period variations, as seen in SXP726 and SXP756. Schmidtke, Cowley, & Udalski (2006) found that sources that exhibited NRPs, with the exception of SXP169, tend not to show orbitally modulated outbursts. SXP756 is now a second exception to this statement. This is most likely due to the physical process causing the variation being related to circumstellar disk phenomena, rather than NRPs in the star.

Chapter 6

Conclusions and Future Work

6.1 Conclusions

Over the past 20 years the SMC has become one of the most deeply studied objects in the sky. There have been numerous X-ray observations, covering almost the entire field, that have detected and positionally located 58 known X-ray pulsars and around 30 HMXB candidates. This group of objects represents by far the largest homogeneous population of X-ray binaries in any galaxy. This thesis has studied a selected number of these X-ray pulsars, presenting both the optical and X-ray data where it exists.

Chapter 3 has concentrated on analysing the optical counterparts to the newly discovered X-ray pulsars found through the *Chandra* Wing survey. The optical counterparts were classified as Be stars from blue and red spectra taken by a variety of telescopes. Their spectral classes fit extremely well into the distribution of other SMC sources. Where it has been possible, the evolution of the Hα line has also been examined, allowing evaluation of possible changes in the circumstellar disk. This has shown SXP967 to have a stable circumstellar disk, unlike the other sources. It is

possible that this stability is due to the circumstellar disk extending out to its truncation radius. For SXP65.8, the brightest of the detected *Chandra* X-ray sources, phase-resolved X-ray spectroscopy has been performed. The analysis suggests that there is a soft underlying component to the X-ray emission, indicative of a separate emission region to the collimated beam. Further intensive X-ray observations of the source during a bright state would help determine the precise origin of this X-ray emission, whether it is from an accretion disk or from the neutron star's stellar surface.

The recent positional location of SXP18.3 enabled an extremely detailed study to be made of its X-ray and optical properties. The positional location by *XMM-Newton* allowed the OGLE data, spanning almost 11 years, to be examined for periodicities. Interestingly, only one year of the OGLE data provided a clear periodic signal. From the comparisons of this period with the *RXTE* data an orbital period of 17.79 d has been proposed. The reasons behind the disappearance of the orbital period during the remainder of the optical light curve are not fully understood. The cause is likely related to exactly how the neutron star removes material from the circumstellar disk. Further detailed optical observations of the circumstellar disk are vital to understanding this, in particular during any subsequent Type-II outbursts. The relatively short orbital period will make studies of the Hα emission line extremely profitable since the evolution of any perturbation of the circumstellar disk will be seen in the line profile.

The OGLE light curves are proving to be extremely valuable when studying these sources. In combination with the *RXTE* light curves, they are enabling many of the properties of the SMC Be/X-ray binaries to be studied. The orbital periods for SXP2.37, SXP172 and SXP202B, 18.62, 68.9, and 229.9 days, respectively, have been measured from the detrended OGLE light curves. Through careful examination of the light curves for SXP726 and SXP756, possible QPVs have been discovered. The cause of these variations has been suggested to be related to the circumstellar disk, but NRPs cannot be ruled out. As a consequence of the recent work of Haberl

et al. (2008a), the counterpart to SXP15.3 has been questioned. This has resulted in a second object being proposed as the true counterpart, which, if found to be true, would make the system unique, in that the HMXB may contain an optical counterpart outside the expected spectral distribution. The OGLE project team have now made available the OGLE light curves for all the SMC sources. These light curves are automatically updated on a daily basis, and are available through their website[1]. This now allows the changes taking place in the circumstellar disk to be studied in real time and jointly with the X-ray monitoring.

6.2 Future Work

Although the group of Be/X-ray binaries in the SMC is beginning to be understood as a population, we are still a long way from being able to study and understand the peculiarities of each system separately. Spectral classifications of almost all the SMC Be/X-ray binary companions have greatly assisted in the study of individual sources. The next step is to try and measure accurate orbital parameters and link these to the X-ray and optical emissions.

One of the most interesting features that has been examined in this thesis is the presence of the short-period QPVs in the circumstellar disks. Many of the SMC sources have been shown to exhibit these variations in their optical light curves, but the cause of these variations is still not entirely clear. It is possible that some of the very short QPVs are in fact non-radial pulsations in the outer envelope of the Be star, but it is not clear that the longer intermediate QPV periods of $\sim$10 d can be caused by the same mechanism. Using the smoothed particle hydrodynamics code of Okazaki et al. (2002), it is possible to introduce features into a disk such as X-ray induced hot spots or one-armed global oscillations. This will allow the emission processes to be tested. Since there are now many systems that are exhibiting these

[1]http://ogle.astrouw.edu.pl/ogle3/xrom/xrom.html

QPVs it may be possible to separate the sources into different categories. These QPVs may also be closely related to the truncation of the disk, and so knowledge of the orbital parameters of these systems is important.

The large outburst from SXP18.3 allowed an estimation of the system's orbital parameters. These orbital values can be used in conjunction with the SPH models to estimate the possible truncation radii for SXP18.3. Comparing both the orbital parameters and truncation radii with future measurements of the Hα line profile, together with any observed X-ray outbursts, will be extremely important if the SMC population is to be understood and fully compared to the Milky Way population.

However, it is not sufficient to study one system only. SXP6.85 located in the middle of the SMC, recently displayed a similar outburst to SXP18.3. The outburst began at the beginning of September 2008 and lasted for several months. Since the optical counterpart was already established (Haberl & Pietsch 2008), follow-up observations were possible. *RXTE* data were taken every two days for a period of around 2 weeks in the middle of the outburst. I plan on examining the data for similar orbitally modulated X-ray period changes. If these variations exist then it will be possible to fit an orbital solution to the data in a similar fashion to SXP18.3.

Continuing Hα observations of all these systems and the other Be/X-ray binaries is vital in understanding both the formation and evolution of the circumstellar disk and the X-ray outbursts. In particular, regular high-resolution optical spectroscopy will enable the circumstellar disk structures to be monitored before and after any X-ray outbursts. Sources such as SXP46.6 exhibit Type-I outbursts every periastron passage, and make ideal targets for this type of study. A series of ESO VLT observations monitoring approximately 20 Be/X-ray binaries in the SMC has recently been carried out covering a 3 month period. These medium and high resolution spectra will allow us to study the development of the disks in extreme detail. A number of the sources experienced X-ray outbursts during this period and will be fundamental to this study. Future observations would be ideally suited to a SALT

or ESO ToO program, since they could be triggered from the *RXTE* monitoring program, allowing the circumstellar disk 'decay' or changes to be studied extremely regularly.

In addition to the X-ray pulsars already studied in this thesis, and the literature, there are a number of other potential HMXBs in the SMC (Shtykovskiy & Gilfanov 2005). Since their initial detection many of these sources have subsequently been found to be pulsars, like SXP893 (Laycock, Zezas, & Hong 2008). The majority of these pulsars are covered in the OGLE and MACHO surveys, but their optical light curves have not yet been examined. By studying these optical light curves prior to future X-ray detections of a pulse period, it will be possible to plan more careful and scientific follow-up observations. This will allow any future X-ray detections to be exploited fully, producing the best possible science.

Bibliography

Alcock C., et al., 1999, PASP, 111, 1539

Baykal A., Stark M.J., Swank J., 2002, ApJ, 569, 903

Besla G., Kallivayalil N., Hernquist L., Robertson B., Cox T. J., van der Marel R. P., Alcock C., 2007, ApJ, 668, 949

Bildsten L., et al., 1997, ApJS, 113, 367

Blay P., Reig P., Martínez Núñez S., Camero A., Connell P., Reglero V., 2004, A&A, 427, 293

Cassinelli J. P., Brown J. C., Maheswaran M., Miller N. A., Telfer D. C., 2002, ApJ, 578, 951

Cherepashchuk A. M., Sazhin M. V., Trifalenkov I. A., 1995, Ap&SS, 229, 265

Clark J. S., Tarasov A. E., Panko E. A., 2003, A&A, 403, 239

Coe M. J., et al., 1994, A&A, 289, 784

Coe M.J. 2000 in "The Be Phenomenon in the Early-Type Stars", IAU Colloquium 175, ASP Conference Proceedings, Vol. 214, ed: M.A. Smith, H.F. Henrichs. Astronomical Society of the Pacific, p.656.

Coe M. J., Haigh N. J., Laycock S. G. T., Negueruela I., Kaiser C. R., 2002, MNRAS, 332, 473

Coe M.J., Edge W.R.T., 2004, MNRAS, 350, 756

Coe M.J., Edge W.R.T., Galache J.L., McBride V.A., 2005, MNRAS, 356, 502

Coe M. J., et al., 2007, MNRAS, 378, 1427

Coe M.J., Schurch M.P.E., Corbet R.H.D., Galache J.L., McBride V.A., Townsend L.J., Udalski A., 2008, MNRAS, 387, 727

Coe M.J., McBride V.A., Bird A.J., Corbet R.H.D., 2008, ATel, 1882, 1

Corbet R. H. D., 1984, A&A, 141, 91

Corbet R.H.D., 1986, MNRAS, 220, 1047

Corbet R.H.D., Marshall F.E., Peele A.G., Takeshima T., 1999, ApJ, 517, 956

Corbet R. H. D., Marshall F. E., Coe M. J., Laycock S., Handler G., 2001, ApJ, 548, L41

Corbet R.H.D., Markwardt C.B., Coe M.J., Edge W.R.T., Laycock S., Marshall F.E., 2003, ATel, 214, 1

Corbet R.H.D., Markwardt C.B., Marshall F.E.,Coe M.J., Edge W.R.T.,Galache J.L., Laycock S., 2004, ATel, 347, 1

Cowley A. P., Schmidtke P. C., McGrath T. K., Ponder A. L., Fertig M. R., Hutchings J. B., Crampton D., 1997, PASP, 109, 21

Cowley A. P., Schmidtke P. C., 2003, AJ, 126, 2949

Covino S., Negueruela I., Campana S., Israel G. L., Polcaro V. F., Stella L., Verrecchia F., 2001, A&A, 374, 1009

Dachs J., Wamsteker W., 1982, A&A, 107, 240

Dickey J.M., Lockman F.J., 1990, A&A, 28, 215

Edge W.R.T., Coe M.J., 2003, MNRAS, 338, 428

Edge W. R. T., Coe M. J., Galache J. L., McBride V. A., Corbet R. H. D., Markwardt C. B., Laycock S., 2004, MNRAS, 353, 1286

Edge W. R. T., 2005, PhDT

Eger P., Haberl F., 2008, ATel, 1453, 1

Eger P., Haberl F., 2008, A&A, 485, 807

Evans C.J., Howarth I.D., Irwin M.J., Burnley A.W., Harries T.J., 2004, MNRAS, 353, 601

Eyles C. J., Skinner G. K., Willmore A. P., Rosenberg F. D., 1975, Nature, 254, 577

Finger M. H., Macomb D. J., Lamb R. C., Prince T. A., Coe M. J., Haigh N. J., 2001, ApJ, 560, 378

Frank J., King A., Raine D.J., 2002, Accretion Power in Astrophysics: Third Edition, by Juhan Frank and Andrew King and Derek Raine, Cambridge University Press, 2002. ISBN 0-521-62957-8

Galache J.L., Laycock S.G.T., Corbet R.H.D., Lochner J., Coe M.J., Schurch M.P.E., Marshall F.E., Markwardt C., 2008, ApJ, (accepted)

Gardiner L. T., Noguchi M., 1996, MNRAS, 278, 191

Ghosh P., Lamb F.K., 1979, ApJ, 234, 296

Grundstrom, E.D., et al., 2007, APJ, 660, 1398

Haberl F., Sasaki M., 2000, A&A, 359, 573

Haberl F., Pietsch W., 2004, A&A, 414, 667

Haberl F., Eger P., Pietsch W., 2008a, A&A, 489 327

Haberl F., Eger P., Pietsch W., Corbet R. H. D., Sasaki M., 2008b, A&A, 485, 177

Haberl F., Pietsch W., 2008, A&A, 484, 451

Hanuschik R. W., Kozok J. R., Kaiser D., 1988, A&A, 189, 147

Harries T. J., Hilditch R. W., Howarth I. D., 2003, MNRAS, 339, 157

Horne J. H., Baliunas S. L., 1986, ApJ, 302, 757

Hubrig S., Yudin R. V., Pogodin M., Schoeller M., Peters G. J., Cure M., 2007, soch.conf, 21

Hughes J.P., Smith R.C., 1994, AJ, 107, 4

Israel G.L., Stella L., Campana S., Covino S., Ricci D., Oosterbroek T., 1998, IAUC 6999, 1

Israel G. L., Stella L., Covino S., Campana S., Mereghetti S., 1999, IAUC, 7101, 1

Israel G.L., et al., 2000, ApJ, 531, 131

Jaschek C., Jaschek M., The Classification of Stars, by Carlos Jaschek and Mercedes Jaschek, Cambridge University Press, 1990. ISBN 0-521-38996-8

Jaschek M., Slettebak A., Jaschek C., 1981, BeSN, 4, 9. As in Jaschek & Jaschek (1990) p151.

Kahabka P., Pietsch W., 1996, A&A, 312, 919

Kahabka P., Pietsch W., Filipovic M.D., Haberl F., 1999, A&AS, 136, 81

Kahabka P., 2000, A&A, 354, 999

Kahabka P., Haberl F., Payne J. L., Filipović M. D., 2006, A&A, 458, 285

Kallivayalil N., van der Marel R. P., Alcock C., Axelrod T., Cook K. H., Drake A. J., Geha M., 2006, ApJ, 638, 772

Kallivayalil N., van der Marel R. P., Alcock C., 2006, ApJ, 652, 1213

Kallivayalil N., van der Marel R. P., Anderson J., Besla G., Alcock C., 2008, arXiv, arXiv:0809.4263

Kato D., et al., 2007, PASJ, 59, 615-647

Kurucz R.L., 1979, ApJS, 40, 1

Lamb R. C., Prince T. A., Macomb D. J., Finger M. H., 1999, IAUC, 7081, 4

Laycock S., Corbet R.H.D., Coe M.J., Marshall F.E., Markwardt C., Lochner J., 2005 ApJS, 161, 96

Laycock S., Zezas A., Hong J., 2008, arXiv, arXiv:0809.1738

Lee U., Osaki Y., Saio H., 1991, MNRAS, 250, 432

Lennon D.J., 1997, A&A, 317, 871

Lewin W. H. G., van der Klis M., 2006, *Compact stellar X-ray sources*, Compact stellar X-ray sources, Cambridge, UK: Cambridge University Press, 2006, Cambridge Astrophysics Series, No. 39. Edited by Walter Lewin & Michiel van der Klis. ISBN 978-0-521-82659-4

Li F., Jernigan G., & Clark G. 1977, IAU Circ., 3125, 1

Li F., & Clark G. 1977, IAU Circ., 3154, 1

Liu Q. Z., van Paradijs J., van den Heuvel E. P. J., 2005, A&A, 442, 1135

Liu Q. Z., Yan J. Z., 2005, NewA, 11, 130

Liu Q. Z., van Paradijs J., van den Heuvel E. P. J., 2006, A&A, 455, 1165

Liu Q. Z., van Paradijs J., van den Heuvel E. P. J., 2007, A&A, 469, 807

Lomb N. R., 1976, Ap&SS, 39, 447

Majid W. A., Lamb R. C., Macomb D. J., 2004, ApJ, 609, 133

Massey P., 2002, ApJS, 141, 81

McBride V.A., Coe M.J., Negueruela I., Schurch M.P.E., McGowan K.E., 2008, MNRAS, 388, 1198

McGowan K.E., et al., 2007, MNRAS, 376, 759

McGowan K.E., Coe M.J., Schurch M.P.E., Corbet R.H.D., Galache J.l., Udalski A., 2008, MNRAS, 384, 821

Meyssonnier N., Azzopardi M., 1993, A&AS, 102, 451

Motch C., Lopes de Oliveira R., Negueruela I., Haberl F., Janot-Pacheco E., 2007, ASPC, 361, 117

Murdin P., Morton D. C., Thomas R. M., 1979, MNRAS, 186, 43P

Negueruela I., 1998, A&A, 338, 505

Negueruela I., Torrejón J. M., Reig P., Ribó M., Smith D. M., 2008, AIPC, 1010, 252

Okazaki A. T., 1991, PASJ, 43, 75

Okazaki A.T., Negueruela I., 2001, A&A, 377, 161

Okazaki A. T., Bate M. R., Ogilvie G. I., Pringle J. E., 2002, MNRAS, 337, 967

Okazaki A. T., Hayasaki K., 2006, ESASP, 604, 171

Osaki Y., 1986, PASP, 98, 30

Osaki Y., 1996, PASP, 108, 39

Owocki S., Gayley K., Cranmer S., 1996, AAS, 28, 881

Paczyński B., 1967, AcA, 17, 355

Press W. H., 2002, Numerical recipes in C++ : the art of scientific computing by William H. Press. xxviii. ISBN 0-521-75033-4.

Pringle J. E., Rees M. J., 1972, A&A, 21, 1

Putman M. E., 2000, PASA, 17, 1

Putman M. E., Staveley-Smith L., Freeman K. C., Gibson B. K., Barnes D. G., 2003, ApJ, 586, 170

Raguzova N. V., 2001, A&A, 367, 848

Reig P., Fabregat J., Coe M. J., 1997, A&A, 322, 193

Reig P., 2007, MNRAS, 377, 867

Sasaki M., Pietsch W., Haberl F., 2003, A&A, 403, 901

Schmidtke P. C., Cowley A. P., Levenson L., Sweet K., 2004, AJ, 127, 3388

Schmidtke P. C., Cowley A. P., Udalski A., 2006, AJ, 132, 971

Schmidtke P. C., Cowley A. P., 2006, AJ, 132, 919

Schmidtke P. C., Cowley A. P., 2008, ATel, 1632, 1

Schurch M.P.E., Coe M.J., McGowan K.E., McBride V.A., Buckley D.A.H., Galache J.L., Corbet R.H.D., 2007, MNRAS, 381, 1561

Schurch M. P. E., Udalski A., 2008, ATel, 1611, 1

Schurch M. P. E., Udalski A., Coe M., 2008, ATel, 1670, 1

Schurch M. P. E., et al., 2009, MNRAS, 392, 361

Schwering P.B.W. & Israel F.P., 1991, A&A, 246, 231

Secchi A., 1878, Die Sterne, Brockhaus, QB801, 15. As in Jaschek & Jaschek (1990) p152.

Sguera V., et al., 2005, A&A, 444, 221

Shakura N. I., Syunyaev R. A., 1973, A&A, 24, 337

Shtykovskiy P., Gilfanov M., 2005, MNRAS, 362, 879

Shtykovskiy P. E., Gilfanov M. R., 2007, AstL, 33, 437

Sidoli L., Paizis A., Mereghetti S., 2006, A&A, 450, L9

Sigut T. A. A., Jones C. E., 2007, ApJ, 668, 481

Skrutskie M.F., et al., 2006, AJ, 131, 1163

Stanimirovic S., Staveley-Smith L., Dickey J. M., Sault R. J., Snowden S. L., 1999, MNRAS, 302, 417

Stella L., White N. E., Rosner R., 1986, ApJ, 308, 669

Szymański M.K., 2005, Acta Astron., 55, 43

Tauris T. M., van den Heuvel E. P. J., 2006, *Compact stellar X-ray sources*, Compact stellar X-ray sources, Cambridge, UK: Cambridge University Press, 2006, Cambridge Astrophysics Series, No. 39. Edited by Walter Lewin & Michiel van der Klis. ISBN 978-0-521-82659-4

Torii K., Kohmura T., Yokogawa J., Koyama K., 2000, IAUC, 7441, 2

Townsend R. H. D., Owocki S. P., Howarth I. D., 2004, MNRAS, 350, 189

Trudolyubov S. P., Priedhorsky W. C., Córdova F. A., 2007, ApJ, 663, 487

Tucholke H.-J., De Boer K.S., Seitter W.C., 1996, A&AS, 119, 91

Udalski A., Kubiak M., Szymański M., 1997, Acta Astron., 47, 319

Udalski, M.J., & Coe, A., 2008, ATel, 1458, 1

Vanbeveren D., De Loore C., Van Rensbergen W., 1998, A&ARv, 9, 63

van den Heuvel E. P. J., 1975, ApJ, 198, L109

Walborn N.R., Fitzpatrick E.L., 1990, PASP, 102, 379

Walter R., Zurita Heras J., 2007, A&A, 476, 335

Wegner W., 2006, MNRAS, 371, 185

Wilson C. A., Finger M. H., Harmon B. A., Scott D. M., Wilson R. B., Bildsten L., Chakrabarty D., Prince T. A., 1997, ApJ, 479, 388

Wilson R. E., Wilson A. T., 1976, ApJ, 204, 551

Woolf N. J., Stein W. A., Strittmatter P. A., 1970, A&A, 9, 252

Yokogawa J., Koyama K., 1998, IAUC 7009, 3

Yokogawa J., Torii K., Imanishi K., Koyama K., 2000, PASJ, 52, L37

Zamanov R., Martí J., 2000, A&A, 358, L55

Zaritsky D., Harris J., Thompson I.B., Grebel E.K., Massey P., 2002, AJ, 123, 855

Zaritsky D., Harris J., 2004, ApJ, 604, 167